Novel Insights in Retinoid Homeostasis during the Feeding-Fasting Transition of Mice

Inaugural-Dissertation
to obtain the academic degree
Doctor rerum naturalium (Dr. rer. nat.)

Submitted to the
Department of Biology, Chemistry, Pharmacy
of
Freie Universität Berlin

by

Julia Sonja Steinhoff
2022

The present doctoral study was carried out from October 2018 to April 2022 at the Institute of Pharmacology at Charité – Universitätsmedizin Berlin under the supervision of Prof. Dr. rer. nat. Michael Schupp.

1st reviewer: Prof. Dr. rer. nat. Michael Schupp

2nd reviewer: Prof. Dr. rer. nat. Nan Ma

Date of defense: August 30, 2022

Herewith I, Julia Sonja Steinhoff, certify that I have prepared and written my thesis independently and that I have not used any sources and aids other than those indicated by me. I affirm that I have not applied for an examination procedure at any other institution or submitted the dissertation in this or any other form to any other faculty as a dissertation.

Table of Contents

List of Figures

[1] The graphic image elements used in figures 6, 7, 8, and 43 were taken from Servier Medical Art by Servier (https://smart.servier.com).

List of Tables

Abbreviations

According to general guidelines on formatting protein and gene nomenclature, in this work for protein symbols all letters are upper-case and not italicized, and for gene symbols the first letter is in upper-case and all letters are italicized.

18s	18S ribosomal RNA (component of the eukaryotic ribosomal small subunit)
36b4	acidic ribosomal phosphoprotein P0
8-Br-cAMP	8-bromo-cyclic adenosine monophosphate
9-*cis* RA	9-*cis* retinoic acid
AAV	adeno-associated virus
AC	adenylate cyclase
acetyl-CoA	acetyl-coenzyme A
ACTB	β-actin
ADIPOQ	adiponectin
ADRB3/ *Adrb3*	β_3-adrenergic receptor
AMPK	adenosine monophosphate-activated protein kinase
ANOVA	ordinary one-way analysis of variance
APS	ammonium persulfate
ATF4	activating transcription factor 4
ATGL/ *Atgl*	adipose triglyceride lipase
ATP	adenosine triphosphate
ATPase	adenosine triphosphatase
atRA	all-*trans* retinoic acid
BAT	brown adipose tissue
BCA	bicinchoninic acid assay
BSA	bovine serum albumin
C/EBPα	CCAAT-enhancer-binding protein α
cAMP	cyclic adenosine monophosphate
CCR	Center for Cardiovascular Research
cDNA	complementary DNA
CGI-58	comparative gene identification-58
ChREBP	carbohydrate-responsive element-binding protein
CIDEA/ *Cidea*	cell death-inducing DNA fragmentation factor α-like effector A
CNS	central nervous system
CRBP1/ *Crbp1*	cellular retinol binding protein 1
CREB	cAMP response element-binding protein

Cyp26a1	cytochrome P450 26A1
Cyp26b1	cytochrome P450 26B1
Cyp2c39	cytochrome P450 2c39
ddH_2O	double distilled water
DG	diacylglycerol
DMEM	Dulbecco's Modified Eagle Medium
DNA	deoxyribonucleic acid
DNase	deoxyribonuclease
EBSS	Earle’s Balanced Salt Solution
ECL	enhanced chemiluminescence
EDTA	ethylenediaminetetraacetic acid
EGTA	ethylene glycol-bis(β-aminoethyl ether)-N,N,N′,N′-tetraacetic acid
ELISA	enzyme-linked immunosorbent assay
eWAT	epididymal white adipose tissue
FADH	flavin adenine dinucleotide (reduced electron carrier)
FBS	fetal bovine serum
FGF	fibroblast growth factor
FGF21/ *Fgf21*	fibroblast growth factor 21
FGFR1c	fibroblast growth factor receptor 1c
FOXO1/ *Foxo1*	forkhead box O1
GATA2	GATA-binding factor 2
GFP	green fluorescent protein
HBSS	Hanks’ Balanced Salt Solution
HPLC	high performance liquid chromatography
Hprt	hypoxanthine-guanine phosphoribosyltransferase
HRP	horseradish peroxidase
HSL/ *Hsl*	hormone-sensitive lipase
Igfbp1	insulin-like growth factor binding protein 1
IN	input
IP	immunoprecipitate
IR	insulin receptor
IRS	insulin receptor substrate
l	liter; equivalent to L; the lower-case letter is used in this dissertation
LPL	lipoprotein lipase
LRAT/ *Lrat*	lecithin retinol acyltransferase
MG	monoacylglycerol

MGL	monoacylglycerol lipase
µl	microliter; equivalent to µL; the lower-case letter is used in this dissertation
ml	milliliter; equivalent to mL; the lower-case letter is used in this dissertation
mRNA	messenger ribonucleic acid
NADH	nicotinamide adenine dinucleotide (reduced electron carrier)
NE	norepinephrine
NEFA	non-esterified fatty acid
P/S	penicillin/streptomycin
PBS	phosphate-buffered saline
Pck1	phosphoenolpyruvate carboxykinase 1
PCR	polymerase chain reaction
PDK1	3-phosphoinositide-dependent protein kinase-1
PFK-2	phosphofructokinase 2
p-HSL	phospho-hormone sensitive lipase
PI3K	phosphoinositide 3-kinase
PIP3	phosphatidylinositol (3,4,5)-trisphosphate
PKA	protein kinase A
PPARα	peroxisome proliferator-activated receptor α
PVDF	polyvinylidene fluoride
qRT-PCR	quantitative real-time polymerase chain reaction
RAN	Ras-related nuclear protein
RAR	retinoic acid receptor
Rarβ2	retinoic acid receptor β2
Ratsat	retinol saturase
RBP4/ *Rbp4*	retinol binding protein 4
RBPR2/ *Rbpr2*	retinol binding protein 4 receptor 2
REH	retinyl ester hydrolases
RNA	ribonucleic acid
RNase	ribonuclease
RSB	resuspension buffer
RXR	retinoid X receptors
S	supernatant
scWAT	subcutaneous white adipose tissue
sd	standard deviation
SDS	sodium dodecyl sulfate
SDS-PAGE	sodium dodecyl sulfate-polyacrylamide gel electrophoresis

sem	standard error of the mean
SHC	src homology and collagen protein
siRNA	small interfering ribonucleic acid
STRA6/ *Stra6*	stimulated by retinoic acid 6
STRA6L/ *Stra6l*	stimulated by retinoic acid 6 like
T_4	thyroxine
TCA	tricarboxylic acid
TEMED	tetramethylethylenediamine
TG	triglycerides
TTR/ *Ttr*	transthyretin (also pre-albumin)
UCP1/ *Ucp1*	uncoupling protein 1
WY	WY 14643

Abstract

Vitamin A, which is also known as retinol, is an essential vitamin and needed for the functionality of vision, immune cells, reproduction, embryonic development, and regulation of cell proliferation and differentiation. Retinol is mobilized from the liver while bound to retinol binding protein 4 (RBP4) and transthyretin (TTR) in order to ensure a successful transport to extrahepatic tissues and to maintain these physiological functions. During fasting, the dietary intake of essential retinol is lacking, which was shown in a preliminary study in mice to induce a shift in the retinoid homeostasis in order to ensure retinoid availability for the organism. It was hypothesized that retinol is reversely transported from adipose tissue to replenish hepatic stores. Moreover, it was suggested that fibroblast growth factor 21 (FGF21) is secreted by the liver to induce this reverse transport.

This study aimed to illuminate which mechanism underlies the changes of hepatic mRNA expression and protein levels of RBP4 and TTR in the fasted state observed in a preliminary study in mice. Therefore, primary murine hepatocytes were used as a model to investigate hepatic regulations. Insulin, glucagon, and their related signaling pathways were identified to regulate RBP4 and TTR. In addition, the question whether there are alterations in the concentrations of apo-RBP4 and holo-RBP4 in serum in times of fasting was investigated, since the export of hepatic retinol was hypothesized to be reduced and repartitioning thereof from adipose tissue was suggested to be enhanced. This was done by using non-denaturing immunoblotting and immunoprecipitation. Also, it was investigated whether FGF21 can mediate a signal and its enhanced secretion can induce reverse transport from adipose tissue to the liver. For this reason, an adeno-associated virus (AAV) was injected into mice, resulting in liver-specific overexpression of FGF21, which led to minor changes in the retinoid homeostasis. The amount of retinoids in the liver and subcutaneous white adipose tissue did not change and the expression of retinol metabolism-associated target genes was induced. In epididymal white adipose tissue, retinyl ester stores were found to have reduced while retinol metabolism-associated target genes remained unaltered. Moreover, hepatic FGF21 overexpression was found to promote the gene and protein expression of uncoupling protein 1 (UCP1) and, thus, so-called browning in subcutaneous white adipose tissue.

Overall, this study found that the ratio of insulin and glucagon, which shifts during the feeding-fasting-transition, can regulate the gene and protein expressions of RBP4 and TTR. Moreover, it was shown that FGF21 can induce minor changes in retinoid homeostasis, but was not identified as the primary regulator of the fasting-induced influences affecting retinoid homeostasis.

Kurzzusammenfassung

Vitamin A, auch bekannt als Retinol, ist ein essentielles Vitamin und wird für die Funktionalität von Sehkraft, Immunzellen, Reproduktion, embryonaler Entwicklung und der Regulation von Zellproliferation und -differenzierung benötigt. Retinol, gebunden an Retinol Binding Protein 4 (RBP4) und Transthyretin (TTR), wird aus der Leber mobilisiert, um einen erfolgreichen Transport zu den extrahepatischen Geweben sicherzustellen und damit diese wichtigen physiologischen Funktionen aufrechtzuerhalten. Das essenzielle Retinol wird bei einer Nahrungskarenz nicht vom Organismus aufgenommen. In vorangegangenen Studien an Mäusen wurde eine Verschiebung der Retinolhomöostase während einer Nahrungskarenz, zur Sicherstellung einer Ausreichenden Versorgung des Organismus, festgestellt. Aus den Daten ergab sich die Hypothese, dass die Retinoidspeicher der Leber während einer Nahrungskarenz von denen des weißen Fettgewebes aufgefüllt werden. Dies soll über die Sekretion und Signalübermittlung von Fibroblast Growth Factor 21 (FGF21) geschehen.

Im Rahmen dieser Arbeit wurde die Fragestellung untersucht, welcher Mechanismus den Veränderungen der haptischen mRNA Expression und der Protein Spiegel von RBP4 und TTR während einer Nahrunskarenz, die in der vorangegangenen Studie in Mäusen beobachtet wurden, zugrunde liegt. Dazu wurden primäre murine Hepatozyten verwendet. Es wurde gezeigt, dass Insulin, Glukagon und ihre zugehörigen Signalwege RBP4 und TTR regulieren. Eine weitere adressierte Fragestellung war, ob Veränderungen in den Serumkonzentrationen von apo-RBP4 und holo-RBP4 durch die Nahrungskarenz messbar sind, da die Hypothese aufgestellt wurde, dass während einer Nahrungskarenz hepatische Retinoide weniger stark mobilisiert werden, und Retinoide aus dem Fettgewebe zurück zur Leber transportiert werden. Dazu wurde ein nicht-denaturierender Immunoblot und eine Immunopräzipitation verwendet. Weiterhin wurde die Fragestellung untersucht, ob die Sekretion von hepatischem FGF21 ein Signal darstellen kann, um den rückwertigen Transport vom Fettgewebe zur Leber zu induzieren. Dazu wurde in der Leber von Mäusen durch eine Injektion eines Adeno-assozierten Viruses (AAV) eine Überexpression von FGF21 induziert, was milde Veränderung in der Retinoidhomöostase hervorrief. Die Menge an Retinoiden in der Leber und im subkutanen weißen Fettgewebe blieben unverändert und die Expression von Zielgenen, die mit dem Metabolismus von Retinol assoziiert sind, wurde induziert. Die Retinylesterspeicher des epididymalen weißen Fettgewebes waren reduziert doch die Expression der Retinol Metabolismus assoziierten Zielgene blieb unverändert. Außerdem wurde beobachtet, dass die hepatische Überexpression von FGF21 die Gen- und Proteinexpression von Uncoupling Protein 1 (UCP1) und damit das sogenannte Browning im subkutanen weißen Fettgewebe fördert.

Zusammenfassend identifizierte diese Studie, dass das Verhältnis von Insulin und Glukagon, das sich während einer Nahrungskarenz verschiebt, die Gen- und Proteinexpression von RBP4 und TTR regulieren kann. Außerdem wurde gezeigt, dass obwohl FGF21 die Retinoidhomöostasie geringfügig beeinflussen kann, FGF21 nicht der Hauptregulator der Retinoidhomöostase während einer Nahrungskarenz ist.

1 Introduction

1.1 Retinoid Homeostasis

Vitamin A, also known as retinol, is one of the fat-soluble vitamins and, as an essential vitamin for vertebrates, is dependent on nutritional intake [1]. Vitamin A and its derivatives, which are referred to as retinoids, are contributors in a number of biological functions: vision, immune cell function, reproduction, embryonic development, and regulation of cell proliferation and differentiation [2-6]. Vitamin A deficiency in humans leads to impaired vision with symptoms like night blindness or complete blindness [7], and, moreover, causes visual defects in newborns through vitamin A deficiency during pregnancy [8].

The biologically active metabolite of vitamin A is all-*trans* retinoic acid (atRA) that functions as a ligand for retinoic acid receptors (RAR) α, β, and γ [9]. 9-*cis* retinoic acid (9-*cis* RA) is a known ligand for retinoid X receptors (RXR) α, β, and γ, although its biological relevance is still unclear and other RXR-activating retinoids, such as 9-*cis*-13,14-dihydroretinoic acid, have also been identified [10-12]. RAR as well as RXR belong to the nuclear receptor family. Another retinol derivative is 11-*cis*-retinal that acts as a chromophore to activate rhodopsin in the visual cycle [13].

1.1.1 Retinol Uptake and Storage

Retinoids reach the intestine after dietary uptake and are packed in the form of retinyl esters together with dietary lipids to create chylomicrons [14, 15]. Approximately 25% of the released chylomicrons directly provide extrahepatic tissues with retinoids, becoming chylomicron remnants owing to the membrane-bound enzyme lipoprotein lipase (LPL), which hydrolyzes triglycerides and retinyl esters to prepare them for their designated purposes in the target tissues [16]. The remaining retinoids are transported within the chylomicron remnants to the liver, where about 80% of all retinoids are stored [17].

The liver is the main organ for uptake, storage, and mobilization of retinoids. While the hepatocytes are the cells involved in uptake and mobilization, the hepatic stellate cells are the ones responsible for storage. After uptake, retinol is bound within the hepatocytes to cellular retinol binding protein 1 (CRBP1) and transported to the hepatic stellate cells by a thus far unknown mechanism [18]. The hepatic stellate cells contain lipid droplets in which retinyl esters can be stored [19]. Lecithin retinol acyltransferase (LRAT) esterifies retinol to mostly retinyl-palmitate, -oleate, and -stearate [20-22]. In order to mobilize the lipophilic retinol from

the liver into the bloodstream and provide retinoids for the physiological functions in the periphery, retinol binding protein 4 (RBP4) is required [23]. First, retinyl ester hydrolases (REH) transform the retinyl esters to retinol, then it is transported to the hepatocyte, and then binds to RBP4 there [24]. The complex consisting of retinol and RBP4 binds to the tetrameric protein transthyretin (TTR, also known as pre-albumin) within the hepatocyte to stabilize the complex during transportation and prevent renal filtration [25, 26]. The complex containing retinol, RBP4, and TTR is secreted into the bloodstream and transported to the target tissues. This secretion is dependent on the availability of retinol [27-29].

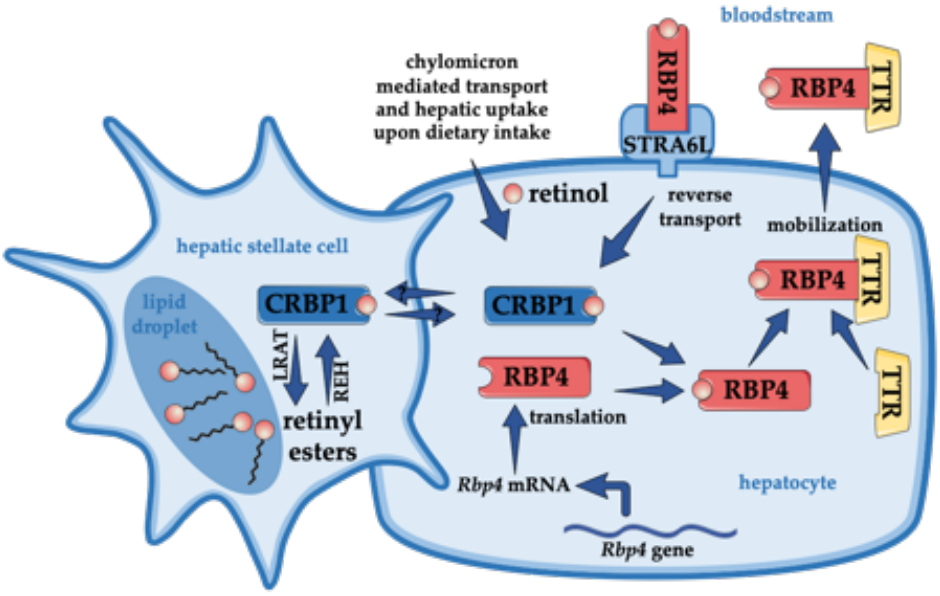

Figure 1: Retinol Uptake, Storage, and Mobilization. Retinol uptake occurs through nutrition and it is transported to the liver within chylomicrons. After uptake, retinol is found coupled to CRBP1 intracellularly. Through a yet unknown mechanism, but one which is thought to be dependent on CRBP1, retinol is transported to hepatic stellate cells, where LRAT transforms it to retinyl esters that can be stored within lipid droplets. In order to mobilize retinoids, retinyl esters are transformed by REH to retinol. Within the hepatocyte, retinol is first bound to RBP4 and then to TTR before the stable complex is released into the bloodstream and transported to target tissues. STRA6L on the surface of liver cells is thought to mediate the reverse transport of retinol. Figure adapted from [30] .

Many extrahepatic tissues express a receptor called ‘stimulated by retinoic acid 6’ (STRA6), that is located on the cell surface and contains nine transmembrane domains [31, 32]. After dissociation of TTR, STRA6 can bind holo-RBP4 and mediate the transport of retinol into the target cell [32-34]. Within the cell, retinol binds to CRBP1, while LRAT initiates its storage [34, 35]. Notably, STRA6 is able to facilitate bi-directional retinol transport to regulate retinoid homeostasis [36]. Mainly in the liver, but also in the intestine and colon, retinol binding protein 4 receptor 2 (RBPR2), later called ‘stimulated by retinoic acid 6 like’ (STRA6L), is responsible for the retinol transport into the cell [37]. However, it remains unknown if the receptor also

mediates its export. An overview of hepatocyte-specific retinoid storage and mobilization is shown in **Figure 1.**

1.1.2 Retinol Transport: Retinol Binding Protein 4 (RBP4)

RBP4 was first discovered in 1963 as a protein that specifically transports retinol in the blood of humans [38]. The 21 kDa protein was described as a single polypeptide chain consisting of 201 amino acids, including an 18 amino acid long N-terminal signal peptide that is cleaved and three disulfide bridges [39, 40]. The analysis of the structure showed that the protein consists of an N-terminal coil, a C-terminal α-helix, and an eight-stranded up-and-down β-barrel. The lipophilic retinol can bind specifically within this β-barrel core and is then transported to target tissues [41]. Two important states of RBP4 are distinguished: the apo-form, which is not bound to retinol, and holo-RBP4, which is bound to its ligand [42].

The concentration of RBP4 in blood – which is approximately 2-3 µM in humans and around 1 µM in mice – remains constant throughout various metabolic conditions [23]. Although the highest level of protein expression was found in the liver, other tissues, mainly adipose tissues, express RBP4 [43-45]. Nevertheless, it was shown that circulating RBP4 derives exclusively from the hepatocytes in mice, since a hepatocyte-specific RBP4 knockout resulted in undetectable RBP4 levels in blood [46]. This finding was supported by the increased serum RBP4 levels in mouse models where the liver specifically overexpressed RBP4 [47, 48]. Moreover, an adipocyte-specific overexpression of RBP4 did not lead to elevated circulating RBP4 levels in mice fed a normal chow [49].

The highest messenger RNA (mRNA) expression was found in the liver, but was also detected in other tissues, such as adipose tissue, kidneys, retinal pigment epithelium, testes, brain, lung, and the choroid plexus [2, 17, 50-53].

1.1.3 Retinol Transport: Transthyretin (TTR)

TTR was first discovered in 1942 and named prealbumin, since it ran ahead of albumin on electrophoresis of plasma and cerebrospinal fluid [54, 55]. The name transthyretin has only been used since 1981, hinting towards its by then well-known function of transporting thyroid hormones and retinol [56, 57].

TTR is mainly expressed by the liver and released into the bloodstream [58]. It is also expressed by the choroid plexus of the brain, which provides TTR for the cerebrospinal fluid [59]. The concentration in the serum remains between 1.8 to 7.2 µM in humans [60] and between 3.6 and 5.4 µM in mice [61] under physiological conditions. The homotetrameric

protein comprises four 14 kDa subunits [62]. Although there are two binding sites for thyroxine (T_4), TTR only transports one T_4 molecule due to negative cooperativity [63-65]. In addition to that, TTR also has four RBP4 binding sites, but only two RBP4 molecules can bind to TTR simultaneously as a result of steric limitations [25, 66]. However, considering the physiological concentrations of both proteins in the bloodstream, TTR is usually only bound to one RBP4 molecule. The affinity of TTR to RBP4 is increased when the latter is bound to retinol [42]. Notably, the binding of T_4 does not alter the binding of RBP4 and *vice versa* [57].

Since its discovery, several functions of TTR have been discussed. Its role in retinol transport is essential to this study. TTR can associate with the complex comprised of RBP4 and retinol within the liver [57]. This complex is released into circulation. Binding TTR allows the RBP4/retinol complex to remain stable during transportation through the bloodstream, since it would otherwise be exposed to renal filtration and catabolism [67, 68]. As was shown in TTR knockout mice and in mice with a liver-specific deletion of TTR, where RBP4 was found to have accumulated in the liver and the serum concentration had decreased dramatically, TTR can promote the secretion of RBP4 [47, 69]. However, the presence of TTR is not absolutely necessary, since RBP4 was still detectable in the serum of TTR knockout mice and the secretion of RBP4 in hepatocytes of mice lacking TTR was not significantly altered compared to the control hepatocytes [66]. Additionally, the retinoid content of the retinoid target tissues in the mice lacking TTR was unchanged [69].

The other described functions of TTR in thyroid hormone transportation and in the central nervous system (CNS) are only briefly mentioned here. T_4, one of the thyroid hormones, is synthesized by the thyroid gland and released into circulation bound to transport proteins, among which is TTR [63]. Thyroid hormones are needed by the organism for developmental functions, tissue differentiation, and regulatory effects on metabolism. Moreover, TTR's involvement in the physiology of the CNS in processes such as behavior, cognition, neuropeptide amidation, neurogenesis, or nerve regeneration is the subject in several studies [70, 71].

1.2 Insulin and Glucagon as Regulators of the Feeding-Fasting Transition

Due to their effects on the metabolism, and glucose homeostasis in particular, both hormones insulin and glucagon are key players in the feeding-fasting transition. In order to regulate glucose homeostasis, the glucagon-to-insulin ratio is higher in times of fasting to promote glycolysis and gluconeogenesis. Feeding induces an elevation of the insulin-to-glucagon ratio, promoting the uptake of glucose and glycogenesis to regulate blood glucose. The insulin and

glucagon signaling insights presented here only focus upon parts relevant for this study, but it should be mentioned that insulin and glucagon coordinate many pathways and participating molecules to fulfill their function as metabolism regulators.

1.2.1 Insulin Signaling

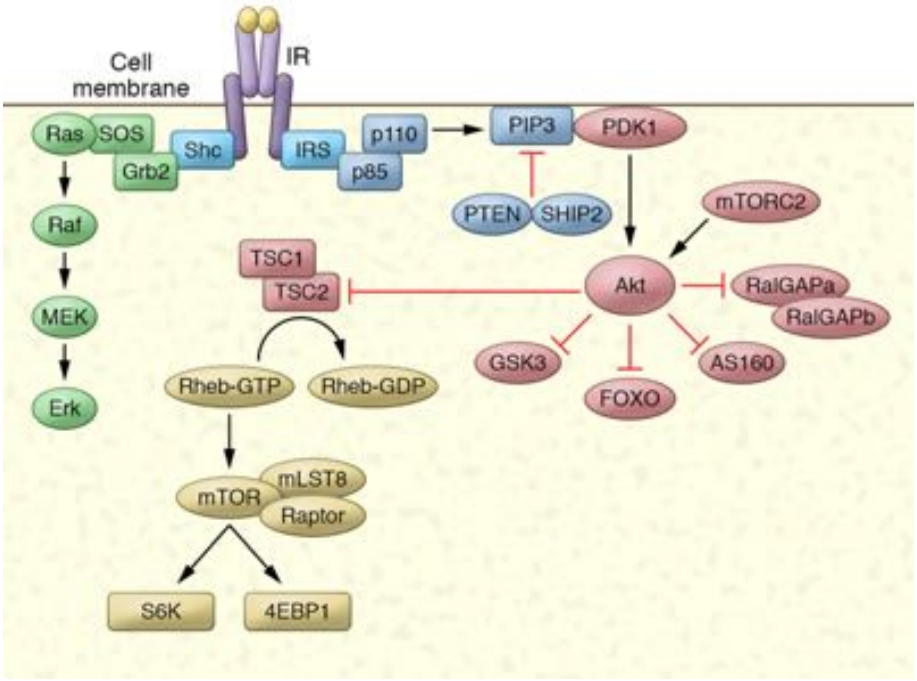

Figure 2: Insulin Signaling Pathway. Insulin activates IR and, in so doing, activates kinase cascades through subsequent phosphorylation. SHC activates the Ras signaling pathway, while IRS induces PDK1-mediated AKT phosphorylation. AKT represents a major regulator of insulin signaling, since it regulates numerous proteins and pathways, among which is FOXO. FOXO is a known regulator of hepatic gluconeogenesis. Figure adapted from [72].

Insulin was discovered a century ago and is widely known to regulate circulating glucose levels [73]. Insulin is secreted by pancreatic β-cells and activates the insulin receptor (IR) [74]. The insulin receptor is a tyrosine kinase receptor that consists of two α- and two β-subunits. Insulin binding to the extracellular α-subunit activates the β-subunit [75-77]. Upon full activation, the β-subunit initiates a conformational change and, thus, induces tyrosine kinase activity. This enables recruitment of proteins to phosphortyrosine sites, which initiates several insulin signaling pathways. Among these recruited proteins are insulin receptor substrates (IRS) [78-80] and 'src homology and collagen protein' (SHC) [81]. They are phosphorylated, resulting in the activation of kinase cascades. SHC activates the Ras pathway and, in turn, induces proliferation, cell differentiation, and protein synthesis [81-84]. IRS activates phosphoinositide 3-kinase (PI3K) by phosphorylation of its p85 and p110 subunits [85, 86]. First phosphatidylinositol (3,4,5)-trisphosphate (PIP3), then 3-phosphoinositide-dependent protein

kinase-1 (PDK1), and finally AKT (also known as protein kinase B) are activated through successive phosphorylation [87, 88]. AKT is a kinase for a variety of proteins, inducing pathways to promote glycolysis, stimulate starch and sucrose metabolism, inhibit lipolysis, and support protein synthesis to name a few [85].

One of the key players in the insulin-mediated signaling of hepatic gluconeogenesis is the fasting-activated transcription factor forkhead box O1 (FOXO1) [89, 90]. AKT phosphorylates and inhibits FOXO1 signaling, since FOXO1 cannot enter the nucleus in its phosphorylated form [90, 91].

The variety of signaling pathways insulin can stimulate illustrates the complexity of its physiology and, at the same time, its significance in the regulation of metabolism. The aforementioned components of the insulin signaling pathway can be found in **Figure 2**.

1.2.2 Glucagon Signaling

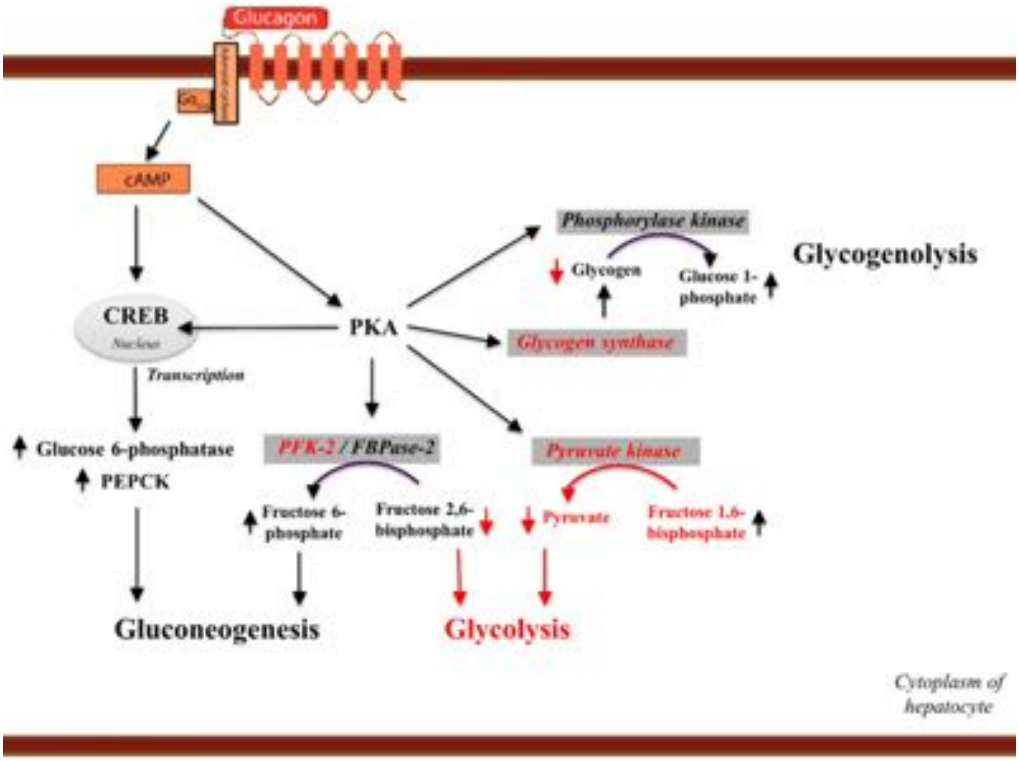

Figure 3: Glucagon Signaling Pathway. Glucagon receptor activation initiates cAMP production that activates PKA. PKA is a central regulator in glucagon signaling and stimulates responses in absence of glucose to support glycogen breakdown and gluconeogenesis. Figure from [92].

Glucagon is secreted by α-cells in the pancreas, and reaches the glucagon receptor via circulation, in order to promote glycogenolysis and gluconeogenesis in fasting periods [93, 94]. This receptor is a G protein-coupled receptor that supports adenylate cyclase (AC) via

$G_{\alpha s}$-signaling after activation [95]. AC subsequently fosters the production of cyclic adenosine monophosphate (cAMP) and, afterwards, protein kinase A (PKA) activity [94]. PKA targets a great number of regulatory proteins in glucagon signaling. Among the most important for glycogen breakdown and gluconeogenesis are phosphorylase kinase, glycogen synthase, pyruvate kinase, cAMP response element-binding protein (CREB), and phosphofructokinase 2 (PFK-2) [96-100]. The cAMP/PKA signaling pathway enables a fast release of glucose from the liver [101, 102]. Similar to insulin signaling, glucagon signaling is complex and highly relevant for the regulation of metabolism. An overview of glucagon signaling is provided in **Figure 3**.

1.3 Fibroblast Growth Factor 21 (FGF21)

FGF21 was discovered in 2000 as a member of the fibroblast growth factor (FGF) superfamily and has since been additionally categorized into a FGF subfamily with atypical characteristics alongside human FGF19, FGF19's murine ortholog FGF15, and FGF23 [103]. In contrast to other members of the FGF superfamily, FGF21 and the aforementioned homologues can circulate as endocrine hormones, since they are not equipped with the typical heparin-binding domain, and are therefore able to be released directly into the bloodstream by the liver [104-106]. FGF21 is found highest expressed in the liver, pancreas, muscles, and adipose tissue, although, evidence has been provided that the principal source of circulating FGF21 in a physiological state is the liver [107, 108]. Notably, FGF21 is able to overcome the blood-brain barrier and act on the brain and CNS, coordinating physiological stress responses there [109].

FGF21 binds to a specific receptor complex, which is comprised of the tyrosine kinase 'fibroblast growth factor receptor 1c' (FGFR1c) and the co-receptor protein β-klotho [110, 111]. Remarkably, interaction with both receptor proteins is necessary for FGF21 to mediate its effects, although β-klotho is thought to be the target receptor and assumed to aid an interaction with FGFR1c [112]. The induced effects include responses to cellular and metabolic stresses in different organs. Serum levels of FGF21 increase through fasting, protein or amino acid restriction, ketogenic and high fat diets, fructose uptake, cold exposure, alcohol consumption, or exercise [106]. Therefore, FGF21 has been described as a regulator of energy and nutrient homeostasis.

Initially, FGF21 was thought to be a regulator of the fasting response. It was shown that hepatic FGF21 transcription and secretion are elevated in the fasted state and a dependence on transcription factor peroxisome proliferator-activated receptor α (PPARα) was described [113, 114].

Interestingly, an increased intake of carbohydrates was shown to induce hepatic FGF21

transcription and secretion into the bloodstream as a result of PPARα's and carbohydrate-responsive element-binding protein's (ChREBP) action [115-119]. FGF21 can then signal on adipose tissue and improve carbohydrate uptake, leading to increased insulin sensitivity [108, 120-122]. This insulin sensitivity-enhancing effect was presumed to be supported by the secretion of the adipokine adiponectin [123, 124]. FGF21 can also signal to the CNS and promote glucose-excited neurons in the ventromedial hypothalamus with the consequence of a reduced simple-sugar intake and sweet taste preference [117, 125, 126].

Thus, FGF21 is upregulated through insufficient carbohydrate intake during fasting, but is also upregulated in times of increased carbohydrate intake. These observations seem contradictory at first. It was hypothesized that FGF21 is a regulator sensitive to both fasting signals (e.g. PPARα activation) and refeeding signals as induced by insulin. Therefore, it has been stated that FGF21 regulates glucose homeostasis in late fasting and then supports the increased carbohydrate intake upon refeeding by improving the glucose uptake to maintain the metabolic nutrient balance [106, 108, 127, 128].

Energy homeostasis of rodents and humans is altered by FGF21. Although numerous studies identified the consequences FGF21 has on the energy balance, the mechanism remains poorly understood to this day. FGF21 has been described as capable of reducing body weight, hepatic triglycerides, cholesterol levels, blood glucose levels, and serum triglyceride levels [106, 129-132]. Through action in the CNS, FGF21 can mediate β-adrenergic signaling that is beneficial for thermogenesis in brown adipose tissue, as well as for browning of white adipocytes, and increasing physical activity to induce weight loss [126, 132-137].

Additionally, FGF21 can regulate protein homeostasis. When amino acid restriction occurs, FGF21 is known to be induced in the liver by 'activating transcription factor 4' (ATF4) and PPARα [138-140]. Subsequently, the produced and secreted FGF21 reaches the brain and promotes a higher food intake to ensure protein intake and maintain physiological functions [141-143]. The increased food intake would facilitate body weight gain, but is prevented by FGF21's signal to the brain that simultaneously enhances physical activity, resulting in a decreased body weight instead [139, 140].

Cold exposure was found to induce FGF21 levels, which are accompanied by elevated levels of uncoupling protein 1 (UCP1) in white adipose tissue, indicating browning to beige adipocytes [144-146].

Various diabetic models exist that involve elevating the FGF21 concentrations in mice either genetically [130] or pharmacologically [129]. Similar studies exist in which diabetic rhesus monkeys were administered FGF21 [131], and they all have similar findings in common. The observed effects on the metabolism and energy homeostasis were weight loss, improved

insulin sensitivity, improved glucose levels and reduced triglyceride levels.

1.4 Physiology and Function of Adipose Tissue

There are three types of adipose tissue: white, brown, and beige adipose tissue. White adipose tissue stores energy, while brown adipose tissue (BAT) dissipates energy as heat, and, finally, beige adipose tissue shares characteristic of both white and brown adipose tissue, enabling it to adjust its functionality to different circumstances.

1.4.1 White Adipose Tissue and Lipolysis

White adipocytes usually comprise a single lipid droplet in which energy is stored in form of triglycerides [147]. The size of the adipocyte depends on the size of the lipid droplet. In a general differentiation, white adipose tissue is separated into subcutaneous white adipose tissue (scWAT) located under the epidermis, and visceral adipose tissue found around internal organs [148]. In addition to storing energy, scWAT provides thermal insulation, and visceral adipose tissue protects the organs from mechanical stress [149]. The visceral adipose tissue depots include epi- and pericardial, perirenal, rectoperineal, mesenteric, and perigonadal white adipose tissue [147]. The perigonadal white adipose tissue is also called epididymal white adipose tissue (eWAT) in males and periovarian adipose tissue in females. The functions and dysfunctions of scWAT and visceral white adipose tissue in the metabolism need to be evaluated specifically. It has been discovered that visceral adipose tissue, especially in association with its expansion in obesity, is linked to insulin resistance and cardiovascular diseases, while scWAT accumulation was shown to be beneficial in metabolic diseases and improves, for example, insulin sensitivity [150-158].

Lipolysis is the process that provides fatty acids and glycerol from white adipose tissue reserves, for example during fasting periods or ketogenic diets [159]. The triglyceride (TG) transformation results in a release of non-esterified fatty acids (NEFA) in three steps mediated by three different enzymes. Adipose triglyceride lipase (ATGL) initiates the first step of hydrolyzing triglycerides to diacylglycerol (DG) [160-162]. This is followed by hormone-sensitive lipase's (HSL) hydrolytic action that transforms diacylglycerol to monoacylglycerol (MG) [163-165]. Monoacylglycerol is converted to glycerol by monoacylglycerol lipase (MGL) [163, 166, 167]. The step initiated by ATGL is rate-limiting for lipolysis [162]. The released NEFAs can be metabolized by β-oxidation and ketone synthesis to provide energy, while glycerol can be used for the gluconeogenesis.

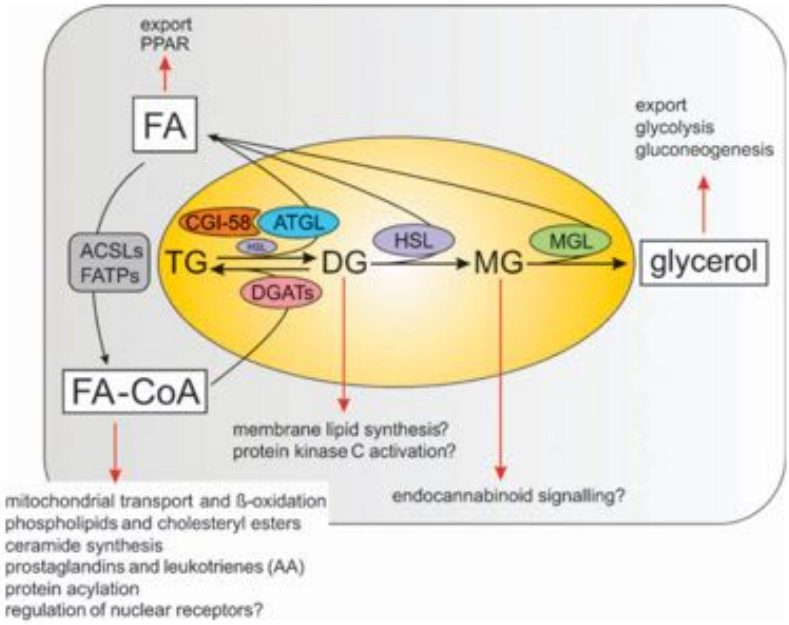

Figure 4: Lipolysis. In order to provide glycerol and fatty acids from adipose tissue reserves for energy production, the lipolytic enzymes ATGL, HSL, and MGL successively break down triglycerides. Figure from [168].

Current literature suggests that the activity of lipolytic enzymes is regulated by post-translational modification rather than altered mRNA expression [168]. ATGL is phosphorylated by adenosine monophosphate-activated protein kinase (AMPK), in turn, activating its hydrolytic function. Moreover, lipid droplet proteins, like comparative gene identification-58 (CGI-58), were shown to act as coactivators of ATGL [169]. The enzymatic activity of HSL is regulated by PKA phosphorylation upon β-adrenergic stimulation and interaction with perilipin [170-173]. Preferentially, HSL hydrolyzes DG, but also TG, MG, and other esters, such as cholesteryl esters and retinyl esters [174, 175]. Lipolysis is known to be altered by numerous hormones, cytokines, and adipokines, as well as complex signaling pathways. Among these molecules are glucagon and glucocorticoids that enhance lipolytic activity, while insulin and insulin-like growth factor are robust inhibitors of lipolysis [168]. **Figure 4** provides an insight into the process of lipolysis, including the aforementioned enzymes.

1.4.2 Brown Adipose Tissue and Non-Shivering Thermogenesis

Non-shivering thermogenesis is a physiological process with the purpose to dissipate energy as heat in BAT [176] and explained in the following [176-179]. Cold exposure activates the sympathetic nervous system and norepinephrine (NE) is released. NE activates β_3-adrenergic receptors in brown fat cells. In doing so, it induces the transcription of UCP1 and promotes

lipolysis [176, 179]. Lipolysis generates NEFAs that are released into the cytoplasm and transported to the mitochondria, where they are metabolized through β-oxidation to substrates for the respiratory chain, including acetyl coenzyme A (acetyl CoA). Acetyl CoA is integrated into the tricarboxylic acid cycle (TCA; also called citric acid cycle CAC), which produces the reduced electron carriers NADH and FADH. These products are oxidized within the mitochondrial respiratory chain in the inner mitochondrial membrane. The subsequent transport of electrons among the inner membrane of the mitochondria is responsible for an electrochemical proton gradient that leads to a proton transport from the matrix to the mitochondrial intermembrane space. Adenosine triphosphatase (ATPase) can couple the energy provided by this gradient in an endothermic reaction to form adenosine triphosphate (ATP). However, the presence of UCP1 in the inner mitochondrial membrane of brown adipocytes inhibits the transformation of energy to ATP, and generates heat instead, since UCP1 allows the reverse transport of protons into the matrix, thereby alleviating the electrochemical proton gradient [176-178]. The complete process of non-shivering thermogenesis is depicted in **Figure 5**, starting from the release of NE due to the activation of the sympathetic nervous system, and finally leading to the generation of heat.

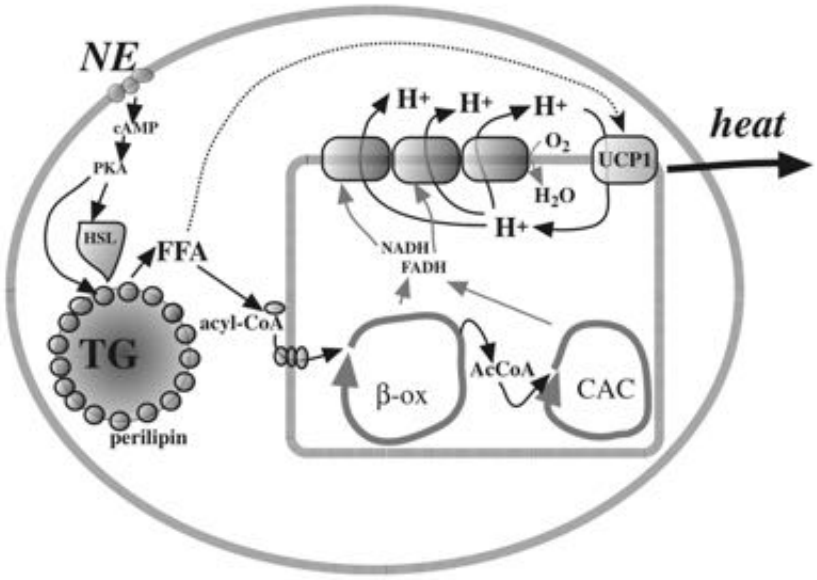

Figure 5: Non-Shivering Thermogenesis. In order to dissipate energy in form of heat, β_3-adrenergic-dependent activation of UCP1 is initiated. β-oxidation and TCA (also called CAC) produce reduced electron carriers NADH and FADH, which are oxidized within the respiratory chain on the mitochondrial inner membrane. Eventually, this results in an electrochemical proton gradient that leads to proton export from the mitochondrial matrix to the mitochondrial intermembrane space. UCP1 enables the reverse transport of protons to the mitochondrial matrix and, thus, dissipates energy in form of heat instead of endothermic energy in form of ATP. Figure from [176].

UCP1 transcription and non-shivering thermogenesis have been confirmed to be induced by retinoids through the interaction with RAR and RXR (especially RARα, RARβ and RXRα), because the retinoic acid-response element was identified in the enhancer region of the UCP1 promoter [180-185]. Moreover, atRA was shown to be a potent activator of UCP1 and supporter of non-shivering thermogenesis, as it was capable of increasing the UCP1-mediated proton transport through the mitochondrial inner membrane [186].

1.4.3 Beige Adipose Tissue and Browning

Browning is defined as the increased presence of brown adipocyte-like cells – so-called beige or brite (brown-in-white) adipocytes – in white adipose tissue [187, 188]. These beige adipocytes are mainly located in scWAT, while only few are found in visceral adipose tissue. They are characterized by the activation of specific proteins that are usually found in brown adipocytes and are activated during non-shivering thermogenesis, among which is UCP1 [176, 189], cell death-inducing DNA fragmentation factor α-like effector A (CIDEA) [190-193], and β_3-adrenergic receptor (ADRB3) [176].

To this day, where beige adipocytes originate from is not fully known. The first hypothesis is that white adipocytes can transform into beige adipocytes [191, 194-197], while the second hypothesis states that the beige adipocytes are differentiated within white adipose tissue from precursor cells [198-201]. Browning can be induced by cold exposure, exercise, β_3-agonists, certain genetic factors, and stimulation by hormones [193]. One of these stimulating molecules is FGF21, which is thought to promote browning of white adipocytes by activating the sympathetic CNS and by induction of thermogenic gene expression in white adipose tissue [144-146]. FGF21 deficiency has been shown to inhibit browning, and, thus, the adaptation to cold [146].

1.5 Preliminary Work

Since retinoids are provided for vertebrates solely by nutrition, mice were fasted for 24 h to investigate how the organism responds to this challenge. The continuous retinoid supply is important for several functions, as mentioned in **Chapter 1.1**, and fasting was expected to induce changes to ensure that these physiological processes would be maintained. In this 24 h fasting experiment with mice, serum retinol levels were found to have remained unaltered at a physiological level of about 0.8 µM. The serum protein concentrations of RBP4, which acts as the transporter of retinol through the bloodstream, did not differ between fed and fasted mice. Since the liver is the main retinoid storage organ, the retinol and retinyl ester concentrations

in the liver were measured. The hepatic retinol content did not change significantly, while the retinyl ester concentration had significantly increased. This was surprising since the dietary intake of retinoids was blocked in this model. Since the liver weight was reduced, this concentration was then calculated as the total amount of retinoids per whole organ and the results showed that the amounts of retinol and retinyl esters were both unaltered.

The fact that due to the lack of dietary intake during fasting, the organism is not provided with the essential retinol, and the RBP4-mediated retinol mobilization, which is thought to constantly take place, would lead one to expect lower hepatic retinoid stores in a fasting challenge. Contrarily, it was observed that the hepatic retinoid content in this model remained constant, which led to the hypothesis that hepatic stores are replenished with retinoids from other tissues to maintain hepatic retinoid homeostasis in times of fasting. For this reason, the retinoid content of other organs was measured. Decreased retinyl ester levels were found in both eWAT and scWAT, leading to the hypothesis that retinoids are reverse transported back to the liver from white adipose tissue in times of fasting. Moreover, this model showed increased hepatic protein and mRNA expression levels of RBP4, while *Ttr* mRNA expression levels and serum protein levels were reduced.

In a next step, a mouse model with forced hepatic retinol mobilization achieved by means of liver-specific and adenovirus-mediated overexpression of RBP4 was established. Over the course of six days, the liver mobilized more than one third of its retinyl ester stores. The phenotype of the mice showed increased NEFA and ketone body concentrations in the serum, indicating towards adipose tissue lipolysis and β-oxidation. Both processes are known to be promoted by FGF21. FGF21 was found to have increased on mRNA level and secreted protein level in this model of forced hepatic retinol mobilization. The developed hypothesis suggests that FGF21 is secreted by the liver to support the crosstalk between the liver and adipose tissue and, in turn, to induce alterations in the retinoid homeostasis.

1.6 Aim of the Study

The preliminary data provided new insights into retinoid homeostasis in times of fasting. Although the observed effects on the retinol transport protein RBP4 as well as TTR are very apparent, which fasting-related mechanism induces the regulation of the mRNA and protein levels remains unclear. Among the most prominent regulators of feeding and fasting under physiological conditions are insulin, glucagon, and PPARα. These molecules – together with altered availability of products of retinol metabolism – are hypothesized to control RBP4 and TTR expression and, thus, influence retinoid homeostasis in the feeding-fasting transition.

The preliminary data showed that the serum levels of RBP4 and retinol were not altered when comparing the fed to the fasted state. The hypothesis proposes that fasting induces the reverse transport of retinoids to the liver. However, since circulating holo-RBP4 derives from the liver in mice, and since retinol could be also transported by other carriers, the question arises whether the concentrations of apo-RBP4 and holo-RBP4 in the bloodstream were altered, even if the total protein levels in the circulation were unchanged, in order to keep hepatic retinoid stores stable and to reverse transport retinoids originating from other tissues to the liver.

FGF21 is secreted by the liver during fasting. It was also elevated in the model of forced RBP4 mobilization in the preliminary data. Therefore, FGF21 is hypothesized to be secreted by the liver to induce hepatic retinoid replenishment from white adipocytes in times of fasting.

The aim of this study is to address the following questions:

1. Which mechanism underlies the changes of hepatic mRNA expression and protein levels of RBP4 and TTR observed in the fasted state *in vivo?*
2. Are the concentrations of apo-RBP4 and holo-RBP4 in the bloodstream altered in times of fasting, since the export of hepatic retinol is thought to be diminished and repartitioning from adipose tissue is suggested to be enhanced?
3. Can the secretion of the hepatokine FGF21 promote crosstalk between the liver and adipose tissue and induce retinoid repartitioning from white adipose tissue to the liver?

2 Materials

2.1 Chemicals and Reagents

The used chemicals and reagents are listed in **Table 1**.

Table 1: Chemicals and Reagents

Substance	Supplier
0.9% saline solution	B. Braun Melsungen AG (Melsungen, DE)
2-mercaptoethanol	Sigma Aldrich (St. Louis, MO, US)
8-bromo-cyclic adenosine monophosphate (8-Br-cAMP)	Enzo Biochem, Inc. (Farmingdale, NY, US)
Acetic acid	Carl Roth GmbH & Co. KG (Karlsruhe, DE)
Acrylamide solution 30%	AppliChem GmbH (Darmstadt, DE)
All-*trans*-retinoic acid (atRA)	Sigma Aldrich (St. Louis, MO, US)
Ammonium persulfate (APS)	Sigma Aldrich (St. Louis, MO, US)
Bovine serum albumin fatty acid free (BSA)	Sigma Aldrich (St. Louis, MO, US)
Bromophenol blue	Sigma Aldrich (St. Louis, MO, US)
Butylated hydroxytoluene	Sigma Aldrich (St. Louis, MO, US)
Chloroform	Merck KGaA (Darmstadt, DE)
Collagenase (Type 1)	Worthington Biochemical Corporation (Lakewood, NJ, US)
D-(+)-Glucose	Sigma Aldrich (St. Louis, MO, US)
Developer solution	Agfa HealthCare NV (Mortsel, BE)
Dimethyl sulfoxide	Acros Organics, Thermo Fisher Scientific Inc. (Waltham, MA, US)
dNTP Mix	Invitrogen, Thermo Fisher Scientific Inc. (Waltham, MA, US)
Earle's Balanced Salt Solution (without $CaCl_2$, without $MgCl_2$) (EBSS)	Gibco, Thermo Fisher Scientific Inc. (Waltham, MA, US)
Ethanol	Merck KGaA (Darmstadt, DE)
Ethylene glycol-bis(β-aminoethyl ether)-N,N,N′,N′-tetraacetic acid (EGTA)	Carl Roth GmbH & Co. KG (Karlsruhe, DE)
Ethylenediaminetetraacetic acid (EDTA)	Sigma Aldrich (St. Louis, MO, US)
Fetal bovine serum (FBS)	Gibco, Thermo Fisher Scientific Inc. (Waltham, MA, US)
Fixation solution	Agfa HealthCare NV (Mortsel, BE)
Glucagon	Sigma Aldrich (St. Louis, MO, US)

Glycine	Carl Roth GmbH & Co. KG (Karlsruhe, DE)
Guanidine hydrochloride	Sigma Aldrich (St. Louis, MO, US)
Hanks' Balanced Salt Solution (with calcium and magnesium; without phenol) (HBSS)	Corning Inc. (Corning, NY, US)
IGEPAL CA-630	Sigma Aldrich (St. Louis, MO, US)
Insulin solution human	Sigma Aldrich (St. Louis, MO, US)
Isoflurane (Forene)	AbbVie Inc. (North Chicago, IL, US)
Isopropanol	Merck KGaA (Darmstadt, DE)
Ketamine 100 mg/ml	CP-Pharma Handelsgesellschaft mbH (Burgdorf, DE)
L(+)-Lactic-acid sodium salt crystalline	AppliChem GmbH (Darmstadt, DE)
M-MLV reaction buffer (5x)	Promega Corporation (Fitchburg, WI, US)
M-MLV reverse transcriptase	Promega Corporation (Fitchburg, WI, US)
Magnesium chloride	Sigma Aldrich (St. Louis, MO, US)
Methanol	Sigma Aldrich (St. Louis, MO, US)
Milk powder	Carl Roth GmbH & Co. KG (Karlsruhe, DE)
Molecular weight marker ProSleve color protein marker	Lonza (Basel, CH)
n-hexane	Sigma Aldrich (St. Louis, MO, US)
No ROX SYBR MasterMix blue dTTP	Eurogentec (Seraing, BE)
Non-reducing lane marker sample buffer (5x)	Thermo Fisher Scientific Inc. (Waltham, MA, US)
OPTI-MEM (with HEPES, 2.4 g/l sodium bicarbonate and L-glutamine)	Gibco, Thermo Fisher Scientific Inc. (Waltham, MA, US)
Penicillin/streptomycin (P/S)	Gibco, Thermo Fisher Scientific Inc. (Waltham, MA, US)
Percoll	Cytiva, Global Life Sciences Solutions USA LLC (Marlborough, MA, US)
phosphatase inhibitor cocktail tablets	F. Hoffmann-La Roche AG (Basel, CH)
Phosphate-buffered saline (PBS) (pH = 7.2; without $CaCl_2$ and $MgCl_2$)	Gibco, Thermo Fisher Scientific Inc. (Waltham, MA, US)
Pierce ECL western blotting substrate	Thermo Fisher Scientific Inc. (Waltham, MA, US)
Ponceau S	Cayman Chemical Company (Ann Arbor, MI, US)
Protease inhibitor cocktail tablets complete, EDTA-free	F. Hoffmann-La Roche AG (Basel, CH)
Protein A sepharose CL-4B	GE Healthcare Bio-Sciences AB (Uppsala, SE)
QIAzol lysis reagent	Quiagen GmbH (Hilden, DE)

Random hexamer primer	Invitrogen, Thermo Fisher Scientific Inc. (Waltham, MA, US)
Retinol	Sigma Aldrich (St. Louis, MO, US)
RNase-free water	Gibco, Thermo Fisher Scientific Inc. (Waltham, MA, US)
Sodium chloride	Merck KGaA (Darmstadt, DE)
Sodium dodecyl sulfate (SDS)	Carl Roth GmbH & Co. KG (Karlsruhe, DE)
Sodium hydroxide solution	Sigma Aldrich (St. Louis, MO, US)
Sodium pyruvate	Sigma Aldrich (St. Louis, MO, US)
Tetramethylethylenediamine (TEMED)	Sigma Aldrich (St. Louis, MO, US)
Tris hydrochloride (tris HCl)	Carl Roth GmbH & Co. KG (Karlsruhe, DE)
Tris(hydroxymethyl)-aminomethane (tris base)	Merck KGaA (Darmstadt, DE)
TritonX-100	Carl Roth GmbH & Co. KG (Karlsruhe, DE)
TRIzol reagent	Thermo Fisher Scientific Inc. (Waltham, MA, US)
Tween 20	Merck KgaA (Darmstadt, DE)
Ultrapure distilled water DNase/RNase free	Invitrogen, Thermo Fisher Scientific Inc. (Waltham, MA, US)
WY 14643	Sigma Aldrich (St. Louis, MO, US)
Xylavet (xylazine) 20 mg/ml	CP-Pharma Handelsgesellschaft mbH (Burgdorf, DE)

2.2 Kits

The used kits are listed in **Table 2**.

Table 2: Kits

Kit	**Supplier**
NEFA-HR (2) kit	FUJIFILM Wako Chemicals Europe GmbH (Neuss, DE)
PeqGOLD total RNA kit	VWR International (Radnor, PA, US)
Pierce BCA protein assay kit	Thermo Fisher Scientific Inc. (Waltham, MA, US)
Quantikine ELISA mouse/rat FGF-21	R&D Systems, Inc. (Minneapolis, MN, US)
Rneasy mini kit	Quiagen GmbH (Hilden, DE)
Triglycerides FS	DiaSys Diagnostic Systems GmbH (Holzheim, DE)

2.3 Buffers and Solutions

All buffers and solutions were prepared in double distilled water (ddH_2O) if not declared otherwise, and are listed in **Table 3**.

Table 3: Buffers and Solutions

Buffer/Solution	Purpose	Composition
APS solution	Preparation of gels for SDS-PAGE	10% [m/v] APS
Blocking solution	Blocking of membrane after western blot	4% [m/v] milk powder in 1:1 TBS/TBST buffer
Collagenase buffer	Isolation of primary murine hepatocytes	52552 u/ml collagenase in HBSS
Digestion buffer	Isolation of primary murine hepatocytes	100 µl of collagenase buffer in 50 ml HBSS (105.1 u/ml)
Electrophoresis buffer (pH 8.3 - 8.8)	Buffer for SDS-PAGE	16.7 mM tris base 8.3 mM tris HCl 192 mM Glycine 0.1% [m/v] SDS
HPLC eluent A	Retinoid quantification	90% [v/v] methanol 10% [v/v] ammonium acetate (0.4 g/l)
HPLC eluent B	Retinoid quantification	90% [v/v] methyl *tert*-butyl ether 8% [v/v] methanol 2% [v/v] ammonium acetate (0.2 g/l)
Loading buffer	Buffer for samples to load on gel for SDS-PAGE	87.5% [m/v] 5x pierce lane marker non-reducing sample buffer 12.5% [m/v] 2-mercaptoethanol
Loading buffer non-denaturing (pH 6.8)	Buffer for samples to load on gel for non-denaturing immunoblot	1.25 mM tris base 27.4 mM glycerol 15 µM bromophenol blue
Percoll buffer	Isolation of primary murine hepatocytes	10% [v/v] PBS (10x) 90% [v/v] Percoll
Perfusion buffer	Isolation of primary murine hepatocytes	0.5 mM EGTA in EBSS
Ponceau S solution	Protein staining on PVDF membrane	0.1% [m/v] Ponceau S in 1% [v/v] acedic acid

Protein lysis buffer	Lysis buffer for protein extraction	2 mM EDTA (pH 8.0) 150 mM NaCl 50 mM NaF 50 mM tris HCl (pH 7.2) 0.5% [m/v] sodium deoxycholate 1% [v/v] IGEPAL CA-630 0.1% [v/v] SDS 1 tablet protease inhibitor cocktail tablets complete, EDTA-free per 50 ml buffer
Resuspension buffer (RSB)	Immunoprecipitation	10 mM tris HCl pH 7.4 100 mM NaCl 2.5 mM $MgCl_2$ 1 tablet protease inhibitor cocktail tablets complete, EDTA-free per 50 ml buffer 1 tablet phosphatase inhibitor cocktail tablets complete, EDTA-free per 50 ml buffer
SDS solution	Compound of gel for SDS-PAGE	10% SDS
Stripping buffer	Buffer to remove already bound antibodies on membranes in western blot analysis	6 M guanidine hydrochloride 0.3% [v/v] tritonX-100 20 mM tris HCl (pH 7.5) 0.1 M 2-mercaptoethanol
Tris-buffered saline (TBS)-buffer	Washing buffer for PVDF membranes; antibody dilution	40.1 mM tris base 159.9 mM tris HCl 137 mM NaCl
Tris-buffered saline buffer with tween (TBST)	Washing buffer for PVDF membranes; antibody dilution	40.1 mM tris base 159.9 mM tris HCl 137 mM NaCl 0.1% [v/v] Tween 20
Transfer buffer (pH 8.1 - 8.5)	Buffer for western blot transfer	25 mM tris base 192 mM Glycine 20% [v/v] methanol 0.05% [v/v] SDS
Tris HCl buffer 0.5 M (pH 6.8)	Buffer for stacking gel for SDS-PAGE	15.3 mM tris base 485 mM tris HCl
Tris HCl buffer 1.5 M (pH 8.8)	Buffer for separation gel for SDS-PAGE	0.3 M tris base 1.2 M tris HCl

2.4 Antibodies

The primary antibodies listed in **Table 4** were used for western blot analysis. The antibodies were diluted in the indicated ratio in a solution of 4% milk powder in a 1:1 TBS/TBST mixture. The p-HSL antibody was diluted in 5% milk powder in TBST while the total HSL antibody and the FOXO1 antibody were diluted in 5% BSA in TBST.

Table 4: Primary Antibodies for the Western Blot Analysis

Antibody	Species	Product ID	Supplier	Dilution
ACTB	Mouse	sc-47778	Santa Cruz Biotechnology, Inc. (Dallas, TX, US)	1:1000
ADIPOQ	Rabbit	#sc-26497	Santa Cruz Biotechnology, Inc. (Dallas, TX, US)	1:1000 - 1:5000
CRBP1	Rabbit	sc-30106	Santa Cruz Biotechnology, Inc. (Dallas, TX, US)	1:1000
FOXO1	Rabbit	#2880S	Cell Signaling Technology, Inc. (Danvers, MA, US)	1:500
HSL	Rabbit	4107S	Cell Signaling Technology, Inc. (Danvers, MA, US)	1:1000
p-HSL (Ser 660)	Rabbit	4126S	Cell Signaling Technology, Inc. (Danvers, MA, US)	1:2000
RAN	Mouse	610341	BD Biosciences (San Jose, CA, US)	1:1000 - 1:2000
RBP4	Rabbit	A0040	Dako Denmark A/S (Glostrup, DK)	1:500 - 1:1000
TTR	Rabbit	A0002	Dako Denmark A/S (Glostrup, DK)	1:333
UCP1	Rabbit	GTX10983	GeneTex Inc (Irvine, CA, US)	1:500

In a second step of the western blot analysis, a horseradish peroxidase (HRP) conjugated secondary antibody was used in accordance with the species of the primary antibody. The antibody was diluted in the indicated concentration in a solution of 4% milk powder in a 1:1 TBS/TBST mixture. The secondary antibodies that were selected are listed in **Table 5**.

Table 5: Secondary Antibodies for the Western Blot Analysis

Antibody	Species	Product ID	Supplier	Dilution
Anti-mouse; HRP conjugated	Goat	31430	Thermo Fisher Scientific Inc. (Waltham, MA, US)	1:1000
Anti-rabbit; HRP conjugated	Goat	31460	Thermo Fisher Scientific Inc. (Waltham, MA, US)	1:1000

Immunoprecipitation involved using an RBP4 antibody to bind RBP4 in the serum of mice and to then precipitate this antigen within the procedure. **Table 6** lists the used RBP4 antibody as well as other antibodies used for specificity testing that was required during the establishment of the method described in **Chapter 4.2.1**.

Table 6: Antibodies for Immunoprecipitation

Antibody	Product ID	Concentration [mg/ml]	Supplier
C/EBPα	sc-61x	2.0	Santa Cruz Biotechnology, Inc. (Dallas, TX, US)
GATA2	sc-9008x	2.0	Santa Cruz Biotechnology, Inc. (Dallas, TX, US)
RBP4	A0040	3.3	Dako Denmark A/S (Glostrup, DK)
TTR	A0002	2.0	Dako Denmark A/S (Glostrup, DK)

2.5 Oligonucleotides

The primers that were used for quantitative real-time polymerase chain reaction (qRT-PCR) were designed with the online tool Primer3 and ordered via SMB Services from Molecular Biology GmbH (Rüdersdorf, DE). The primers were produced by Sigma Aldrich (St. Louis, MO, US). The used primers and their sequences (from 5’ to 3’) are listed in **Table 7**.

Table 7: Primers

Gene	Primer direction	Primer
18s	Forward	AAACGGCTACCACATCCAAG
	Reverse	GGCCTCGAAAGAGTCCTGTA
36b4	Forward	TCATCCAGCAGGTGTTTGACA
	Reverse	GGCACCGAGGCAACAGTT
Adrb3	Forward	GGCCCTCTCTAGTTCCCAG
	Reverse	TAGCCATCAAACCTGTTGAGC
Atgl	Forward	CAACGCCACTCACATCTAC
	Reverse	GTTGAAGGAGGGATGCAGA
Cidea	Forward	AGGGACACCACGCATTTCAT
	Reverse	CCGATTTCTTTGGTTGCTTG
Crbp1	Forward	GCGCGCTCGACGTCAAC
	Reverse	ACGATCTCTTTGTCTGGCTTCAG
Cyp26a1	Forward	TCTCCAACCTGCACGATTCC
	Reverse	CGGCTGAAGGCCTGCAT
Cyp26b1	Forward	AGAGCAGCAAGGAACATGGC
	Reverse	AGTTGCATGATCAAGGATGTGC
Cyp2c39	Forward	TCCTCTTGAACACGGTCCTC
	Reverse	TAACGGCCTTGGCATTGTTT
Fgf21	Forward	CCTGGGTGTCAAAGCCTCTA
	Reverse	GTCCTCCAGCAGCAGTTCTC
Foxo1	Forward	CTACGAGTGGATGGTGAAGAGC
	Reverse	CCAGTTCCTTCATTCTGCACTCG
Hprt	Forward	TGCTGACCTGCTGGATTACA
	Reverse	TATGTCCCCCGTTGACTGAT
Hsl	Forward	CACCCATAGTCAAGAACCCCTTC
	Reverse	TCTACCACTTTCAGCGTCACCG
Igfbp1	Forward	ACGAGCACCTTGTTCAGCTC
	Reverse	GCAGCTGCTCCTCTGTCATC
Lrat	Forward	TATGGCTCTCGGATCAGTCC
	Reverse	TAATCCCAAGACAGCCGAAG
Pck1	Forward	ATCATCTTTGGTGGCCGTAG
	Reverse	CCTCAGATCTCATGGCTGCT
Rarβ2	Forward	TGCTCAATCCATCGAGACAC
	Reverse	CTTGTACACCCGAGGAGGAG

Ratsat	Forward	CCCATCAAGCAAGGATCCAA
	Reverse	ATGGGTACCAGCGCAGTCA
Rbp4	Forward	GCAGGAGGAGCTGTGCCTAGA
	Reverse	GGAGGGCCTGCTTTGACAGT
Stra6	Forward	GCAGACCAGCTACTCCGAGA
	Reverse	GAGACAGGAGGCTACGCTTG
Stra6l	Forward	ACTCCCTGACCTGGTTTGTG
	Reverse	GTGAGGGCCAGTAGAAAACG
Ttr	Forward	CGTACTGGAAGACACTTGGCATT
	Reverse	GAGTCGTTGGCTGTGAAAACC
Ucp1	Forward	GGGCCCTTGTAAACAACAAA
	Reverse	ACTGGAGAGGCCAGGAGTGT

2.6 Small Interfering Ribonucleic Acid (siRNA)

The used siRNAs (Eurogentec, Liège, BE) and their sequences (from 5' to 3') are listed in **Table 8**.

Table 8: siRNAs

siRNA	**Sequence**
siControl	UUG-AUG-UGU-UUA-GUC-GCU-A(UU)
siFoxo1	UUG-CUC-AUA-AAG-UCG-GUG-C(UU)

2.7 Adeno-Associated Viruses (AAV)

The AAVs were produced and the genomic copies were quantified by PD Dr. Stefan Weger from the Institute of Virology of the Charité – Universitätsmedizin Berlin. The viruses and their titers are shown in **Table 9**.

Table 9: Adeno-Associated Viruses

Virus	**Titer [genomic copies/ml]**
AAV2/8-LP1 FGF21	$4.39x10^{11}$
AAV2/8-LP1 GFP	$4.80x10^{11}$

2.8 Cell Line and Culture Conditions

Primary murine hepatocytes were isolated from the livers of male C57BL/6J mice. The cells were cultured in Dulbecco's Modified Eagle Medium (DMEM) high glucose (+ 4,5 g/l glucose, + L-glutamine, - pyruvate) (Gibco, Thermo Fisher Scientific Inc., Waltham, MA, US) supplemented with 10% FBS and 1% P/S. Indicated experimental settings required the use of DMEM no glucose (- glucose, + L-glutamine, - pyruvate) (Gibco, Thermo Fisher Scientific Inc., Waltham, MA, US) with or without FBS and P/S. The isolated primary murine hepatocytes were incubated at 37 °C in a humidified atmosphere containing 5% CO_2.

2.9 Experimental Animals and Husbandry

Male C57BL/6J mice were used in all described experiments. The mice were obtained from the Forschungseinrichtung für Experimentelle Medizin (Research Facility for Experimental Medicine) of the Charité – Universitätsmedizin Berlin and kept in their facility in the Center for Cardiovascular Research (CCR) of the Charité – Universitätsmedizin Berlin. In this pathogen-free environment, the mice can be kept under standardized conditions, where the room temperature is set to 22 ± 2 °C, the humidity is 60 ± 15%, and a 12 h day-and-night rhythm is maintained.

The mice were kept in cages of different sizes: type I with a maximum of three mice, type II with a maximum of five mice, and type III with a maximum of eight mice. The animals were placed into new cages by trained personnel twice per week, which contained the dry litter FS14/Fichte (Altromin Spezialfutter GmbH & Co. KG, Lage, DE) and to which objects were added for environmental enrichment. The animals were fed *ad libitum* with the standard diet V1124-300 (ssniff-Spezialdiäten GmbH, Soest, DE) and water. All procedures for the animal experiments were approved by the Landesamt für Gesundheit und Soziales Berlin (State Office for Health and Social Affairs Berlin) under the numbers O 0400/17, G 0056/16, and G 0130/17 while complying with the national and European laws for laboratory animal experiments.

2.10 Consumables

The employed consumables are listed in **Table 10**.

Table 10: Consumables

Consumable	Supplier
0.5 ml insulin syringe U-100 0.3 mm (30G) x 12 mm	B. Braun Melsungen AG (Melsungen, DE)
15 ml and 50 ml PP conical tubes	Corning Inc. (Corning, NY, US)
6-well, 12-well, and 24-well plates	Corning Inc. (Corning, NY, US)
C30 analytical column	YMC Europe GmbH (Dinslaken, DE)
Cannula Sterican (different sizes)	B. Braun Melsungen AG (Melsungen, DE)
Cell culture dish, 100 mm	Corning Inc. (Corning, NY, US)
Cell scraper 16 cm	Sarstedt AG & Co. KG (Nümbrecht, DE)
Contour next glucose test strips	Ascensia Diabetes Care Holdings AG (Basel, CH)
Disposable scalpel	Feather Safety Razor Co., Ltd (Osaka, JP)
Ear tags	H. Hauptner und Richard Herberholz GmbH & Co. KG (Solingen, DE)
Filter paper	Bio-Rad Laboratories (Hercules, CA, US)
FreeStyle precision pro β-ketone test strips	Abbott Laboratories (Chicago, IL, US)
Hard-shell PCR plates 364 wells and 96 wells	Bio-Rad Laboratories (Hercules, CA, US)
Medical X-RAY film 100 NIF 18 x 24	FUJIFILM Europe GmbH (Düsseldorf, DE)
Microseal PCR plate sealing film, adhesive	Bio-Rad Laboratories (Hercules, CA, US)
Micro pestle	VWR International (Radnor, PA, US)
Microplate, 96-well, flat-bottom	Greiner Bio-One GmbH (Kremsmünster, AT)
Nylon mesh (250 µm)	Klein & Wiehler oHG (Königswinter, DE)
Parafilm PM-996	Bemis Company, Inc. (Neenah, WI, US)
PCR-tubes	neoLab Migge GmbH (Heidelberg, DE)
Pipette tips (10 µl, 200 µl, 1000 µl)	Sarstedt AG & Co. KG (Nümbrecht, DE)
Polyvinylidene fluoride (PVDF) membrane	Bio-Rad Laboratories (Hercules, CA, US)
Safe seal tube 1.5 ml	Sarstedt AG & Co. KG (Nümbrecht, DE)
Safe seal tube 2 ml PP	Sarstedt AG & Co. KG (Nümbrecht, DE)
Serological pipettes (5 ml, 10 ml, 25 ml)	Sarstedt AG & Co. KG (Nümbrecht, DE)
Solofix lancets	B. Braun Melsungen AG (Melsungen, DE)
Syringe filter, minisart NML, CA, 28 mm, 0.2 µm, sterile	Sartorius AG (Göttingen, DE)
Syringes without cannula (0.5 ml, 1 ml)	B. Braun Melsungen AG (Melsungen, DE)
Vasofix safety peripheral venous catheter 22 G	B. Braun Melsungen AG (Melsungen, DE)

2.11 Equipment

Table 11 contains a comprehensive list of all equipment used.

Table 11: Equipment

Article	Supplier
Analytical balance	Sartorius AG (Göttingen, DE)
Biofuge 13-R centrifuge	Heraeus (Berlin, DE)
Biofuge universal 32-R centrifuge	Heraeus (Berlin, DE)
Centrifuge 5415 R	Eppendorf AG (Hamburg, DE)
Centrifuge 5810 R	Eppendorf AG (Hamburg, DE)
CFX connect real-time PCR detection system	Bio-Rad Laboratories (Hercules, CA, US)
Chemidoc imaging system	Bio-Rad Laboratories (Hercules, CA, US)
ContourXT glucose meter	Ascensia Diabetes Care Holdings AG (Basel, CH)
Equipment for polyacrylamide gels	Bio-Rad Laboratories (Hercules, CA, US)
Equipment for western blot	Bio-Rad Laboratories (Hercules, CA, US)
Film cassette	GE Heathcare GmbH (Solingen, DE)
Film developer Agfa CURIX 60	Agfa HealthCare NV (Mortsel, BE)
FreeStyle precision neo	Abbott Laboratories (Chicago, IL, US)
Heating plate MR 2002	Heidolph Instruments GmbH & Co.KG (Kelheim, DE)
HERA safe working bench	Thermo Fisher Scientific Inc. (Waltham, MA, US)
HPLC system	Shimadzu (Kyōto, JP)
Incubator	Heraeus (Berlin, DE)
Microprocessor pH meter 743	Knick Elekronische Messgeräte GmbH & Co. KG (Berlin, DE)
Microscope Leica DM IL LED	Leica Mikrosysteme Vertrieb GmbH (Wetzlar, DE)
Mini-PROTEAN tetra cell system	Bio-Rad Laboratories (Hercules, CA, US)
MiniSpin plus benchtop centrifuge	Eppendorf AG (Hamburg, DE)
MiniTrans-blot cell (Western Blot system)	Bio-Rad Laboratories (Hercules, CA, US)
Mortar and pestle	Jizerská porcelánka s.r.o. (Desná, CZ)
NanoDrop ND-1000 spectrophotometer	PEQLAB Biotechnologie GmbH (Erlangen, DE)
Neubauer counting chamber	LO-Laboratories GmbH (Lancing, UK)

PTC-200 peltier thermal cycler	Bio-Rad Laboratories (Hercules, CA, US)
Restrainer rotating tail injector RTI	Braintree Scientific, Inc. (Braintree, MA, US)
Rotamax 120 shaker	Heidolph Instruments GmbH & Co.KG (Kelheim, DE)
Scale Kern 470	KERN & SOHN GmbH (Balingen-Frommern, DE)
STA-multipurpose peristaltic pump 131900	DESAGA GmbH (Heidelberg, DE)
Thermomixer comfort	Eppendorf AG (Hamburg, DE)
Tissue tearor homogenizer	Biospec Products, Inc. (Breda, NL)
Ultrasonic bath Sonorex RK 52 H	BANDELIN electronic GmbH & Co. KG (Berlin, DE)
Vortex genie 2	Scientific Industries, Inc. (Bohemia, NY, US)
VWR pellet mixer	VWR International (Radnor, PA, US)
water bath Köttermann 3042	Köttermann GmbH & Co. KG (Uetze, DE)
xMark microplate spectrophotometer	Bio-Rad Laboratories (Hercules, CA, US)

2.12 Software

All software used to obtain, process, analyze, and present the data has been listed in **Table 12**.

Table 12: Software

Software	Purpose	Supplier
CFX Manager, Software Version 3.1	qRT-PCR signal detection	Bio-Rad Laboratories (Hercules, CA, US)
EndNote X9, software version 9.3.3	References management	Clarivate Analytics (Philadelphia, PA, US)
GraphPad PRISM 9, software version 9.3.0	Scientific graphing and statistical analysis	GraphPad Software Inc. (San Diego, CA, US)
Image J, software version 1.53k	Protein signal quantification for western blot analysis	National Institutes of Health (Bethesda, MD, US)
Image Lab, software version 6.1.0	Protein signal detection for western blot	Bio-Rad Laboratories (Hercules, CA, US)
Microplate Manager 6, software version 6.2	Measurement of colorimetric signals	Bio-Rad Laboratories (Hercules, CA, US)
MS Office 2019	Data processing and presentation	Microsoft Corporation (Redmond, WA, US)
ND-1000, software version 3.8.1	RNA quantification	Thermo Fisher Scientific Inc. (Waltham, MA, US)

3 Methods

3.1 Molecular Biological Methods

3.1.1 RNA Extraction from Primary Murine Hepatocytes

The extraction of RNA from primary murine hepatocytes was performed using VWR's peqGold total RNA kit according to the manufacturer's manual. The lysed RNA is bound to a silica-based matrix in a column, washed, and eventually eluted in 40 µl RNase-free water. The concentration of RNA in the sample was determined with a NanoDrop ND-1000 spectrometer and the samples were stored at -80 °C.

3.1.2 RNA Extraction from Liver Tissue

The extraction of RNA from liver tissue was performed with Quiagen's RNeasy mini kit, where the lysed RNA is bound to a silica-based matrix in a column, washed, and eventually eluted in RNase-free water. The manufacturer's instructions were adapted. Approximately 50 mg of liver tissue from the right liver lobe was used and mechanically homogenized in 500 µl QIAzol lysis reagent. Another 500 µl of QIAzol lysis reagent were added after the homogenization and incubated for 5 minutes at room temperature. Thereafter, 200 µl chloroform per 1 ml were added and the tube was vortexed thoroughly for 15 seconds. The samples were incubated for 3 minutes at room temperature before they were centrifuged for 15 minutes at 12.000 x g and 4 °C. The upper aquatic phase was transferred into a new tube and mixed with one volume of 70% ethanol. This mixture was added to the provided column of Quiagen's RNeasy mini kit and centrifuged for 15 seconds at 10,000 rpm. Then, 700 µl of the provided RW1 buffer were added to the filter and, after centrifugation for 15 seconds at 10,000 rpm, 500 µl of the provided RPE buffer were added and the centrifugation step repeated. Next, another 500 µl of RPE buffer were added and centrifuged for 2 minutes at 10,000 rpm. The column was then incubated for 3 minutes at room temperature before 30 µl of RNase-free water were added to the filter and the RNA was eluted into a new tube by means of centrifugation for 1 minute at 10,000 rpm. The concentration of RNA in the sample was determined with a NanoDrop ND-1000 spectrometer and the samples were stored at -80 °C.

3.1.3 RNA Extraction from White Adipose Tissue

The entire excised white adipose tissue piece was homogenized in liquid nitrogen with the help of a mortar and a pestle until it became a powder. The extraction of RNA from eWAT and scWAT was performed with Quiagen's RNeasy mini kit. The underlying principle is explained in **Chapter 3.1.2**. The manufacturer's instructions were adapted. Therefore, approximately 70 mg of tissue were used and mechanically homogenized in 500 µl of QIAzol lysis reagent. Another 500 µl of QIAzol lysis reagent were added after the homogenization and incubated for 5 minutes at room temperature. Thereafter, 200 µl chloroform per 1 ml were added and the tube was vortexed thoroughly for 15 seconds. The samples were incubated for 3 minutes at room temperature before they were centrifuged for 15 minutes at 13,000 rpm and 4 °C. The upper aquatic phase was transferred into a new tube and mixed with one volume of 70% ethanol. This mixture was added to the provided column of Quiagen's RNeasy mini kit and centrifuged for 15 seconds at 10,000 rpm. The filtrate was discarded and the filter washed once with 350 µl of the provided RW1 buffer. Thereafter, a mixture of 10 µl DNase stock solution and 70 µl RDD buffer from the RNase-free DNase set was added directly on the filter and incubated for 15 minutes at room temperature. The filter was then washed, first with 500 µl RW1 buffer and then with 500 µl of the provided RPE buffer by addition on the filter and centrifugation at 10,000 rpm for 15 seconds. For the last step of washing, 500 µl of RPE buffer were added on the filter and centrifuged for 2 minutes at 10,000 rpm. To dry the filter, it was centrifuged for 1 minute at 10,000 rpm, before the filter was placed on a new 1.5 ml tube and the RNA was eluted with 40 µl of RNase-free water added directly on the filter and incubated for 5 minutes at room temperature. After centrifugation for 1 minute at 10,000 rpm, the same 40 µl of RNase-free water were added to the filter once more, incubated, and centrifuged as described above before the concentration of RNA in the sample was determined with a NanoDrop ND-1000 spectrometer and the samples were stored at -80 °C.

3.1.4 Complementary DNA (cDNA) Synthesis

Each sample of 1 µg RNA, which had been calculated using the results of the NanoDrop ND-1000 measurement, was mixed with 0.25 µg of random hexamer primer and ultrapure water to a volume of 15 µl. This mixture was heated to 70 °C for 5 minutes, after which the samples were cooled down to 4 °C. A mixture consisting of 5.0 µl M-MLV reaction buffer (5x), 1.25 µl dNTP mix, 1.0 µl M-MLV reverse transcriptase, and 2.75 µl of ultrapure water to a total volume of 10 µl per sample was prepared and added to the samples as indicated in **Table 13**. This mixture was then incubated for 1 h at 37 °C and the synthetized cDNA samples were stored at -20 °C.

Table 13: Composition of Reverse Transcriptase Mixture for cDNA Synthesis

Reagent	Volume [µl]	Concentration
5x M-MLV reaction buffer	5.0	1x
dNTP mix [10 mM]	1.25	0.5 mM per dNTP
M-MLV reverse transcriptase [200 u/µl]	1.0	200 u
Ultrapure water	2.75	
Total volume	10	

3.1.5 Quantitative Real-Time Polymerase Chain Reaction (qRT-PCR)

The principle of this method is to amplify the DNA through PCR and to quantify it by adding a fluorescent dye that intercalates with the DNA. The fluorescent signal is then related to the PCR product. A standard curve was generated for the qRT-PCR. To obtain a 1:5 dilution in 220 µl of ultrapure water, up to 5 µl of each cDNA sample were taken, mixed together, and considered the highest concentrated sample for the standard curve. Three more dilutions, each in a 1:10 ratio, were prepared, resulting in four samples for the standard curve (100%, 10%, 1%, 0.1%). The remaining volume of the samples was diluted in a 1:10 ratio in ultrapure water.

For one sample, a mixture containing 0.1 µl forward primer for the target gene, 0.1 µl reverse primer for the target gene, 2.5 µl 2x fast start universal SYBR green master (ROX), and 0.3 µl of ultrapure water to a total volume of 3 µl was prepared as described in **Table 14**. This mixture and 2 µl of the diluted samples or standards were pipetted together on a 384-well plate and measured with the CXF Connect Real-Time System using the suitable program, as explained in **Table 15**. With the help of the standard curve, the relatively expressed mRNA levels could be quantified in relation to so-called house keeper genes, which are robustly expressed genes that are usually not regulated.

Table 14: Mixture for qRT-PCR

Reagent	Volume [µl]	Concentration
Forward primer [5 µM]	0.1	200 nM
Reverse primer [5 µM]	0.1	200 nM
2x fast start universal SYBR green master (ROX)	2.5	1x
Ultrapure water	0.3	
Total volume	3.0	

Table 15: Program for qRT-PCR

qRT-PCR	Temperature [°C]	Time	Cycles
Initial denaturation	95	10 minutes	1
Denaturation of DNA-primer hybridization/ amplification	95	15 seconds	40
Annealing	60	1 minutes	40
Melting curve	95 60 → 95	30 seconds 30 seconds	1

3.2 Protein Biochemical Methods

3.2.1 Isolation of Protein Extracts from Cultivated Cells

The cells were cultured in 12-well plates and treated as indicated in each experimental setup. Thereafter, they were washed twice with ice-cold PBS, carefully scratched from the surface of the plate in ice-cold PBS, and centrifuged for 5 minutes at 5,000 rpm. The supernatant was discarded and the cell pellet reconstituted in an adequate amount of protein lysis buffer. The cells were sonicated five times at the lowest intensity and centrifuged for 30 minutes at 13,000 rpm and 4 °C afterwards. The supernatant was transferred into a new tube and stored at -20 °C.

3.2.2 Isolation of Protein Extracts from Liver Tissue

Approximately 50 mg of liver from the right liver lobe were placed in 500 µl of ice-cold protein lysis buffer and were homogenized with a micro pestle, sonicated five times at the lowest intensity, and centrifuged for 30 minutes at 13,000 rpm and 4 °C. The supernatant was transferred into a new tube and stored at -80 °C.

3.2.3 Isolation of Protein Extracts from White Adipose Tissue

The entire excised white adipose tissue piece was homogenized in liquid nitrogen with the help of a mortar and a pestle until it became a powder. Approximately 30 to 50 mg of tissue were taken for protein isolation, 200 µl of protein lysis buffer were added, and the samples were then frozen again in liquid nitrogen. After thawing the samples, they were again homogenized by vortexing them thoroughly. They were sonicated 20 times at medium intensity, and

centrifuged for 30 minutes at 13,000 rpm and 4 °C. The supernatant was transferred into a new tube and stored at -80 °C.

3.2.4 Protein Concentration Measurement

The protein concentration was measured with the Pierce BCA protein assay kit. In this assay the protein reduces Cu^{2+} to Cu^{+}, and, in a second reaction, bicinchoninic acid forms a complex with Cu^{+} that can be detected photometrically. The manufacturer's instructions were adapted. For the assay, the working reagent was prepared with the provided reagents A and B in a 50:1 ratio. 5 µl of each standard and sample were pipetted into a flat-bottom 96-well plate. Subsequently, 95 µl of the prepared working reagent were added and incubated for 30 minutes at 37 °C. The samples, as well as the standard curve, were measured with a photometer in duplicates at a wavelength of 562 nm. Using a standard curve, a relation between the photometrical signal and the protein concentration was determined and used to calculate the protein concentration of the samples.

3.2.5 Sodium Dodecyl Sulfate-Polyacrylamide Gel Electrophoresis (SDS-PAGE)

Proteins can be separated according to their molecular weight with an SDS-PAGE.

Table 16: Gel Preparation for SDS-PAGE

Reagent	10% separating gel	12% separating gel	15% separating gel	18% separating gel	stacking gel
ddH2O	4.1 ml	3.35 ml	2.4 ml	1.35 ml	3.05 ml
1.5 M tris HCl buffer pH 8.8	2.5 ml	2.5 ml	2.5 ml	2.5 ml	-
0.5 M tris HCl buffer pH 6.8	-	-	-	-	1.25 ml
10% SDS solution	100 µl	100 µl	100 µl	100 µl	50 µl
acrylamide solution 30%	3.3 ml	4.0 ml	5.0 ml	6.0 ml	0.65 ml
10% APS solution	75 µl	75 µl	75 µl	75 µl	50 µl
TEMED	7.5 µl	7.5 µl	7.5 µl	7.5 µl	6 µl

The polyacrylamide gels measuring 1.5 mm thick were produced as shown in **Table 16** using the designated equipment. Afterwards, the gel was placed in an electrophoresis chamber filled

with electrophoresis buffer. Between 10 and 50 µg of protein were diluted in protein loading buffer, boiled for 20 minutes (to reliably denature the tetrameric TTR) or heated to 95 °C for 5 minutes, centrifuged for 3 minutes at 13,000 rpm at room temperature, and then loaded onto the gel along with a molecular weight size marker. The protein concentration of the serum samples and supernatant samples was not measured, and equal volumes of all samples were directly added to the protein loading buffer instead before proceeding as explained for the cell lysates. Serum samples were diluted in a 1:30 ratio to prevent a protein overload. The SDS-PAGE was started at a voltage of 80 V through the stacking gel, while afterwards the voltage was raised to 120 V.

3.2.6 Non-Denaturing Gel Electrophoresis

In order to separate apo-RBP4 and holo-RBP4 on an immunoblot, a non-denaturing gel electrophoresis was performed. Therefore, the above-mentioned procedure for the SDS-PAGE was adapted as follows. The serum samples were diluted in bromophenol blue loading buffer, which does not contain 2-mercaptoethanol, in a 1:30 ratio and not centrifuged, boiled, or heated. The gels were prepared according to **Table 16**, but without using SDS. Then the samples were loaded onto the gels together with a molecular weight size marker. The electrophoresis buffer in the electrophoresis chamber was prepared as explained in **Table 3**, but without the addition of SDS. The electrophoresis was conducted at a voltage of 124 V at 4 °C.

3.2.7 Western Blot Analysis

Following the separation of the proteins in the acrylamide gel, the proteins were transferred onto a membrane to detect and analyze the proteins. Therefore, the separating gel was placed on a PVDF membrane that was activated in methanol for 1 minute and placed between filters and sponges in a so-called sandwich. The cassette and a cooling unit were placed in the tank exactly as described in the manufacturer's manual. The tank was filled with transfer buffer and a voltage of 80 V was applied for 2 h while the tank was kept on ice; respectively, a voltage 29 V was applied overnight at 4 °C. After the transfer, the membrane was washed three times for 5 minutes in ddH_2O, air-dried, reactivated for 1 minute in methanol, stained with 0.1% Ponceau S solution for 10 minutes, and imaged. The membrane was then de-stained by placing the membrane in 0.1 M NaOH solution three times for 5 minutes, and then washed three times for 5 minutes in TBST buffer, before moving to the blocking for 1 h in 4% milk solution. The membrane was incubated overnight at 4 °C in primary antibody solution containing the antibody to the protein of interest. After three washing steps lasting 10 minutes

each in TBST, the membrane was incubated for 1 hour at room temperature in a secondary antibody solution that contained an HRP-conjugated antibody against the species of the primary antibody. Thereafter, the membrane was washed three times for 10 minutes in TBST and the signal of the protein of interest was detected with an enhanced chemiluminescence (ECL) western blotting substrate solution following the manufacturer's instructions. The signal was detected on the Biorad ChemiDoc imaging system or with a film on the Curix 60 developer with an appropriate exposition time so that the bands were visible, but not saturated. In order to be able to detect p-HSL and HSL that display bands on the same level, the membranes were stripped after the first incubation with p-HSL. They were incubated three times for 10 minutes in 4 ml of stripping buffer on a rotative shaker, after which they were washed four times for 3 minutes in TBST. Afterwards, the incubation with the first antibody against HSL and the following steps were performed as described above.

3.2.8 Immunoprecipitation of RBP4

With the aim to precipitate RBP4 from murine serum, the method of immunoprecipitation was adjusted and a new protocol was established within this study.

For this purpose, an indicated antibody volume was added to 50 µl of serum and incubated for 4 h at 4 °C while rotating. Then, an indicated volume of sepharose beads (50% slurry in RSB) was added to the samples and incubated for another 3 h at 4 °C while rotating. Aiming to separate the supernatant from the sepharose beads, the samples were centrifuged at 1,000 rpm for 1 minute. The supernatant, as well as the sepharose beads, which had been re-suspended in 100 µl RSB, were frozen at -80 °C.

3.3 Analytical Methods

3.3.1 FGF21 Enzyme-Linked Immunosorbent Assay (ELISA)

In order to determine the concentration of FGF21 in mouse serum, the Quantikine ELISA kit mouse/rat FGF-21 was used. In this quantitative sandwich ELISA the antigen of interest is bound to an antibody that was pre-coated on a provided microplate. A second antibody, which is linked to an enzyme, is added and binds to the antigen. The enzyme can transform an added substrate and the measured photometrical signal is proportional to the bound antigen. The assay was performed exactly as instructed by the manufacturer. The standard curve revealed a relation between the absorption and concentration, which was used to calculate the concentration of the samples.

3.3.2 Quantitative Determination of Non-Esterified Fatty Acids (NEFA)

The quantitative determination of the NEFAs in murine serum was conducted with the NEFA (HR2) kit using an enzymatic colorimetric method. The enzyme Acyl-CoA synthase leads to the transformation of NEFAs to Acetyl-CoA, which is then oxidized by Acyl-CoA oxidase to 2,3-trans-Enoyl-CoA and hydrogen peroxide. The enzymatic action of peroxidase causes a blue/purple product to form, which can be quantified with a photometer. The manufacturer's instructions were adapted. Therefore, 5 µl of each standard and sample were added to 150 µl of the provided reagent R1 in a flat-bottomed 96-well plate in duplicates and incubated for 10 minutes at 37 °C. Then, 75 µl of the provided reagent R2 were added to each well. Following an incubation period of 10 minutes at 37 °C, the samples as well as the standard curve were measured with a photometer at a wavelength of 546 nm. The obtained standard curve was utilized to establish a correlation between the absorbance and the NEFA concentration, which, in turn, was used to calculate the concentration of the samples.

3.3.3 Quantitative Determination of Serum Triglycerides

The quantitative determination of the triglycerides in murine serum was carried out with the DiaSys triglycerides FS kit using a colorimetric enzymatic method. The activity of glycerol-3-phosphateoxidase creates a product that can be quantified with a photometer. The manufacturer's instructions were adapted. For this reason, 200 µl of the provided reagent were added to 5 µl of the standard and samples on a flat-bottomed 96-well plate and were then incubated for 10 minutes at 37 °C. The absorbance was subsequently measured at a wavelength of 500 nm with a photometer. The obtained standard curve enabled a correlation between the absorbance and the triglyceride concentration and was utilized to calculate the triglyceride concentration of the samples.

3.3.4 Extraction of Serum Retinol

The extraction of serum retinol was performed with the help of Andrea Hurtienne and Apl. Prof. Dr. Jens Raila from the Department of Physiology and Pathophysiology of Nutrition at the Institute of Nutritional Science at the University of Potsdam, Germany.

100 µl of distilled water were added to a volume of 100 µl serum and mixed thoroughly before adding 200 µl of 99.5% ethanol. Then, 1000 µl n-hexane (supplemented with 0.05% butylated hydroxytoluene) were added and rotated for 15 minutes at room temperature to achieve an even mixture. After centrifugation for 10 minutes at 1,500 x g, the supernatant was transferred

to a new tube and the extraction steps were repeated once more starting from the addition of n-hexane. The supernatants from both extractions were dried with nitrogen at 37 °C until the solvents were completely evaporated. The residue was dissolved in isopropanol and then centrifuged for 5 minutes at 2,000 x g. The retinol content was measured using HPLC.

3.3.5 Extraction of Tissue Retinoids

The extraction of tissue retinoids was performed with the help of Andrea Hurtienne and Apl. Prof. Dr. Jens Raila from the Department of Physiology and Pathophysiology of Nutrition at the Institute of Nutritional Science at the University of Potsdam, Germany.

100 µl of distilled water were added to 100 mg of the tissue sample, and were mixed thoroughly before adding 1 ml of a 2:3 [v/v] extraction mixture of isopropanol and n-hexane and rotating for 15 minutes at room temperature to achieve an even mixture. After centrifugation for 10 minutes at 1,500 x g, the supernatant was transferred to a new tube (tube A) and the extraction steps starting from the addition of the extraction mixture were repeated once more. A total of 2 ml of 0.1 M NaCl were added to the supernatants from both extractions in tube A and incubated for 30 minutes at room temperature. The supernatant was transferred to a new tube (tube B), while 2 ml of n-hexane were added to tube A, mixed thoroughly, and incubated for 30 minutes at room temperature. Thereafter, the supernatant from tube A was transferred to tube B and the extraction process with n-hexane was repeated in tube A. The extract collected in tube B was dried at 37 °C with nitrogen until the solvents were completely evaporated. The residue was dissolved in isopropanol and then centrifuged for 5 minutes at 2,000 x g. The retinoid content was measured using HPLC.

3.3.6 High Performance Liquid Chromatography (HPLC) Measurement of Retinoids

The HPLC measurement of retinoids was performed with the help of Andrea Hurtienne and Apl. Prof. Dr. Jens Raila from the Department of Physiology and Pathophysiology of Nutrition at the Institute of Nutritional Science at the University of Potsdam, Germany.

The HPLC was performed at 20 °C, the flow rate was set to 0.2 ml/minute, and the signal was detected with a photodiode array at 200 to 550 nm. A C30-bonded, silica-based reverse-phase column with a particle size of 5 µm was used. The protocol for the gradient dilution of the eluents is shown in **Table 17**.

Table 17: Protocol for HPLC Gradient Dilution

Time [minutes]	Volume eluent A [%]	Volume eluent B [%]
0	95	5
1	93	7
2	85	15
3	80	20
11	75	25
21	45	55
29	13	87
32	7	93
33	1	99
47	1	99
47.1	95	5
60	stop	stop

3.4 Cell Biological Methods

3.4.1 Isolation of Primary Murine Hepatocytes

Primary murine hepatocytes were isolated from male C57BL/6J mice between the ages of seven and 30 weeks. A combination of ketamine (80 mg/kg body weight) and xylazine (12 mg/kg body weight) was injected intraperitoneally for anesthesia. Successful anesthesia was confirmed by testing the reflex between the toes. Next, the mouse was fixated and the prepared abdomen was carefully cut open to access the liver. A venous catheter was inserted into the vena cava cranially and the liver was flushed with a perfusion buffer at a speed of 4 ml/minute, which quickly resulted in swelling of the liver. The portal vein was cut so that the blood and the buffer could drain from the organ. Successful perfusion was confirmed by a change of color of the liver from dark brown to light brown. Immediately after that, the liver was perfused with a digestion buffer at the same speed using the same catheter. When the digestion was successful, the liver was transferred to a 100 mm cell culture dish and the gallbladder removed before quickly moving into a sterile environment.

The following steps were all performed in DMEM high glucose. A total of 25 ml of DMEM were added to the liver, it was crushed by applying gentle pressure with two cell scrapers on the liver, and then was passed through a mesh. This procedure was repeated with another 25 ml of DMEM before spinning the cells at 850 rpm for 10 minutes at 30 °C. The pellet was carefully

resuspended in 25 ml of DMEM to which then 25 ml of Percoll buffer were added. After centrifugation at 850 rpm for 10 minutes at 30 °C, the cells were washed by carefully resuspending the cell pellet in 25 ml DMEM and subsequent centrifugation for 3 minutes at 850 rpm and 30 °C. The pellet was carefully resuspended in an appropriate volume of DMEM and the cells were counted in a Neubauer chamber. The cells were seeded on 12-well plates with a density of approximately 400,000 cells per well. 10 minutes after seeding, the plates were shaken carefully by hand to ensure an even distribution of the cells, and, then, the cells were allowed to settle for 4 to 6 h before they were used for experiments.

3.4.2 Lipofection

Lipofection was used for the transfection of RNA into the primary murine hepatocytes and to induce the knockdown of an indicated target gene. After allowing the isolated primary murine hepatocytes to settle for 4 to 6 h, the medium was changed to DMEM high glucose with 10% FBS and 1% P/S. For a single well on a 12-well plate containing approximately 400,000 cells, 1 nmol (5 µl) of siRNA was mixed with 45 µl of Optimem. Then, 4 µl of Lipofectamin was mixed with 46 µl of Optimem per well and incubated for 5 minutes at room temperature. The siRNA mixture and the Lipofectamin mixture were combined and incubated for 20 minutes at room temperature. Thereafter, 90 µl of this mixture were added to the cells dropwise and incubated overnight. The next morning, the media was replaced with DMEM high glucose with 10% FBS and 1% P/S and the cells were cultured for 72 h if not indicated otherwise.

3.5 Animal Experiments

3.5.1 Experimental Design for the Study on the Serum of Fed and Fasted Mice

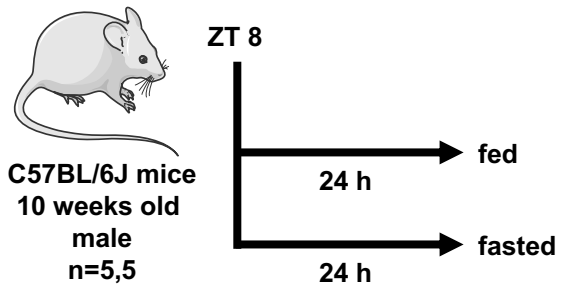

Figure 6: Procedure for 24 h Fasting and Subsequent Immunoblot. C57BL6/J mice were fed *ad libitum* or fasted for 24 h before they were euthanized and subject to testing. The collected serum was used for a non-denaturing immunoblot.

This experiment was conducted on ten-week-old male C57BL6/J mice (**Figure 6**). After letting the mice adjust to their new environment for one week, five mice were fed *ad libitum* for 24 h, and another five mice fasted for 24 h before they were euthanized by means of a final heart puncture while under inhaled anesthesia with isoflurane.

3.5.2 Experimental Design for the Immunoprecipitation Study on the Serum of Fed and Fasted Mice

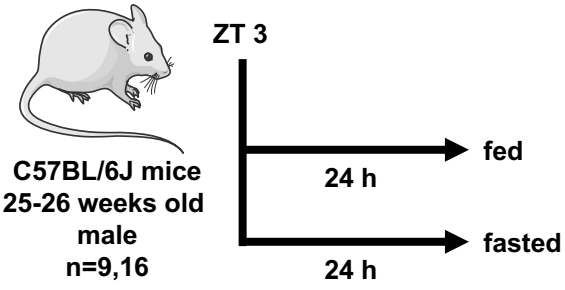

Figure 7: Procedure for 24 h Fasting and Subsequent Immunoprecipitation of Serum RBP4. C57BL6/J mice were fed *ad libitum* or fasted for 24 h before they were euthanized and subject to testing. The collected serum was used for RBP4 immunoprecipitation.

In this experiment, 25 to 26-week-old old male C57BL6/J mice were tested (**Figure 7**). After letting the mice adjust to their new environment for one week, nine mice were fed *ad libitum* for 24 h, and another 16 mice fasted for 24 h before they were euthanized as stated before.

3.5.3 Experimental Design for the Study on FGF21 Overexpression

This experiment was performed with 8 to 10-week-old male C57BL6/J mice (**Figure 8**). After letting the mice adjust to their new environment for one week, seven mice were injected with AAV-LP1-GFP and another seven mice were injected with AAV-LP1-FGF21. After two weeks, blood samples were collected from the submandibular vein, the blood glucose and blood ketones were measured, and the FGF21 concentration in the serum was determined. The mice were weighed weekly. 24 days after injection, the blood glucose and ketones were analyzed before the mice were euthanized as explained before and the serum and organs harvested for further analysis.

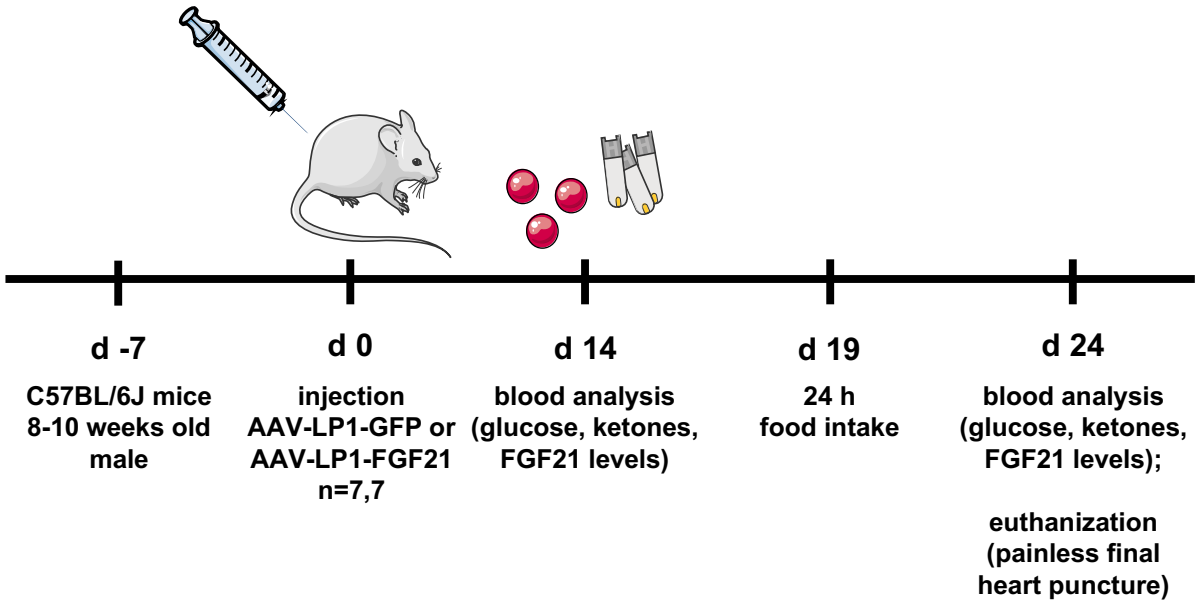

Figure 8: Procedure for AAV-Mediated GFP and FGF21 Overexpression. C57BL6/J mice were injected with AAV-LP1-GFP or AAV-LP1-FGF21. Their blood was analyzed on day 14. After 19 days, their food intake was recorded for 24 h. On day 24, their blood was analyzed, the mice euthanized, and the serum and organs harvested for further analysis.

3.5.3.1 Gene Transfer Through AAV

FGF21 was expressed with the help of AAV serotype 2/8. The AAV injection has been shown to induce liver-specific effects due to the LP1 promotor [47]. The control animals were treated with AAV2/8-LP1-GFP, which caused the liver-specific overexpression of green fluorescent protein (GFP). In order to determine the appropriate amount of necessary virus, a pilot study was performed in which three different virus titers were tested and the hepatic *Fgf21* mRNA expression (**Figure 9A**) as well as the serum levels of FGF21 (**Figure 9B**) were measured. For the subsequent main study, a titer of $0.2 \bullet 10^{11}$ genomic copies/µl was used.

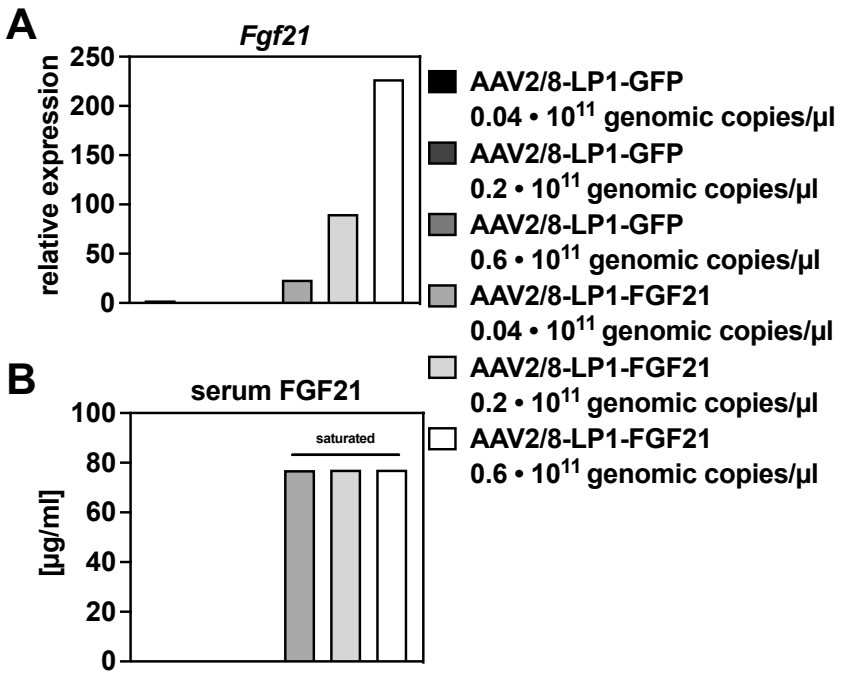

Figure 9: Pilot Study for Titer Testing. The mice were tail vein-injected with AAV2/8-LP1-GFP or AAV2/8-LP1-FGF21 at indicated concentrations. 24 days after injection, (A) the mRNA expression of *Fgf21* was analyzed by qPCR, (B) and the FGF21 serum levels were measured using ELISA. The data is presented as one bar per mouse (n=1,1,1,1,1,1).

3.5.3.2 Intravenous Application in the Tail Vein

The AAV was administered by means of a tail vein injection. For this purpose, the mouse was fixated in a restrainer and the tail was submerged in a water bath heated to 42 °C for 30 seconds to ensure dilation and visibility of the vein. The AAV was diluted in 0.9% saline to a total volume of 250 µl, and was then injected into the prepared tail vein. Gentle pressure was applied on the vein to prevent blood or the AAV solution from leaking. The mice were checked each day for irregularities.

3.5.3.3 Blood Collection from the Submandibular Vein

Blood was withdrawn from the submandibular vein for blood parameter analysis at indicated time points. The mouse was restrained by hand and the vein accessed. The puncture point was located at the back of the jaw. A lancet was used to puncture the vein until blood flowed and could be collected. Then, gentle pressure with a gauze was used to stop the bleeding. The mice were checked the next day for irregularities.

3.5.3.4 Body Weight

The mice were weighed weekly and on the day of euthanization using a scale with an accuracy of 0.1 g. The daytime measurements were conducted was always the same.

3.5.3.5 Food Intake

The mice were put in individual cages for 24 h. The amounts of food at the beginning and the end were determined by weighing them on a scale with an accuracy of 0.1 g and the difference was calculated.

3.5.3.6 Organ and Tissue Weight

The organs and tissues were weighed immediately after harvesting on the day of euthanization on a pre-tared aluminum foil in which they were wrapped, quickly frozen in liquid nitrogen, and stored long-term at -80 °C. An analytical balance with an accuracy of 0.1 mg was used.

3.5.3.7 Fluorescence Microscopy

A thin piece of the right liver lobe was cut after organ harvesting and weight determination. It was placed on a slide, set up under a suitable microscope, and an image was captured.

3.5.3.8 Blood Glucose

The blood glucose was measured on the indicated days throughout the experiment as well as on the day of euthanization. Blood was collected by carefully scratching the tail with a scalpel and immediately applying the blood to a glucose test strip to measure the glucose concentration in duplicates. If the deviation was higher than 10%, another measurement was necessary. The blood glucose concentration was always measured at the same time of day.

3.5.3.9 Blood Ketones

The blood ketones were measured on the indicated days during the experiment and on the day the animals were euthanized. The blood was collected by carefully scratching the tail with a scalpel. The collected blood was applied directly onto a ketone test strip to measure the ketone concentration. As was the case for the blood glucose concentration as well, the blood ketone concentration was always measured at the same time of day.

3.6 Statistical Analysis

The results have been expressed as mean values and, in the case of the cell culture experiments, the standard deviation (sd) was calculated. In the case of animal experiments, the standard error of the mean (sem) was determined. Each *in vitro* experiment was conducted at least three times and a representative result is shown. A student's t-test was used to test for significance between two groups of *in vitro* experiments, while an ordinary one-way analysis of variance (ANOVA) was performed to test for significance between more than two groups. For correction purposes after multiple testing using ordinary one-way ANOVA analysis, Dunnett's multiple comparison test was conducted. The student's t-test was used to test for significance in animal experiments. Based on previous experiences, a normal distribution was assumed.

4 Results

4.1 The Mechanism Behind the Regulation of RBP4 and TTR in Feeding and Fasting

The preliminary study has shown that RBP4 and TTR mRNA regulation, protein expression, and secretion are altered during fasting periods, as was described in **Chapter 1.5**. The following experiments aim to uncover the mechanism behind these findings and, therefore, focus on the PPARα signaling pathway, retinol metabolites, the glucagon signaling pathway, and the insulin signaling pathway.

4.1.1 The Regulation of RBP4 and TTR by the PPARα Signaling Pathway

The PPARα signaling pathway is induced during fasting [202]. The objective was to test whether PPARα activation could promote changes in the *Rbp4* and *Ttr* mRNA levels like those observed in times of fasting. For this reason, the PPARα agonist WY 14643 (WY) was used to stimulate the isolated primary murine hepatocytes.

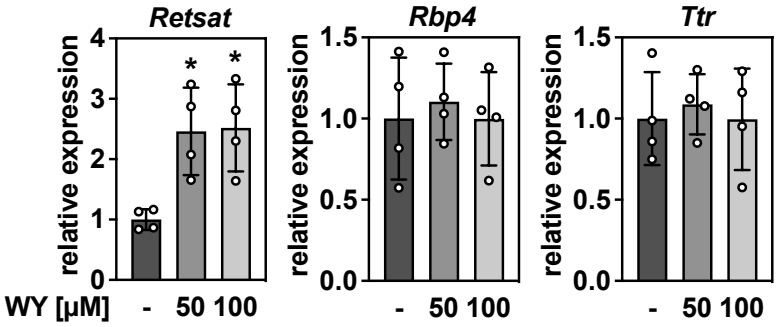

Figure 10: *Rbp4* and *Ttr* Gene Regulation Is Not Altered by PPARα Activation. Primary murine hepatocytes were isolated and then incubated with WY at the indicated concentrations for 21 h under serum-free conditions in DMEM without glucose and supplemented with 2 mM pyruvate and 20 mM lactate. The mRNA expression levels of *Retsat*, *Rbp4*, and *Ttr* were determined by qPCR. The data is presented as individual data points and mean ± sd (n=4,4,4) and **P*<0.05 is considered statistically significant when compared to control conditions that were not incubated with WY.

WY treatment increased the expression of retinol saturate (*Retsat*), a known PPARα target gene [203-205], validating this approach (**Figure 10**). Both *Rbp4* and *Ttr* mRNA levels were not influenced by the stimulation with WY (**Figure 10**).

4.1.2 The Regulation of RBP4 and TTR by Metabolites of Retinoid Homeostasis

A vitamin A deficient diet [206] and fasting [207] were shown to reduce hepatic retinoic acid levels. Retinoic acid is generated from retinol within the retinoid metabolism by enzymatic actions [17]. In the next step, the question whether alterations in the availability of participants of retinoid homeostasis could induce a regulation of *Rbp4* and *Ttr* on mRNA level was investigated. For this reason, primary murine hepatocytes were exposed to either retinoic acid or retinol.

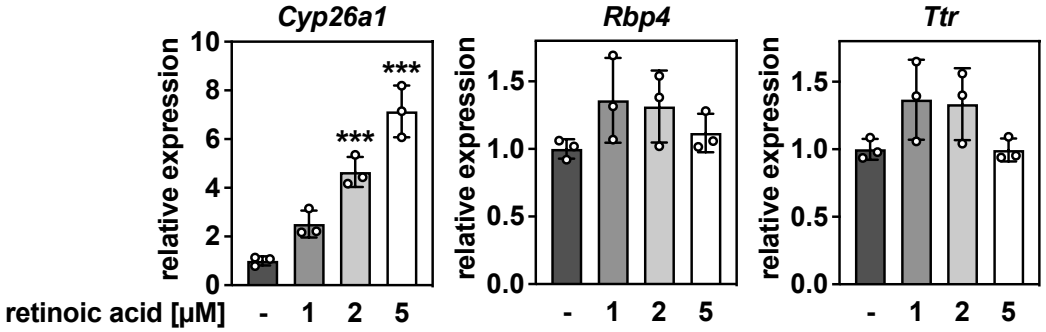

Figure 11: *Rbp4* and *Ttr* Gene Regulation Is Not Altered by Increased Retinoic Acid Availability. Primary murine hepatocytes were isolated and then incubated with retinoic acid at the indicated concentrations for 21 h under serum-free conditions in DMEM without glucose and supplemented with 2 mM pyruvate, 20 mM lactate, and 0.1% BSA. The mRNA expression levels of *Cyp26a1*, *Rbp4*, and *Ttr* were determined by qPCR. The data is presented as individual data points and mean ± sd (n=3,3,3,3) and ****P*<0.001 is considered statistically significant when compared to control conditions that were not incubated with retinoic acid.

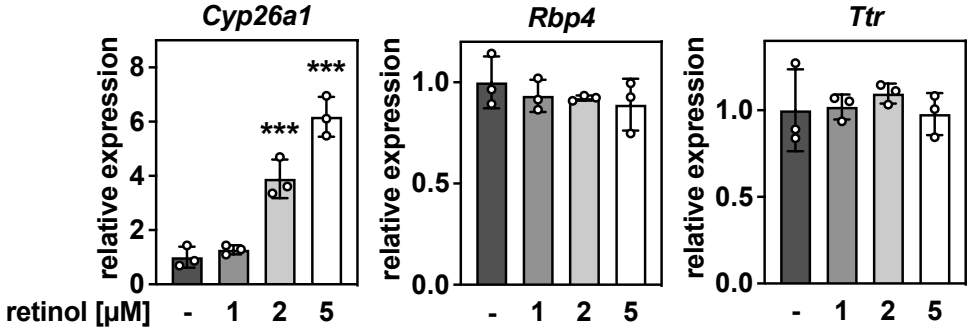

Figure 12: *Rbp4* and *Ttr* Gene Regulation Is Not Altered by Increased Retinol Availability. Primary murine hepatocytes were isolated and then incubated with retinol at the indicated concentrations for 21 h under serum-free conditions in DMEM without glucose and supplemented with 2 mM pyruvate, 20 mM lactate, and 0.1% BSA. The mRNA expression levels of *Cyp26a1*, *Rbp4*, and *Ttr* were determined by qPCR. The data is presented as individual data points and mean ± sd (n=3,3,3,3) and ****P*<0.001 is considered statistically significant when compared to control conditions that were not incubated with retinol.

In order to confirm that retinoic acid was in fact transported into the cells and, therefore, was able to mediate its effects, cytochrome P450 26A1 (*Cyp26a1*) was used as a control gene. Its mRNA expression is upregulated by retinol [208] and retinoic acid [209]. Retinoic acid treatment upregulated the mRNA expression of this control gene in a dose-dependent manner (**Figure 11**). Neither the *Rbp4*, nor the *Ttr* mRNA expression levels were altered by retinoic acid stimulation (**Figure 11**).

The stimulation with retinol, which was shown to be successful as indicated by a dose-dependent upregulation of the target gene *Cyp26a1*, also did not promote changes in the mRNA expression levels of *Rbp4* and *Ttr* in hepatocytes (**Figure 12**).

4.1.3 The Regulation of RBP4 and TTR by the Glucagon Signaling Pathway

Glucagon and the downstream second messenger cAMP are major regulators of homeostasis in feeding and fasting, as explained in **Chapter 1.2.2**, and are hypothesized to additionally regulate hepatic RBP4 and TTR expression and secretion.

In the first step, the influence of the second messenger cAMP, a downstream molecule of glucagon, was tested in the form of the synthetic and more stable 8-Br-cAMP. Therefore, primary murine hepatocytes were exposed to increasing doses of this molecule. The mRNA expression levels of phosphoenolpyruvate carboxykinase 1 (*Pck1*), which was used as a control gene since it is known to be upregulated by glucagon and cAMP signaling [210], responded in a dose-dependent manner with significant changes compared to the control samples (**Figure 13A**). The 8-Br-cAMP treatment led to increasing mRNA expression levels of *Rbp4*, with a significant approximately 1.9-fold change when subject to the highest 8-Br-cAMP dose compared to the control (**Figure 13A**). The *Ttr* mRNA expression levels increased significantly in all groups that were incubated with 8-Br-cAMP compared to the control group (**Figure 13A**).

The immunoblot analysis did not show a significant change in the protein levels of RBP4 in the hepatocyte lysates, but still displayed a trend of elevated protein levels after 8-Br-cAMP treatment (**Figure 13B**). The TTR levels in this immunoblot analysis increased significantly for the two highest 8-Br-cAMP doses used (**Figure 13B**). Both proteins were secreted into the supernatant dose-dependently to a significant lower extent when exposed to 8-Br-cAMP (**Figure 13C**). This effect was even stronger for the secretion of RBP4, in which case the highest 8-Br-cAMP dose led to a reduction of secretion by 96%. In case of TTR, the reduction equaled 86%.

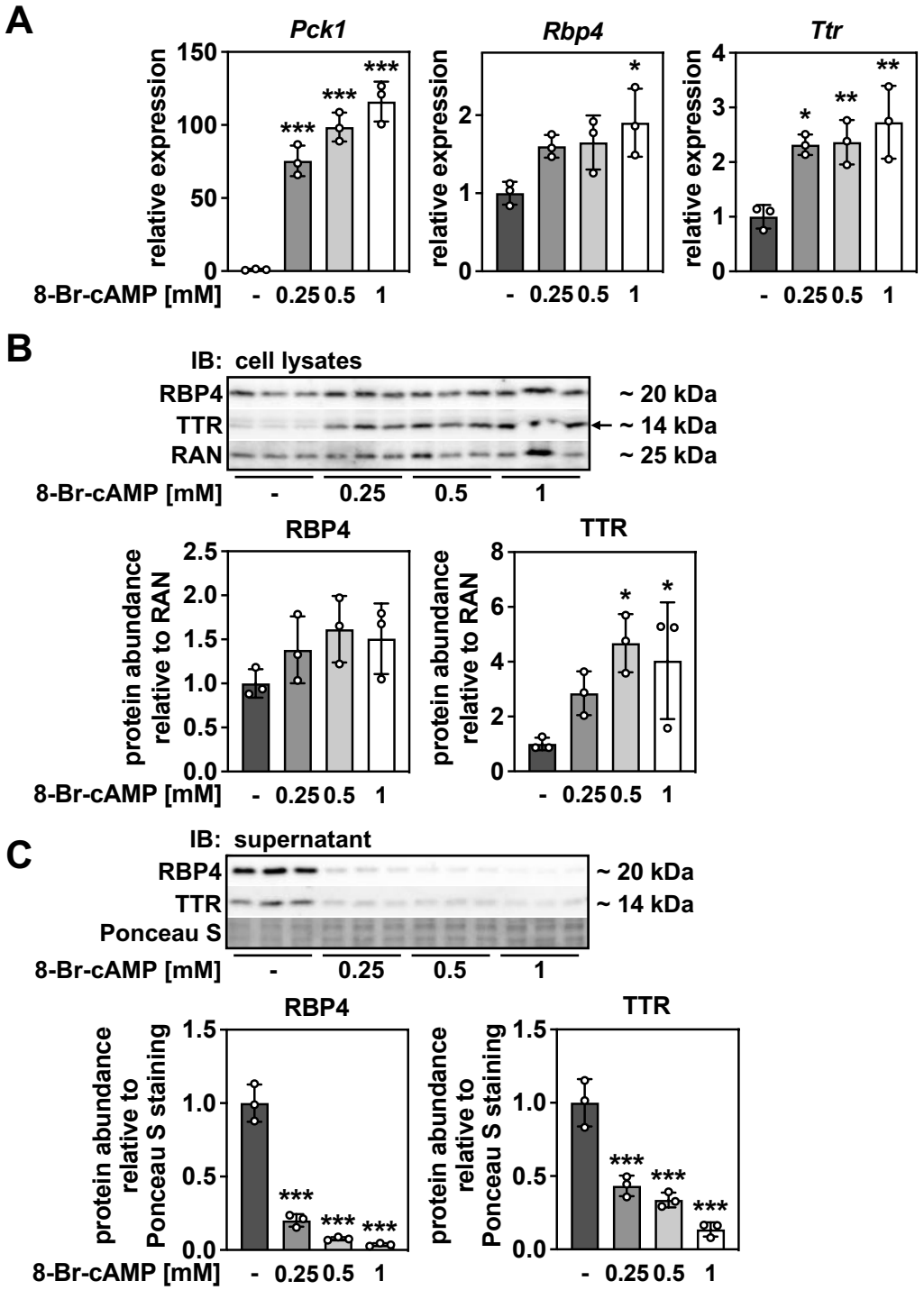

Figure 13: *Rbp4* and *Ttr* Gene Expression Is Upregulated and the Secretion Inhibited by 8-Br-cAMP Treatment. Primary murine hepatocytes were isolated and then incubated with 8-Br-cAMP at the indicated concentrations for 21 h under serum-free conditions in DMEM without glucose and supplemented with 2 mM pyruvate and 20 mM lactate. (A) The mRNA expression levels of *Pck1*, *Rbp4*, and *Ttr* were determined by qPCR. (B) Cell lysates were analyzed by immunoblotting for the protein expression of RBP4 and TTR and a densitometric analysis was performed using image processing software. (C) Supernatants were analyzed by immunoblotting for the protein expression of RBP4 and TTR and a densitometric analysis was performed using image processing software. The data is presented as individual data points and mean ± sd (n=3,3,3,3) and **P*<0.05, ***P*<0.01, and ****P*<0.001 are considered statistically significant when compared to control conditions that were not incubated with 8-Br-cAMP.

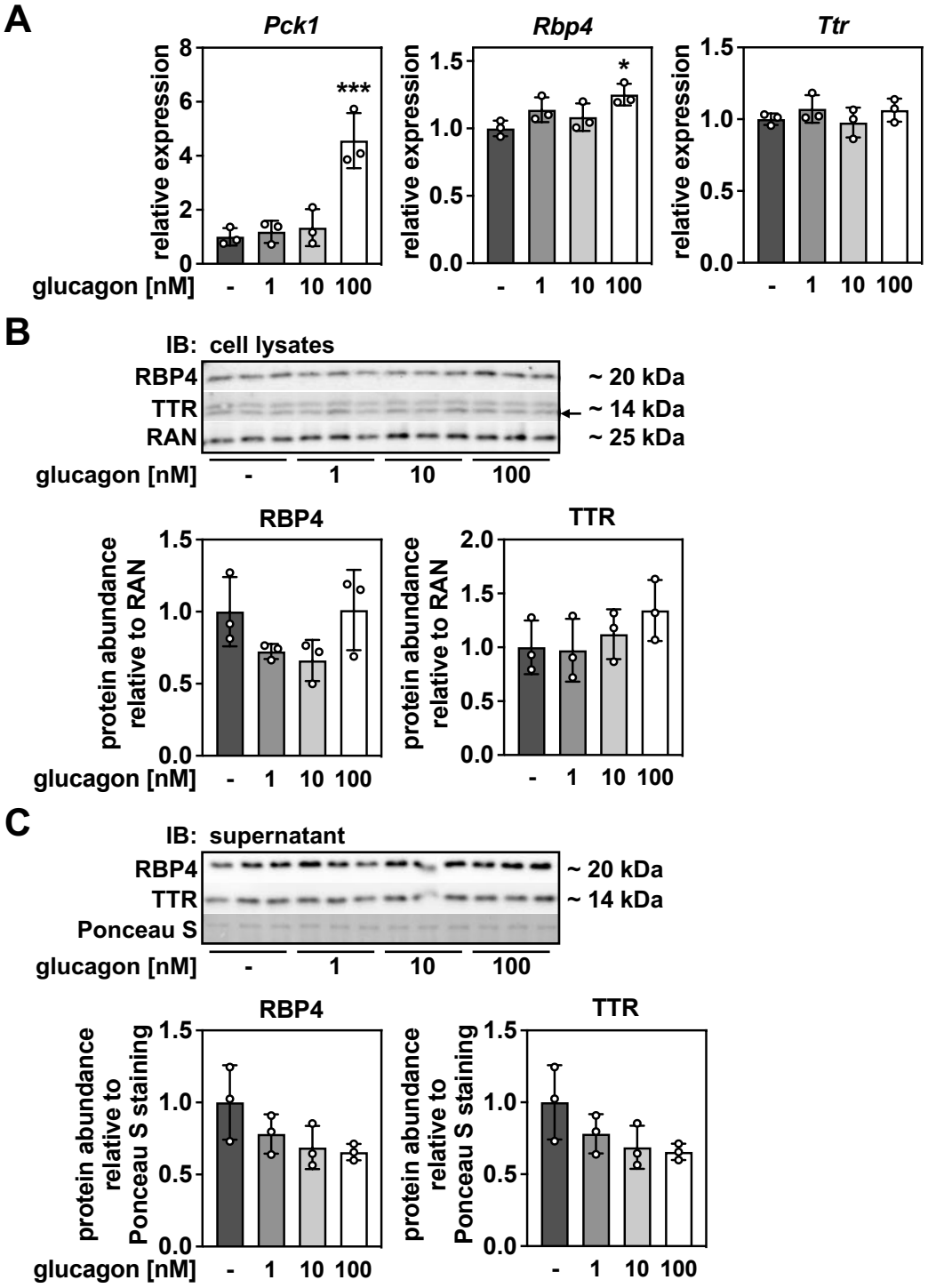

Figure 14: ***Rbp4 Gene Expression Is Upregulated by Glucagon Stimulation.*** Primary murine hepatocytes were isolated and then incubated with glucagon at the indicated concentrations for 21 h under serum-free conditions in DMEM without glucose and supplemented with 2 mM pyruvate and 20 mM lactate. (A) The mRNA expression levels of *Pck1, Rbp4,* and *Ttr* were determined by qPCR. (B) Cell lysates were analyzed by immunoblotting for protein expression of RBP4 and TTR and a densitometric analysis was performed using image processing software. (C) Supernatants were analyzed by immunoblotting for protein expression of RBP4 and TTR and a densitometric analysis was performed using image processing software. The data is presented as individual data points and mean ± sd (n=3,3,3,3) and **P*<0.05 and ****P*<0.001 are considered statistically significant when compared to control conditions that were not incubated with glucagon.

In order to test the effects of glucagon, the primary murine hepatocytes were exposed to increasing concentrations of glucagon. The control gene *Pck1* showed a dose-dependent increase in its mRNA expression level, and significant changes were detected for incubation with 100 nM glucagon (**Figure 14A**). Moreover, the *Rbp4* mRNA expression level increased approximately 1.25-fold in this group, while the *Ttr* mRNA expression level remained unchanged (**Figure 14A**). The hepatic protein expression showed no significant change for both RBP4 and TTR expression levels (**Figure 14B**). The secretion of RBP4 and TTR did not change significantly, but a dose-dependent trend was observed for both proteins, showing that both seem to have been secreted into the supernatant to a lesser extent compared to the control samples (**Figure 14C**).

4.1.4 The Regulation of RBP4 and TTR by the Insulin Signaling Pathway

Another regulator of the feeding-fasting homeostasis is insulin, which is known to be the counterpart of the aforementioned glucagon, as described in **Chapter 1.2.1**. Therefore, the next step was to investigate the role of insulin in RBP4 and TTR regulation during the states of feeding and fasting in primary murine hepatocytes.

The ‘insulin-like growth factor binding protein 1’ (*Igfbp1*) gene, which is a target gene of FOXO1 and can be inhibited by insulin [211], was used as a control gene. It displayed a dose-dependent, significant decrease of its mRNA expression level when stimulated with insulin (**Figure 15A**). The mRNA expression of *Rbp4* did not change significantly, although the mRNA levels displayed a visible decreasing trend (**Figure 15A**). The mRNA levels of *Ttr* were decreasing significantly and in a dose-dependent manner (**Figure 15A**).

The analysis of the protein levels in the cell lysates showed that the RBP4 levels were significantly decreased and that this effect was dependent on the insulin dose the primary murine hepatocytes were exposed to (**Figure 15B**). In the following analysis the secretion of both RBP4 and TTR into the supernatant was investigated. The secretion of RBP4 did not show significant changes, although the standard deviation was high and a trend of increased secretion after insulin treatment was observed (**Figure 15C**). The secretion of TTR was unaltered in comparison to the control samples (**Figure 15C**).

In a next step, the effects of FOXO1 on the *Rbp4* and *Ttr* mRNA expression levels were tested. For this purpose, primary murine hepatocytes were depleted of the FOXO1 protein by siRNA (**Figure 16A**). This reduced the *Foxo1* mRNA levels by 85%, and also decreased those of the FOXO1 target gene *Igfbp1*, which was used as a control gene (**Figure 16B**). The depletion of FOXO1 diminished the mRNA expression level of *Rbp4*, which was reduced by about 45%, while the *Ttr* mRNA expression level remained unaltered (**Figure 16B**).

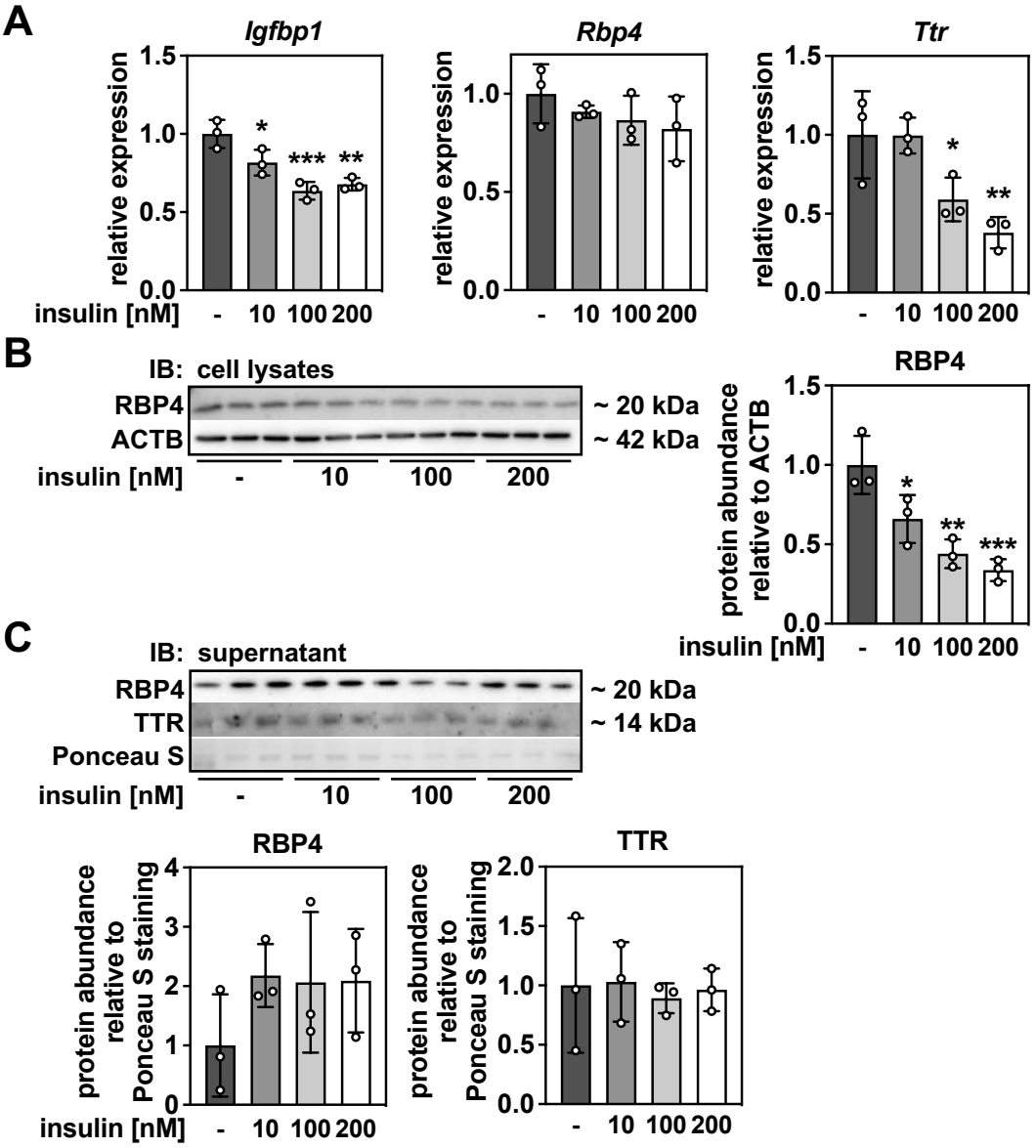

Figure 15: *Rbp4* and *Ttr* Gene Expression Is Suppressed by Insulin Stimulation and the Hepatic RBP4 Protein Levels Are Reduced. Primary murine hepatocytes were isolated, and then incubated overnight under serum-free conditions in DMEM with 25 mM glucose. The next morning, the medium was changed and the primary hepatocytes were incubated for another 24 h in DMEM with 25 mM glucose supplemented with 10% FBS and 1% PS. Thereafter, the primary murine hepatocytes were incubated with insulin at the indicated concentrations for 24 h under serum-free conditions in DMEM with 25 mM glucose. (A) The mRNA expression levels of *Igfbp1, Rbp4,* and *Ttr* were determined by qPCR. (B) Cell lysates were analyzed by immunoblotting for protein expression of RBP4 and a densitometric analysis was performed using image processing software. (C) Supernatants were analyzed by immunoblotting for protein expression of RBP4 and TTR and a densitometric analysis was performed using image processing software. The data is presented as individual data points and mean ± sd (n=3,3,3,3) and **P*<0.05, ***P*<0.01, and ****P*<0.001 are considered statistically significant when compared to control conditions that were not incubated with insulin.

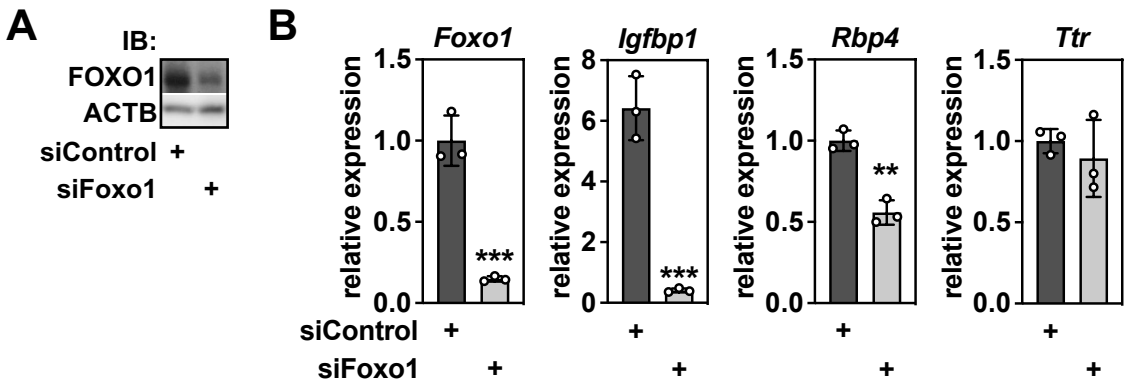

Figure 16: *Rbp4* Gene Expression Is Regulated by FOXO1 Signaling Pathway. Primary murine hepatocytes were isolated and then incubated overnight under serum-free conditions in DMEM with 25 mM glucose with 1 nmol siRNA. The next morning, the medium was changed and the primary hepatocytes were incubated for 72 h in DMEM with 25 mM glucose supplemented with 10% FBS and 1% PS. (A) Cell lysates were analyzed by immunoblotting for protein expression of FOXO1. (B) The mRNA expression levels of *Foxo1, Igfbp1, Rbp4*, and *Ttr* were determined by qPCR. The data is presented as individual data points and mean ± sd (n=3,3) and $^{**}P<0.01$ and $^{***}P<0.001$ are considered statistically significant when compared to control conditions that were incubated with control siRNA.

4.2 The Homeostasis of apo-RBP4 and holo-RBP4 in Feeding and Fasting

Although the total protein levels of RBP4 in the bloodstream of fasted mice appeared to be unaltered compared to fed mice in the preliminary study, the performed measurement of the total RBP4 by western blot does not provide information on the retinol loading in this state. This study aims to determine the apo-RBP4 and holo-RBP4 levels, and detect changes during the feeding-fasting transition as part of the suggested transport mechanisms leading to a replenishment of hepatic retinoid stores.

4.2.1 The apo-RBP4 Levels Are Increased in the Serum of Fasted Mice

The mice were either fed *ad libitum* or fasted for 24 h, and their serum was analyzed for proteins related to retinol transport. The levels of total RBP4 in the serum remained stable in the feeding-fasting transition, while the levels of TTR were reduced in the fasted state by about 60% (**Figure 17A**).

In a control experiment, the extraction of retinol from its carrier RBP4 with hexane led to reduced holo-RBP4 levels and increased apo-RBP4 levels depending on the number of extractions performed (**Figure 17B**). This proves that this non-denaturing immunoblot can show both forms of RBP4.

The protein levels of apo-RBP4 in fed and fasted mice were detected using this method, and revealed a significant increase of the apo-RBP4 levels in the serum of fasted mice. About 8% of the total RBP4 appeared in the apo form in fasted mice, while this was only about 1% of the total protein in the fed state (**Figure 17B**).

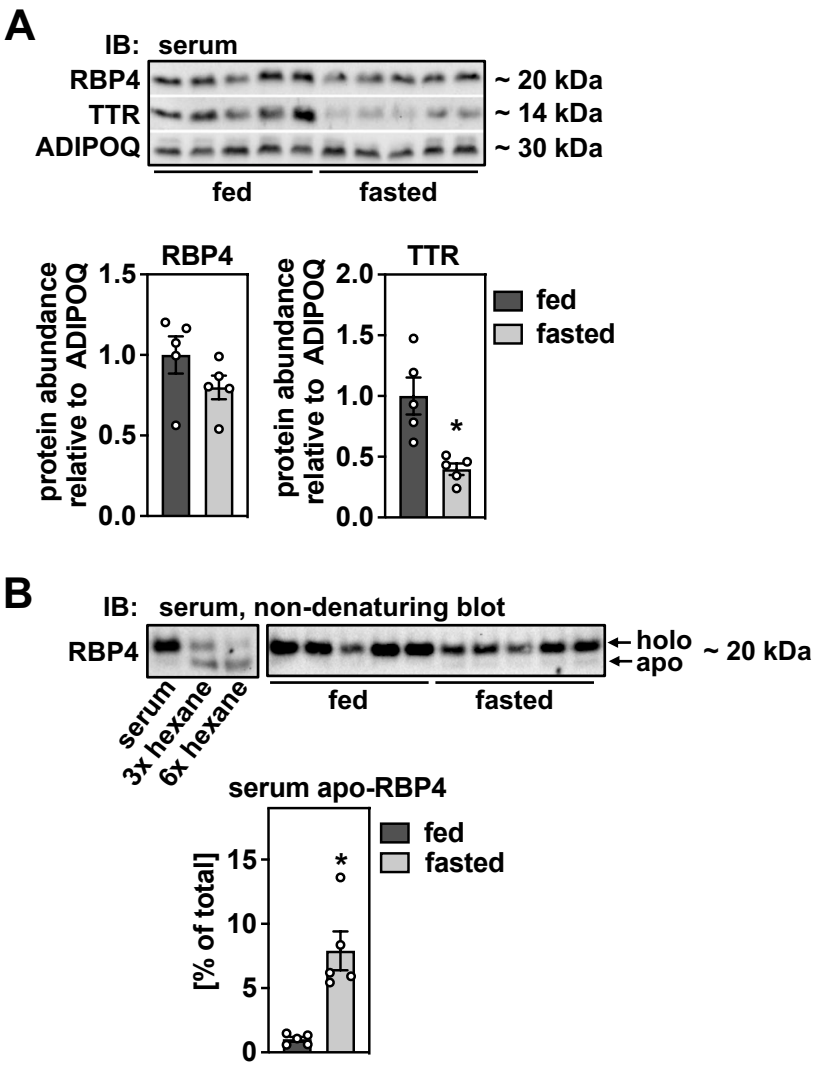

Figure 17: Total Serum RBP4 Levels Remain Unaltered, apo-RBP4 Levels Increase, and TTR Levels Decrease during Fasting. The mice were fed *ad libitum* or fasted for 24 h. (A) The serum was analyzed by immunoblotting for protein expression of RBP4 and TTR and a densitometric analysis was performed using image processing software. (B) The serum was analyzed by non-denaturing immunoblotting for protein expression of holo-RBP4 and apo-RBP4. Control samples were obtained by extracting serum with hexane three or six times as indicated. The densitometric analysis of holo-RBP4 and apo-RBP4 was performed using image processing software. The data is presented as individual data points and mean ± sem (n=5,5) and **P*<0.05 is considered statistically significant when compared to fasted mice.

4.2.2 The Immunoprecipitation of RBP4 from the Serum of Fed and Fasted Mice Leads to Lower Retinol Levels in Serum

In order to remove RBP4 from murine serum, an immunoprecipitation assay was established and used to analyze the serum of fed and fasted mice.

The amount of RBP4 antibody as well as the amount of sepharose beads needed to remove the maximum amount of RBP4 from the serum was determined. A total of 62.5 µg of RBP4 antibody (**Figure 18A**) and 75 µl of a slurry consisting of 50% sepharose beads (**Figure 18B**) per 50 µl serum led to the best results.

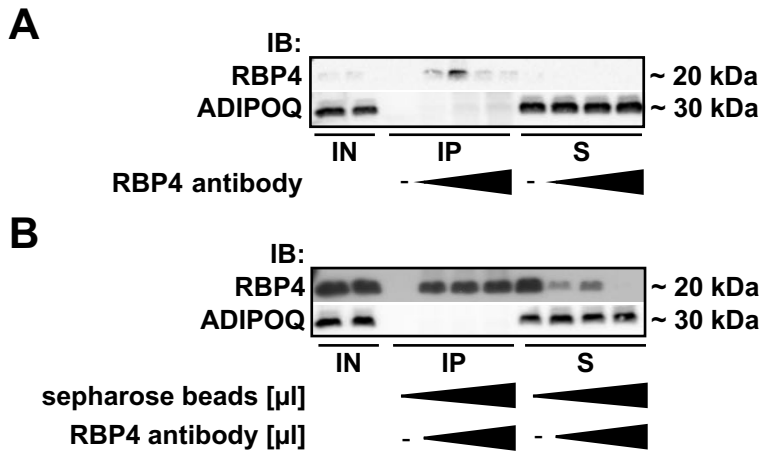

Figure 18: RBP4 Immunoprecipitation Decreases RBP4 in Supernatant and Enriches RBP4 in Precipitate Dependent on Antibody and Sepharose Dose. The serum of mice was collected and immunoprecipitation conducted. (A) Serum was precipitated using 0 to 41 µg of antibody per 50 µl of serum. The input (IN), immunoprecipitate (IP), and supernatant (S) were analyzed by immunoblotting for protein expression of RBP4 and ADIPOQ. (B) The serum was precipitated using 0 to 61.5 µg of antibody and 0 to 75 µl of a slurry (consisting of 50% beads) per 50 µl serum. Input (IN), immunoprecipitate (IP), and supernatant (S) were analyzed by immunoblotting for protein expression of RBP4 and ADIPOQ. The data is presented as individual samples.

Once this had been completed, an analysis regarding whether retinol could be measured in the supernatant and in the precipitate after conducting the immunoprecipitation was carried out. The RBP4 levels in the supernatant had reduced by about 90% compared to the RBP4 levels in the input (**Figure 19A**). The quantification of the retinol content in the supernatant and the precipitate demonstrates that the retinol levels were reduced by more than 75% in the supernatant. Moreover, the remaining retinol was found in the fraction of the sepharose beads. When added, the retinol in both fractions equals 100% of the retinol found in the input (**Figure 19B**).

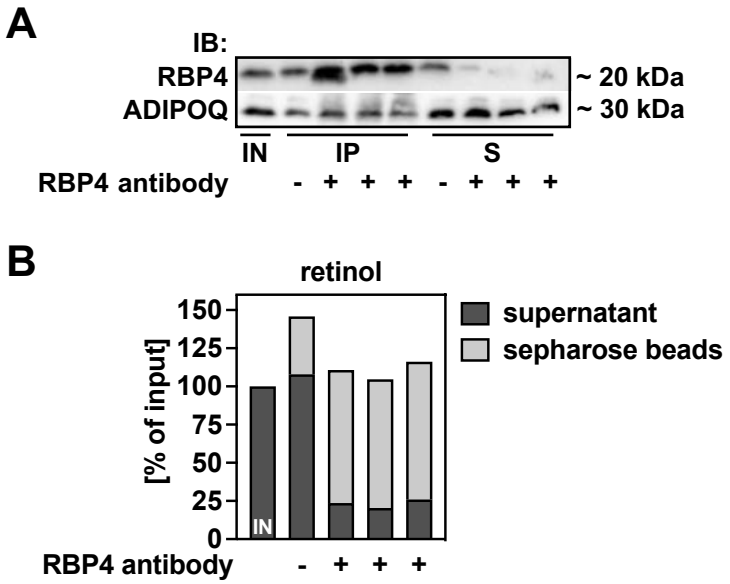

Figure 19: RBP4 Immunoprecipitation Decreases RBP4 and Retinol in Supernatant and Enriches RBP4 and Retinol in Precipitate. The serum of mice was collected and immunoprecipitation conducted using 62.5 µg of RBP4 antibody and 75 µl of a slurry (consisting of 50% beads) per 50 µl serum. (A) Input (IN), immunoprecipitate (IP), and supernatant (S) were analyzed by immunoblotting for protein expression of RBP4 and ADIPOQ. (B) The retinol content was determined by HPLC measurement. The data is presented as individual samples.

The precipitation of RBP4, and with that of the bound retinol, was thought to result from a specific reaction of the RBP4 antibody and not from unspecific binding. In an attempt to verify this, whether immunoprecipitation with other antibodies would result in similar effects on RBP4 and retinol was tested next. For this purpose, the experiment was not only performed with the RBP4 antibody, but also with antibodies against TTR, GATA-binding factor 2 (GATA2), and CCAAT-enhancer-binding protein α (C/EBPα). The same concentration was used for all four antibodies per 50 µl serum. The quantification of the RBP4 levels in the supernatant after immunoprecipitation with the RBP4-specific antibody and the analysis of retinol content in the supernatant after the immunoprecipitation confirmed the results shown in **Figures 18** and **19**. Both displayed significant reductions: RBP4 by approximately 95% (**Figure 20A**), and retinol by about 85% (**Figure 20B**). Moreover, the RBP4 (**Figure 20A**) and retinol (**Figure 20B**) quantification in those samples that were immunoprecipitated with any of the other three tested antibodies did not show this reduction. The levels in the supernatant for RBP4 and retinol were still at 100% compared to the input.

These preliminary experiments confirmed that this method reduced the serum RBP4 content alongside with the retinol content in the serum. The reduction of the serum retinol was shown to lead to a complementary increase of retinol in the sepharose beads fraction. Additionally, these effects were found to have been specifically caused by the use of an antibody against RBP4. For this reason, the method of RBP4 immunoprecipitation was shown to be a reliable

method for analyzing the concentration of non-RBP4-bound retinol in the serum of fed or fasted mice.

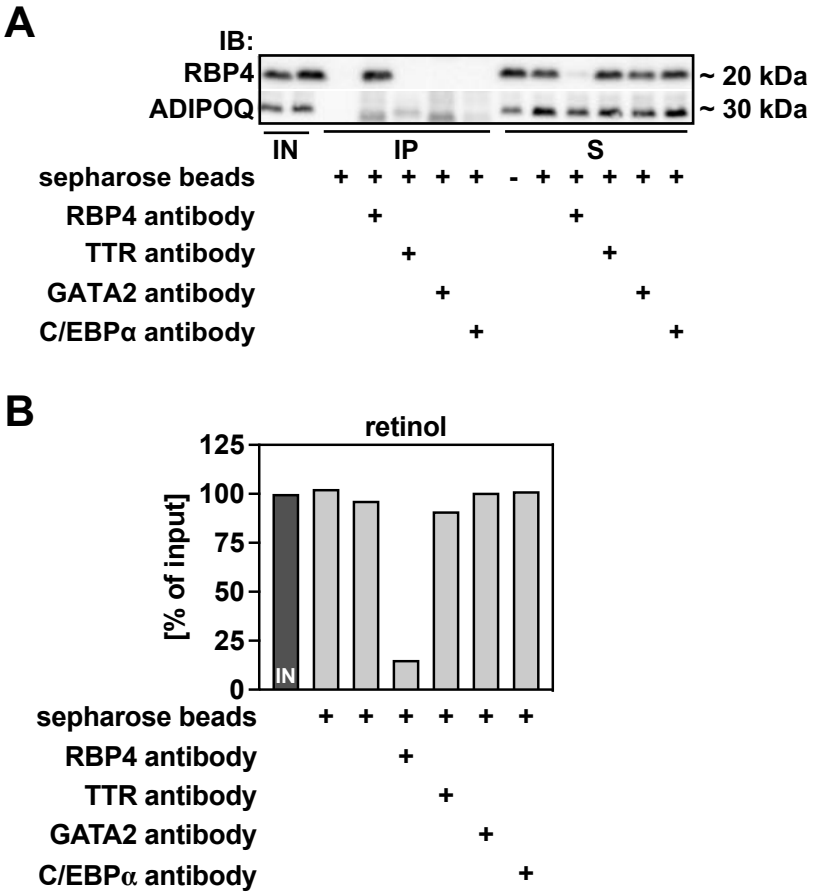

Figure 20: RBP4 Immunoprecipitation Success Is Solely Guaranteed by Use of RBP4-Specific Antibody. The serum of mice was collected and immunoprecipitation conducted using 62.5 µg of indicated antibody and 75 µl of a slurry (consisting of 50% beads) per 50 µl serum. (A) Input (IN), immunoprecipitate (IP), and supernatant (S) were analyzed by immunoblotting for protein expression of RBP4 and ADIPOQ. (B) Retinol content in supernatant was determined by HPLC measurement. The data is presented as individual samples.

The RBP4 serum levels in the then performed experiment did not differ for fed and fasted animals, as shown exemplarily in **Figure 21A**, since the input levels of RBP4 remained unaltered. This figure also shows that there was not a significant discrepancy regarding the amount of RBP4 precipitated from the serum of both groups, resulting in a mean RBP4 reduction of 88%. The RBP4 immunoprecipitation did not remove TTR from the supernatant, as seen in the IP samples on the immunoblot (**Figure 21A**). The analysis of the retinol concentrations in the serum before immunoprecipitation showed no significant change from fed to fasted animals (**Figure 21B**), while the retinol content in the supernatant was significantly lower in the fasted mice after the immunoprecipitation of RBP4 from the serum (**Figure 21C**).

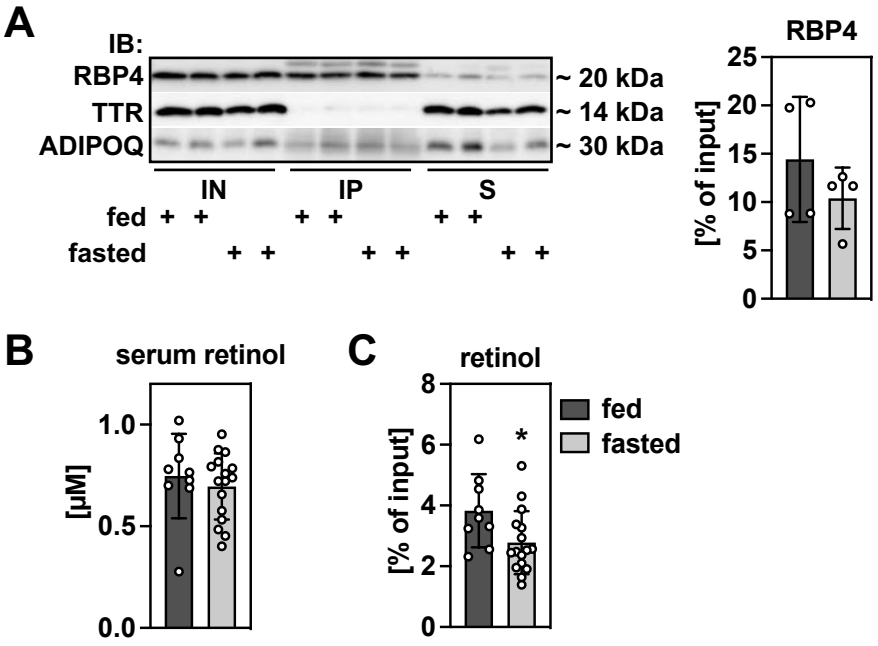

Figure 21: Fasting Results in Lower Retinol Levels in the Supernatant after RBP4 Immunoprecipitation. The mice were fed *ad libitum* or fasted for 24 h, the serum collected, and an immunoprecipitation with 62.5 µg of RBP4 antibody and 75 µl of a slurry (consisting of 50% beads) per 50 µl serum conducted. (A) Input (IN), immunoprecipitate (IP), and supernatant (S) were analyzed by immunoblotting for protein expression of RBP4, TTR, and ADIPOQ. (B) Retinol content was determined in serum before immunoprecipitation and (C) in supernatant after immunoprecipitation by HPLC measurement. For (A) exemplary sera are presented. For densitometric analysis, exemplary immunoblot densitometry data is presented as individual data points and mean ± sem. For (B) and (C) the data is presented as individual data points and mean ± sem (n=9,16) and **P*<0.05 is considered statistically significant when compared to fed mice.

4.3 Hepatic FGF21 Overexpression in a Murine *in vivo* Model

An *in vivo* model with a liver-specific overexpression of FGF21 was established and analyzed in order to investigate whether FGF21 is secreted by the liver to promote a crosstalk between the liver and adipose tissue, thus, inducing a reverse transport of retinoids from white adipose tissue to the liver. AAV2/8-LP1-FGF21 was used to achieve the liver-specific overexpression of FGF21 in mice. The mice in the control group were injected with AAV2/8-LP1-GFP.

4.3.1 The Efficiency of the Liver-Specific Overexpression of FGF21

Liver-directed gene transfer via AAV provides a stable expression of the episomal transgene [212]. A microscopic analysis confirmed the presence of GFP in the hepatocytes and with that the successful use of AAV2/8-LP1-GFP (**Figure 22A**). Since GFP was present in the hepatocytes, a green fluorescent light was emitted that is not normally expressed in

mammalian cells. In contrast, the injection of AAV2/8-LP1-FGF21 did not result in any fluorescent signal (**Figure 22A**). The efficiency of *Fgf21* overexpression (AAV2/8-LP1-FGF21) was assessed by means of an mRNA analysis that showed a 200-fold increase in the expression level compared to the control group (AAV2/8-LP1-GFP) (**Figure 22B**). The serum concentration of FGF21 had also increased more than 200-fold and exceeded the linear range of the used ELISA, even after dilution (**Figure 22C**).

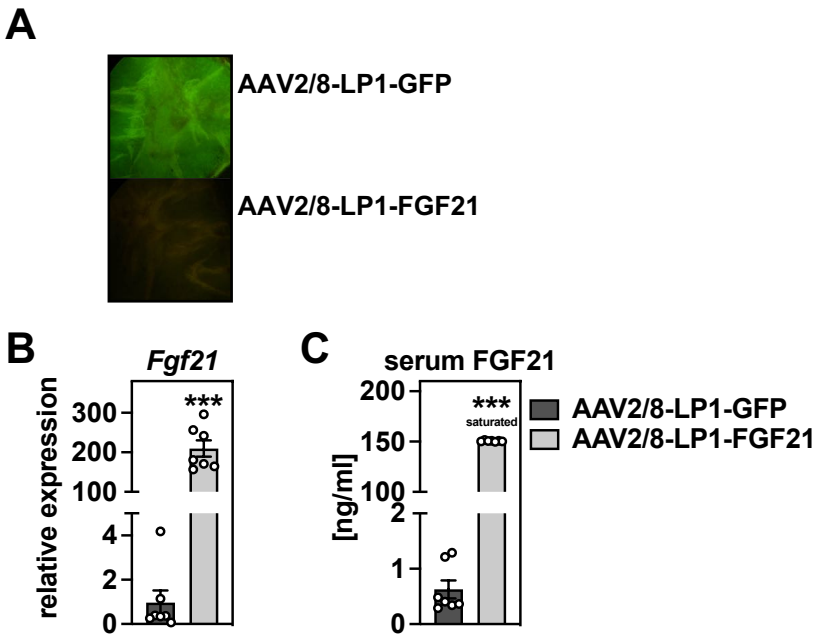

Figure 22: Liver-Specific AAV2/8-LP1-FGF21 Expression Increases Hepatic *Fgf21* mRNA Levels and FGF21 Secretion. The mice were tail vein-injected with AAV2/8-LP1-GFP or AAV2/8-LP1-FGF21. Then, 24 days after injection, (A) microscopic images of the fluorescent GFP signal in the liver were obtained. (B) The mRNA expression of *Fgf21* was analyzed using qPCR, (C) and the serum FGF21 levels were measured using an ELISA. The data is presented as individual data points and mean ± sem (n=7,7) and ****P*<0.001 is considered statistically significant when compared to mice with liver-specific GFP expression.

4.3.2 Body Weight Changes after AAV Injection

The body weights of the mice were measured weekly to analyze the metabolic effects of the FGF21 overexpression (**Figure 23A**). On the day of the injection, there was no significant difference between the control group that was injected with AAV2/8-LP1-GFP and the group that received AAV2/8-LP1-FGF21. Seven days after the injection, the body weight of the group overexpressing FGF21 (AAV2/8-LP1-FGF21) had significantly decreased compared to the GFP-overexpressing control group (AAV2/8-LP1-GFP). This difference became more prominent over the course of 24 days, since the GFP control mice (AAV2/8-LP1-GFP)

displayed a normal, age-related weight increase common in mice fed *ad libitum*. In comparison, the mice overexpressing FGF21 (AAV2/8-LP1-FGF21) constantly lost weight. This effect was not due to a change in their food intake as this was monitored for 24 hours and no difference was found (**Figure 23B**).

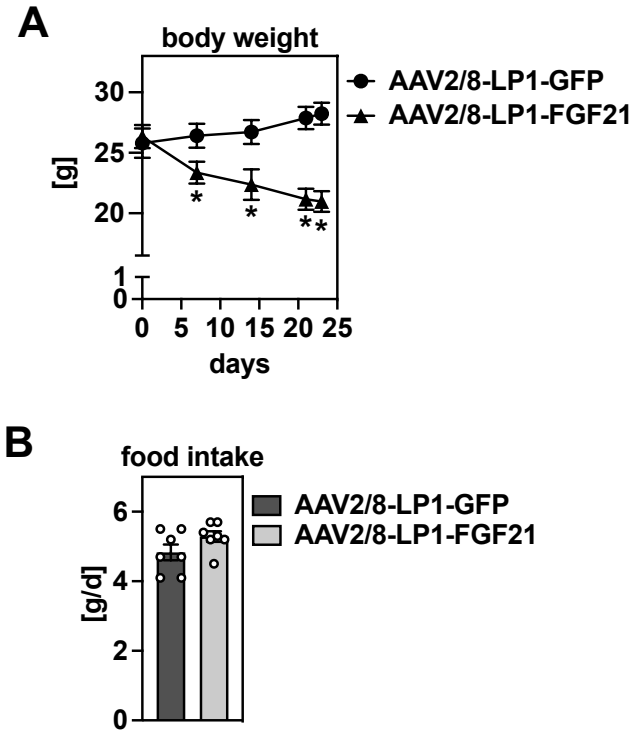

Figure 23: Liver-Specific AAV2/8-LP1-FGF21 Expression Decreases Body Weight. The mice were tail vein-injected with AAV2/8-LP1-GFP or AAV2/8-LP1-FGF21. (A) Their body weights were measured weekly. (B) On day 19 after injection, the mice were kept separate from one another and their food intake was measured for 24 h. The data is presented as mean ± sem (n=7,7) for (A), and individual data points and mean ± sem (n=7,7) for (B), and **P*<0.001 is considered statistically significant when compared to mice with liver-specific GFP expression.

4.3.3 The Changes in the Metabolic Blood and Serum Parameters Caused by FGF21 Overexpression

The blood and serum parameters of both groups were analyzed at the end of the experiment to further characterize the metabolic impact of FGF21 overexpression.

Since FGF21 is known influence glucose homeostasis, as described in **Chapter 1.3**, the blood glucose was measured in both groups after *ad libitum* feeding. It was found to have significantly reduced in the FGF21-overexpressing mice (AAV2/8-LP1-FGF21) in comparison to the GFP control group (AAV2/8-LP1-GFP) (**Figure 24A**).

Ketogenesis is induced during fasting to provide an alternative source of energy and it has been shown to be promoted by FGF21 [114]. For this reason, the ketone bodies in the blood were measured at the end of the experiment, but no significant difference was found (**Figure 24B**).

NEFAs were quantified in the serum of both groups to examine the influence of FGF21 overexpression on lipolysis, since previous studies have shown that FGF21 can cause NEFA levels to increase [114]. No significant difference in both groups was detected (**Figure 24C**). The serum concentration of the triglycerides was significantly reduced in previous studies [114, 130] and this was also the case here for the group that was injected with AAV2/8-LP1-FGF21 compared to the AAV2/8-LP1-GFP control (**Figure 24D**).

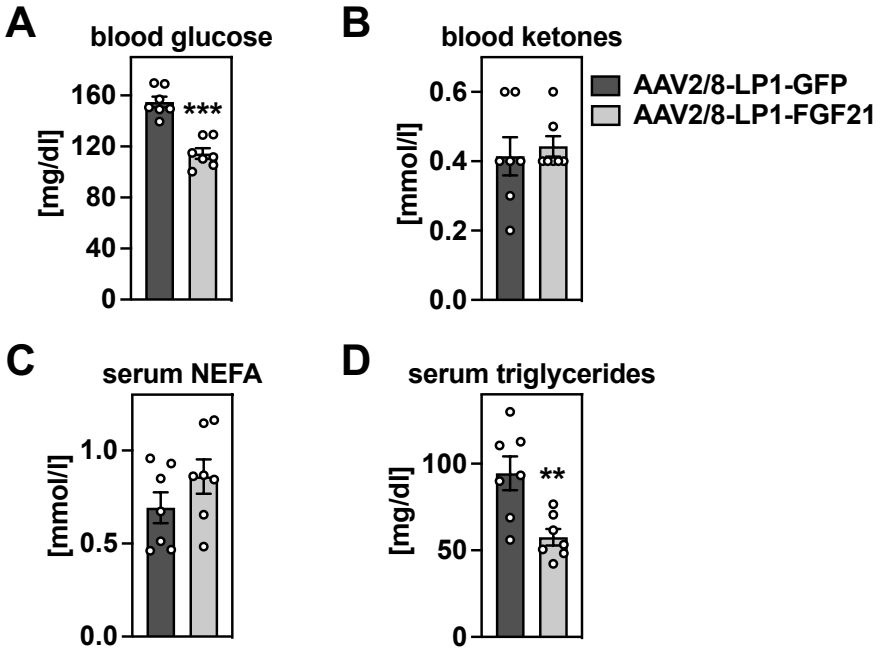

Figure 24: Liver-Specific AAV2/8-LP1-FGF21 Expression Alters Metabolic Blood and Serum Parameters. The mice were tail vein-injected with AAV2/8-LP1-GFP or AAV2/8-LP1-FGF21. Then, 24 days after injection, (A) the blood glucose levels, (B) blood ketone levels, (C) serum NEFA levels, (D) and serum triglyceride levels were determined. The data is presented as individual data points and mean ± sem (n=7,7) and $^{**}P<0.01$ and $^{***}P<0.001$ are considered statistically significant when compared to mice with liver-specific GFP expression.

4.3.4 The Effects of FGF21 Overexpression on Organ Weights

The body weight of mice injected with AAV2/8-LP1-FGF21 decreased drastically, as described in **Chapter 4.3.2**. Subsequently, an analysis was performed to see if the organ weights had reduced as well. The liver weight (**Figure 25A**) and eWAT weight (**Figure 26A**) were

significantly decreased in the FGF21-overexpressing mice (AAV2/8-LP1-FGF21) compared to the control animals (AAV2/8-LP1-GFP). This was also significant when the organ weight was normalized in relation to the total body weight of each individual mouse (**Figures 25B** and **26B**). scWAT did not display a significant change in organ weight (**Figure 27A**), but showed a non-significant trend towards increased fat mass in the FGF21-overexpressing mice (AAV2/8-LP1-FGF21) when normalized in relation to the total body weight (**Figure 27B**). The weight of BAT did not change significantly (**Figures 28A** and **28B**).

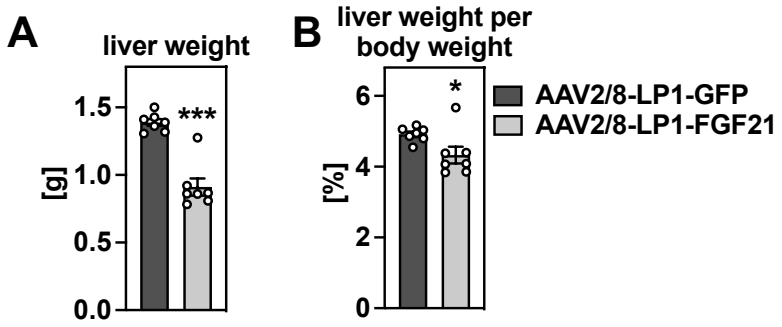

Figure 25: Liver-Specific AAV2/8-LP1-FGF21 Expression Reduces Liver Mass. The mice were tail vein-injected with AAV2/8-LP1-GFP or AAV2/8-LP1-FGF21. (A) Then, 24 days after injection, the organs were harvested and the liver weight determined. (B) Liver weights were normalized in relation to the individual body weight on day 24 after injection. The data is presented as individual data points and mean ± sem (n=7,7) and **P*<0.05 and ****P*<0.001 are considered statistically significant when compared to mice with liver-specific GFP expression.

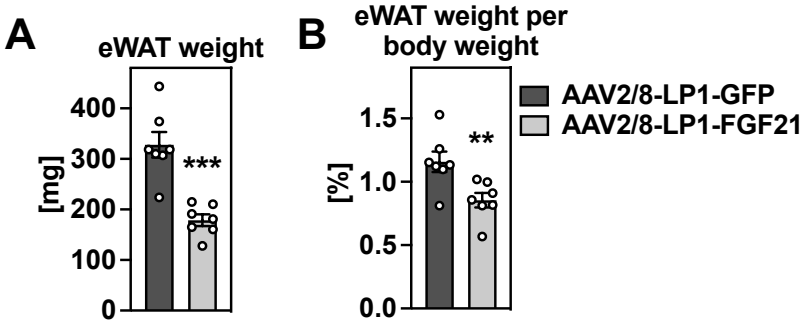

Figure 26: Liver-Specific AAV2/8-LP1-FGF21 Expression Reduces eWAT Mass. The mice were tail vein-injected with AAV2/8-LP1-GFP or AAV2/8-LP1-FGF21. (A) Then, 24 days after injection, the organs were harvested and eWAT weight determined. (B) eWAT weights were normalized in relation to the individual body weight on day 24 after injection. The data is presented as individual data points and mean ± sem (n=7,7) and ***P*<0.01 and ****P*<0.001 are considered statistically significant when compared to mice with liver-specific GFP expression.

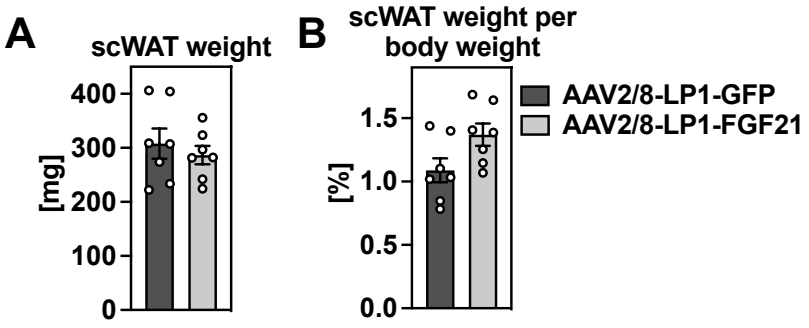

Figure 27: Liver-Specific AAV2/8-LP1-FGF21 Expression Does Not Alter scWAT Mass. The mice were tail vein-injected with AAV2/8-LP1-GFP or AAV2/8-LP1-FGF21. (A) Then, 24 days after injection, the organs were harvested and scWAT weight determined. (B) scWAT weights were normalized in relation to the individual body weight on day 24 after injection. The data is presented as individual data points and mean ± sem (n=7,7) and **P*<0.05 is considered statistically significant when compared to mice with liver-specific GFP expression.

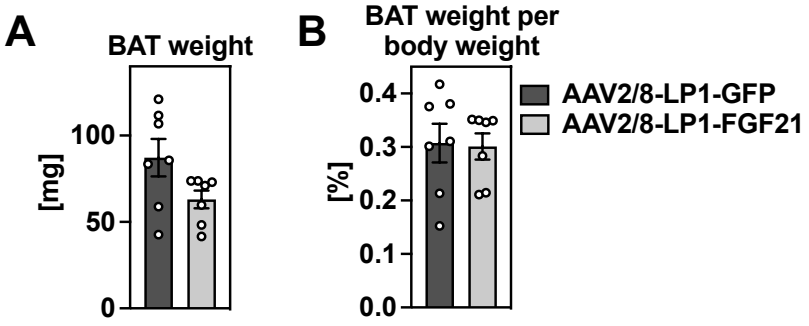

Figure 28: Liver-Specific AAV2/8-LP1-FGF21 Expression Does Not Alter BAT Mass. The mice were tail vein-injected with AAV2/8-LP1-GFP or AAV2/8-LP1-FGF21. (A) Then, 24 days after injection, the organs were harvested and BAT weight determined. (B) BAT weights were normalized in relation to the individual body weight on day 24 after injection. The data is presented as individual data points and mean ± sem (n=7,7) and **P*<0.05 is considered statistically significant when compared to mice with liver-specific GFP expression.

4.3.5 The Effects of FGF21 Overexpression on Retinoid Content in Serum, Liver, and Adipose Tissue

In order to determine whether FGF21 has an impact on retinoid homeostasis and can induce repartitioning of retinoids from adipose tissue to the liver, the next step was to analyze the retinoid levels in serum, liver, and white adipose tissue.

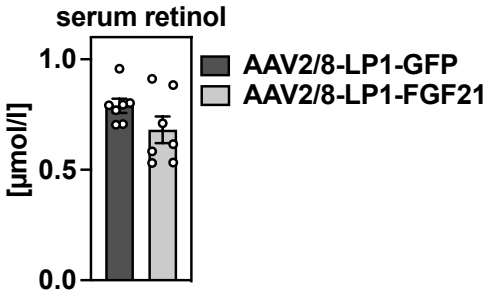

Figure 29: Liver-Specific AAV2/8-LP1-FGF21 Expression Does Not Alter Serum Retinol Levels. The mice were tail vein-injected with AAV2/8-LP1-GFP or AAV2/8-LP1-FGF21. Then, 24 days after injection, the serum was isolated and the retinol levels were measured using HPLC. The data is presented as individual data points and mean ± sem (n=7,7) and **P*<0.05 is considered statistically significant when compared to mice with liver-specific GFP expression.

The serum retinol levels were not altered when comparing the control group (AAV2/8-LP1-GFP) and the FGF21-overexpressing group (AAV2/8-LP1-FGF21) (**Figure 29**).

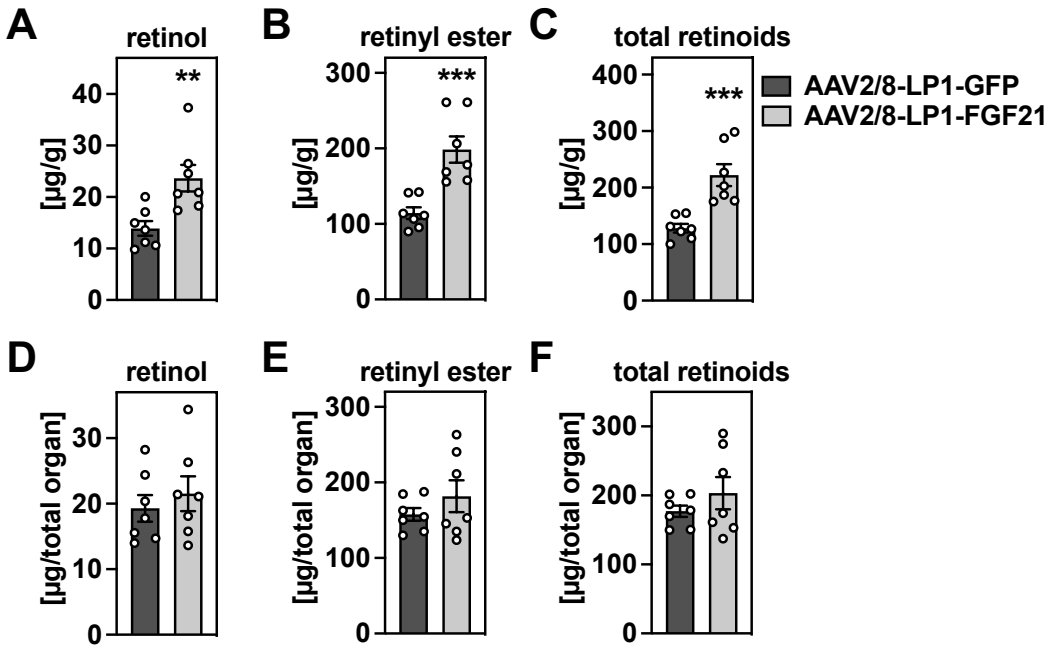

Figure 30: Liver-specific AAV2/8-LP1-FGF21 Expression Elevates Hepatic Retinoid Concentrations but Not Retinoid Content. The mice were tail vein-injected with AAV2/8-LP1-GFP or AAV2/8-LP1-FGF21. Then, 24 days after injection, the liver was harvested and (A) the retinol (B) and retinyl ester levels were determined. (C) The total retinoids were calculated by adding the retinol and retinyl esters together. The hepatic concentrations were normalized in relation to the organ weight and calculated as the amounts of (D) retinol, (E) retinyl ester, (F) and total retinoids per whole liver. The data is presented as individual data points and mean ± sem (n=7,7) and ***P*<0.01 and ****P*<0.001 are considered statistically significant when compared to mice with liver-specific GFP expression.

The retinol concentration (**Figure 30A**) in the livers of mice overexpressing FGF21 (AAV2/8-LP1-FGF21) as well as the retinyl ester concentration (**Figure 30B**) were significantly

increased in comparison to the control group (AAV2/8-LP1-GFP). Accordingly, a significant increase was also found when combing these results to the concentration of total retinoids (**Figure 30C**). Nonetheless, as shown in **Figure 25A**, the liver weight had significantly decreased in FGF21-overexpressing mice (AAV2/8-LP1-FGF21), and it became obvious that the amounts of retinol (**Figure 30D**), retinyl ester (**Figure 30E**), and total retinoids (**Figure 30F**) in the whole liver did not change comparing both groups when the concentration of retinoids was calculated as µg for the entire organ.

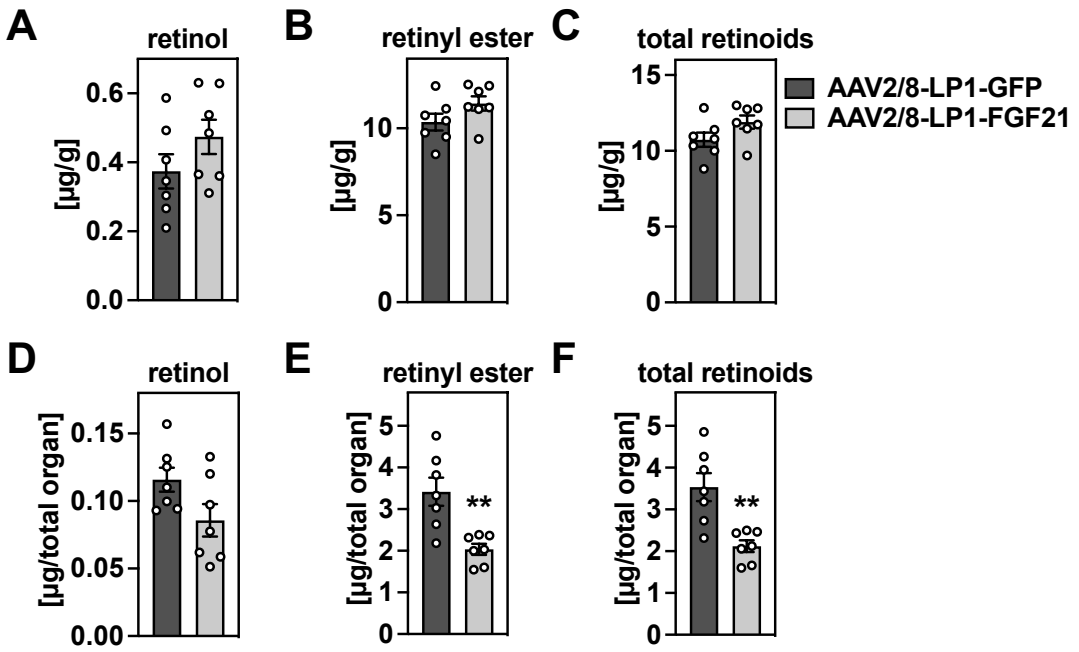

Figure 31: Liver-Specific AAV2/8-LP1-FGF21 Expression Does Not Alter Retinoid Concentrations but Decreases Retinyl Ester Content per Whole eWAT. The mice were tail vein-injected with AAV2/8-LP1-GFP or AAV2/8-LP1-FGF21. Then, 24 days after injection, the eWAT was harvested and (A) the retinol (B) and retinyl ester levels were determined. (C) The total retinoids were calculated by adding the retinol and retinyl esters together. The concentrations in eWAT were normalized in relation to the organ weight and calculated as the amounts of (D) retinol, (E) retinyl ester, (F) and total retinoids per whole eWAT. The data is presented as individual data points and mean ± sem (n=7,7) and $^{**}P<0.01$ is considered statistically significant when compared to mice with liver-specific GFP expression.

Subsequently, the concentration of retinoids in eWAT was analyzed. The retinol concentration (**Figure 31A**), retinyl ester concentration (**Figure 31B**), as well as the total retinoid concentration (**Figure 31C**) were unaltered. This was not the case when the total amounts per complete organ were calculated. The amount of retinyl esters per whole organ (**Figure 31E**) and the total retinoid content per whole organ (**Figure 31F**) decreased significantly after AAV2/8-LP1-FGF21 injection, while the retinol content per whole organ (**Figure 31D**) displayed a non-significant decreasing trend.

In the case of scWAT, the findings were a stark contrast to those obtained for the eWAT. The

concentrations of retinol (**Figure 32A**), retinyl ester (**Figure 32B**), and total retinoids (**Figure 32C**) were significantly higher in scWAT of FGF21-overexpressing mice (AAV2/8-LP1-FGF21) compared to the control group (AAV2/8-LP1-GFP). The calculation of retinoids per whole organ showed these increases only as part of what could be considered a non-significant trend (**Figures 32D**, **32E**, and **32F**).

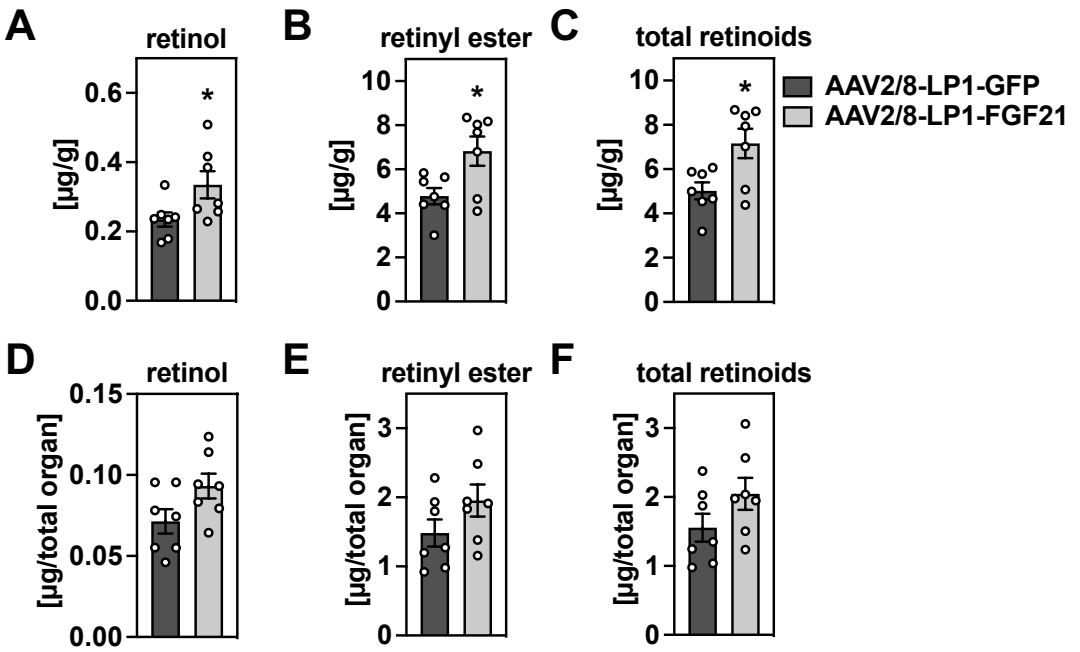

Figure 32: Liver-Specific AAV2/8-LP1-FGF21 Expression Increases scWAT Retinoid Concentrations but Not the Retinoid Content per Whole scWAT. The mice were tail vein-injected with AAV2/8-LP1-GFP or AAV2/8-LP1-FGF21. Then, 24 days after injection scWAT was harvested and (A) retinol, (B) and retinyl ester levels determined. (C) The total retinoids were calculated by adding the retinol and retinyl esters together. The concentrations in scWAT were normalized in relation to the organ weight and calculated as the amounts of (D) retinol, (E) retinyl ester, (F) and total retinoids per whole scWAT. The data is presented as individual data points and mean ± sem (n=7,7) and **P*<0.05 is considered statistically significant when compared to mice with liver-specific GFP expression.

4.3.6 The Influence of FGF21 on Gene and Protein Expression Levels of Molecules Related to Retinoid Homeostasis

A qRT-PCR was completed to analyze the effect of liver-specific FGF21 overexpression on the expression levels of retinoid homeostasis-related genes. The gene expression was analyzed in the liver tissue, eWAT, and scWAT.

In the livers of FGF21-overexpressing mice (AAV-LP1-FGF21), the mRNA levels of cytochrome P450 2c39 (*Cyp2c39*), which is a gene involved in atRA catabolism [213], and retinoic acid receptor β2 (*Rarβ2*) were significantly increased in comparison to the control

group (AAV-LP1-GFP) (**Figure 33A**). In contrast, there was no significant difference detectable for RAR target genes *Cyp26a1*, *Lrat,* and *Stra6l* (**Figure 33A**). The measured genes related to retinol transport or binding – *Rbp4*, *Ttr*, and *Crbp1* – remained unaltered, although a trend of upregulated *Rbp4* gene expression with a *P*-value of 0.06 was observed in FGF21-overexpressing mice (AAV-LP1-FGF21) compared to the control mice (AAV-LP1-GFP) (**Figure 33B**).

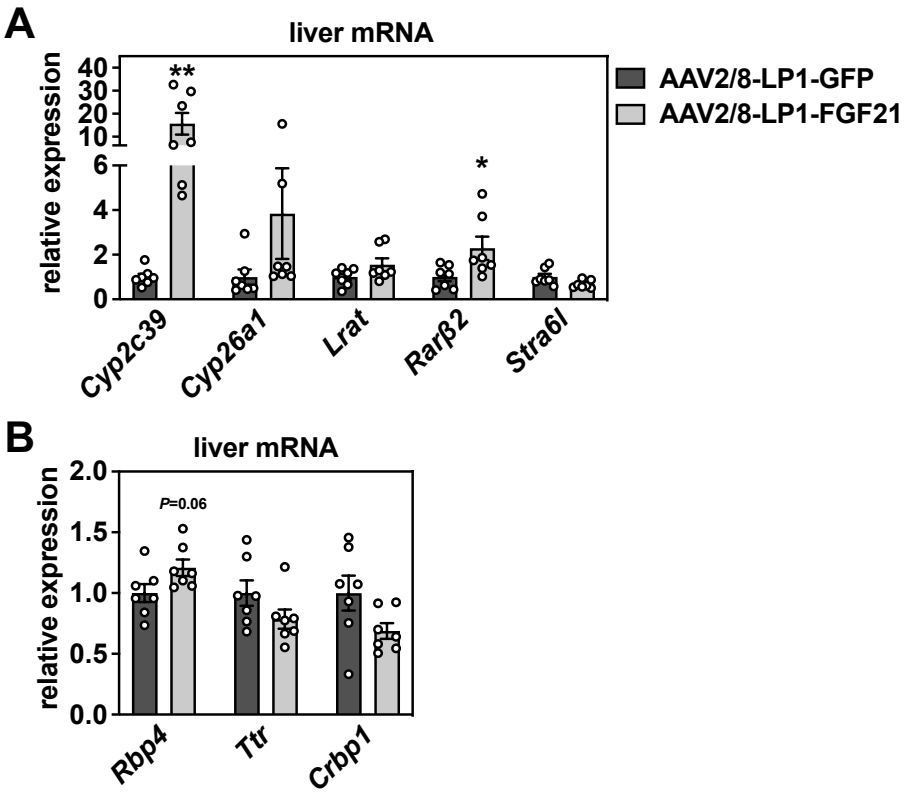

Figure 33: Liver-Specific AAV2/8-LP1-FGF21 Expression Induces Transcriptional Responses of Retinoid Homeostasis-Related Genes in the Liver. The mice were tail vein-injected with AAV2/8-LP1-GFP or AAV2/8-LP1-FGF21. Then, 24 days after injection, the liver was harvested. (A) The mRNA expression levels of *Cyp2c39*, *Cyp26a1*, *Lrat*, *Rarβ2*, and *Stra6l,* and of (B) retinol transport or binding-related genes *Rbp4*, *Ttr*, and *Crbp1* were determined by qPCR. The data is presented as individual data points and mean ± sem (n=7,7) and **P*<0.05 and ***P*<0.01 are considered statistically significant when compared to mice with liver-specific GFP expression.

In eWAT no significant change in mice injected with AAV-LP1-GFP or AAV-LP1-FGF21 was found regarding the RAR target genes cytochrome P450 26b1 (*Cyp26b1*), *Lrat*, *Rarβ2,* and *Stra6* (**Figure 34A**). The gene expression of the retinol transporter *Rbp4* had significantly increased in FGF21 overexpression (AAV-LP1-FGF21) compared to the control mice (AAV-LP1-GFP) (**Figure 34B**). The *Crbp1* gene expression did not change (**Figure 34B**).

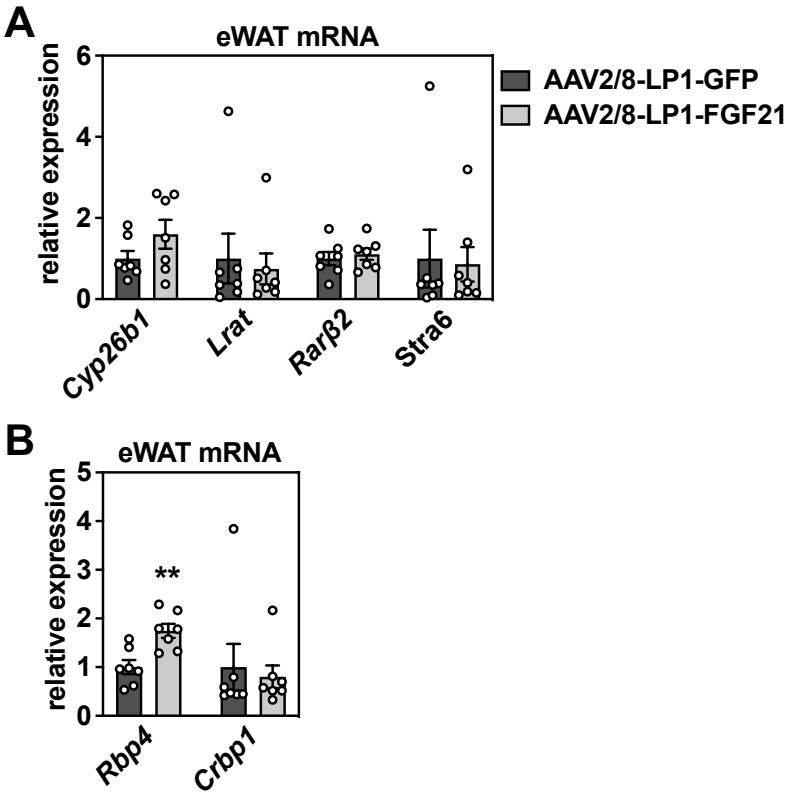

Figure 34: Liver-Specific AAV2/8-LP1-FGF21 Expression Does Not Alter Transcriptional Responses of Genes Related to RAR Signaling but Induces *Rbp4* Expression in eWAT. The mice were tail vein-injected with AAV2/8-LP1-GFP or AAV2/8-LP1-FGF21. Then, 24 days after injection, eWAT was harvested. (A) The mRNA expression levels of RAR signaling-related genes *Cyp26b1*, *Lrat*, *Rarβ2*, and *Stra6*, and of (B) retinol transport or binding-related genes *Rbp4* and *Crbp1* were determined by qPCR. The data is presented as individual data points and mean ± sem (n=7,7) and ***P*<0.01 is considered statistically significant when compared to mice with liver-specific GFP expression.

The gene expression of *Rarβ2* in scWAT was significantly upregulated by the FGF21 overexpression (AAV-LP1-FGF21), while, in contrast, the other RAR target genes – *Cyp26b1*, *Lrat,* and *Stra6* – did not display any significant changes compared to the control group (AAV-LP1-GFP) (**Figure 35A**). The expression of *Rbp4* showed a significant upregulation in scWAT of mice who received AAV-LP1-FGF21 compared to the control mice (AAV-LP1-GFP) (**Figure 35B**). *Crbp1* gene expression remained unaltered (**Figure 35B**).

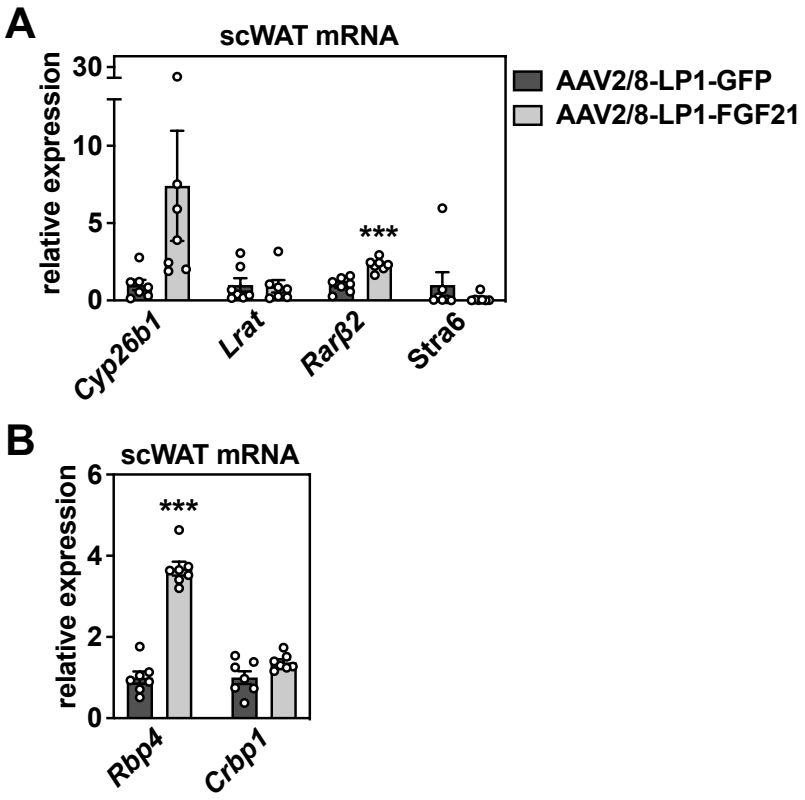

Figure 35: Liver-Specific AAV2/8-LP1-FGF21 Expression Induces Transcriptional Responses of Genes Related to RAR Signaling and Induces *Rbp4* Expression in scWAT. The mice were tail vein-injected with AAV2/8-LP1-GFP or AAV2/8-LP1-FGF21. Then, 24 days after injection, scWAT was harvested. (A) The mRNA expression levels of RAR signaling-related genes *Cyp26b1*, *Lrat*, *Rarβ2*, and *Stra6*, and of (B) retinol transport or binding-related genes *Rbp4* and *Crbp1* were determined by qPCR. The data is presented as individual data points and mean ± sem (n=7,7) and ***P<0.001 is considered statistically significant when compared to mice with liver-specific GFP expression.

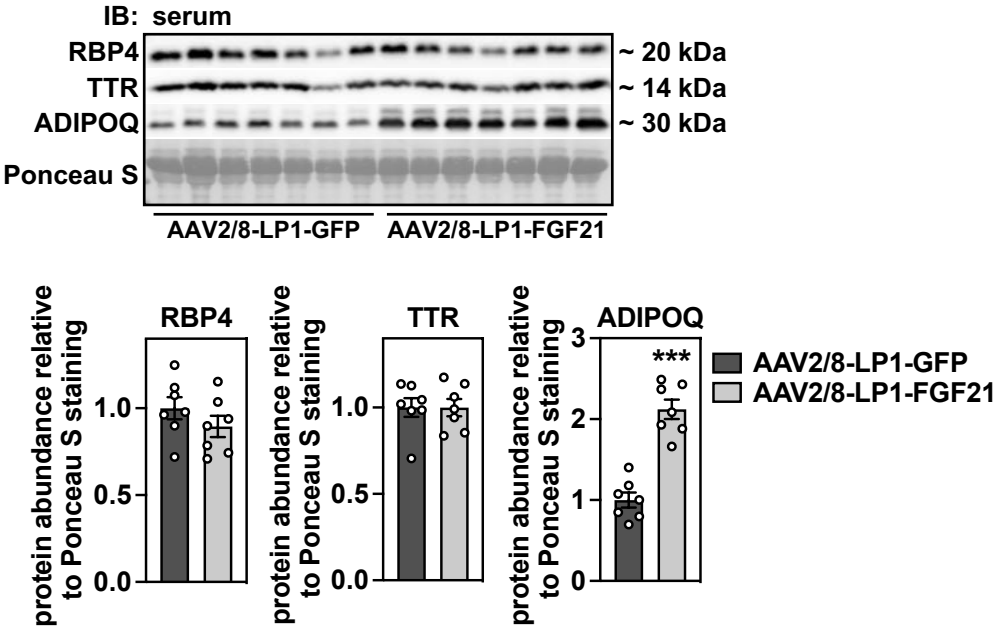

Figure 36: Liver-Specific AAV2/8-LP1-FGF21 Expression Does Not Alter Serum Levels of RBP4 and TTR but Promotes Those of ADIPOQ. The mice were tail vein-injected with AAV2/8-LP1-GFP or AAV2/8-LP1-FGF21. Then, 24 days after injection, the serum was collected. The serum was analyzed by immunoblotting for protein expression of RBP4, TTR, and ADIPOQ and a densitometric analysis was performed using image processing software. The data is presented as individual data points and mean ± sem (n=7,7) and ****P*<0.001 is considered statistically significant when compared to mice with liver-specific GFP expression.

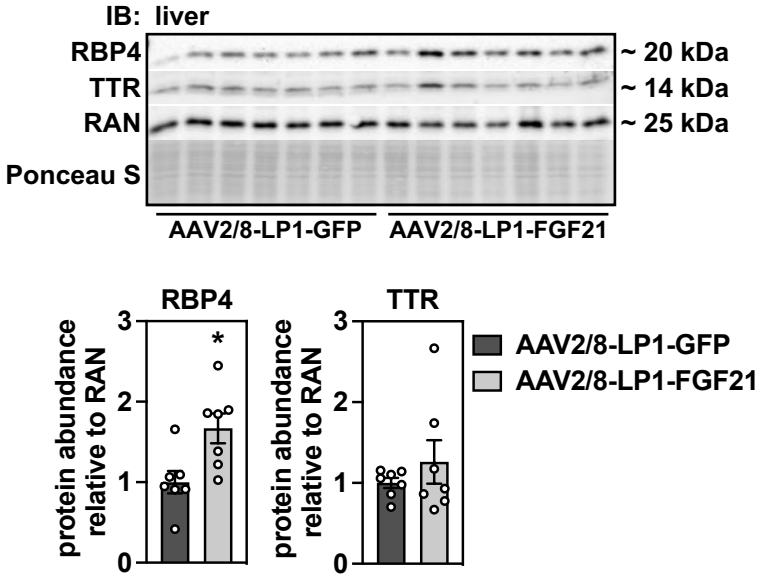

Figure 37: Liver-Specific AAV2/8-LP1-FGF21 Expression Increases Hepatic RBP4, but Not TTR Levels. The mice were tail vein-injected with AAV2/8-LP1-GFP or AAV2/8-LP1-FGF21. Then, 24 days after injection, the liver was harvested. The liver tissue was analyzed by immunoblotting for protein expression of RBP4 and TTR and a densitometric analysis was performed using image processing software. The data is presented as individual data points and mean ± sem (n=7,7) and **P<0.05* is considered statistically significant when compared to mice with liver-specific GFP expression.

Next, the expression of proteins related to retinol binding and transport was analyzed in the serum, liver, and adipose tissue to supplement the data found in the gene expression analysis.

The protein levels of RBP4 and TTR in the serum were unaltered when comparing between FGF21-overexpressing mice (AAV-LP1-FGF21) and control mice (AAV-LP1-GFP) (**Figure 36**). The detection and quantification of ADIPOQ in these sera revealed an approximately two-fold increase in the group overexpressing FGF21 (AAV-LP1-FGF21) compared to the control group (AAV-LP1-GFP) (**Figure 36**). The RBP4 protein levels in the liver were significantly elevated 1.7-fold in the AAV-LP1-FGF21 group compared to the AAV-LP1-GFP group, whereas the TTR levels remained unchanged (**Figure 37**). The protein levels of RBP4 and CRBP1 in eWAT did not change when comparing both groups (**Figure 38**). Moreover, the RBP4 and CRBP1 protein levels in scWAT also did not change significantly either (**Figure 39**).

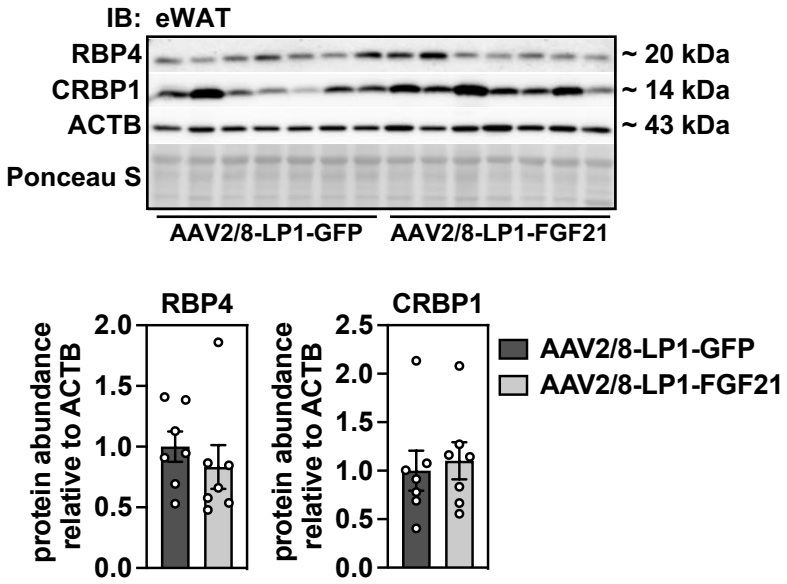

Figure 38: Liver-Specific AAV2/8-LP1-FGF21 Expression Does Not Alter Protein Expression of RBP4 and CRBP1 in eWAT. The mice were tail vein-injected with AAV2/8-LP1-GFP or AAV2/8-LP1-FGF21. Then, 24 days after injection, eWAT was harvested. eWAT was analyzed by immunoblotting for protein expression of RBP4 and CRBP1 and a densitometric analysis was performed using image processing software. The data is presented as individual data points and mean ± sem (n=7,7) and **P*<0.05 is considered statistically significant when compared to mice with liver-specific GFP expression.

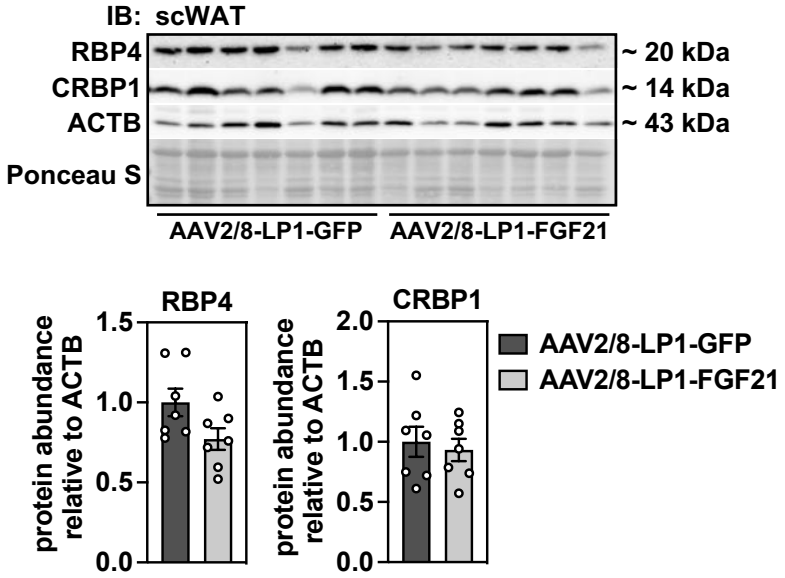

Figure 39: Liver-Specific AAV2/8-LP1-FGF21 Expression Does Not Alter Protein Expression of RBP4 and CRBP1 in scWAT. The mice were tail vein-injected with AAV2/8-LP1-GFP or AAV2/8-LP1-FGF21. Then, 24 days after injection, scWAT was harvested. scWAT was analyzed by immunoblotting for protein expression of RBP4 and CRBP1 and a densitometric analysis was performed using image processing software. The data is presented as individual data points and mean ± sem (n=7,7) and **P*<0.05 is considered statistically significant when compared to mice with liver-specific GFP expression.

4.3.7 The Effects of FGF21 on Lipolytic Enzymes

The weight loss of mice overexpressing FGF21 indicated that enhanced lipolysis was taking place. Previous studies have shown that lipolytic enzymes are capable of retinyl ester hydrolyzation in white adipose tissue and it was suggested that they can also mobilize them [175]. These suggested capabilities are the reason this study directs a special focus on the lipases ATGL and, in particular, HSL in the presented model of liver-specific FGF21 overexpression in mice.

The gene expression levels of *Hsl* and *Atgl* were significantly upregulated in eWAT of liver-specific FGF21 overexpression (AAV-LP1-FGF21) compared to the control group (AAV-LP1-GFP) (**Figure 40A**). A 1.4-fold change was observed for *Hsl* gene expression, and a 1.7-fold change for *Atgl*. The total HSL protein levels did not change, although a trend towards increased total HSL levels was visible in the group that received the AAV-LP1-FGF21 (**Figure 40B**). The p-HSL protein levels in relation to the total HSL levels were significantly decreased in eWAT of FGF21-overexpressing mice (AAV-LP1-FGF21) (**Figure 40B**).

The analysis of the gene expression in scWAT of both enzymes revealed a significant upregulation with a 3.8-fold change for *Hsl* and a 5.3-fold change for *Atgl* in scWAT of

AAV-LP1-FGF21-injected mice compared to the control group (AAV-LP1-GFP) (**Figure 41A**). The analysis of the protein levels of HSL showed increased levels of total HSL and decreased levels of p-HSL in relation to total HSL in scWAT of FGF21-overexpressing mice (AAV-LP1-FGF21) (**Figure 41B**).

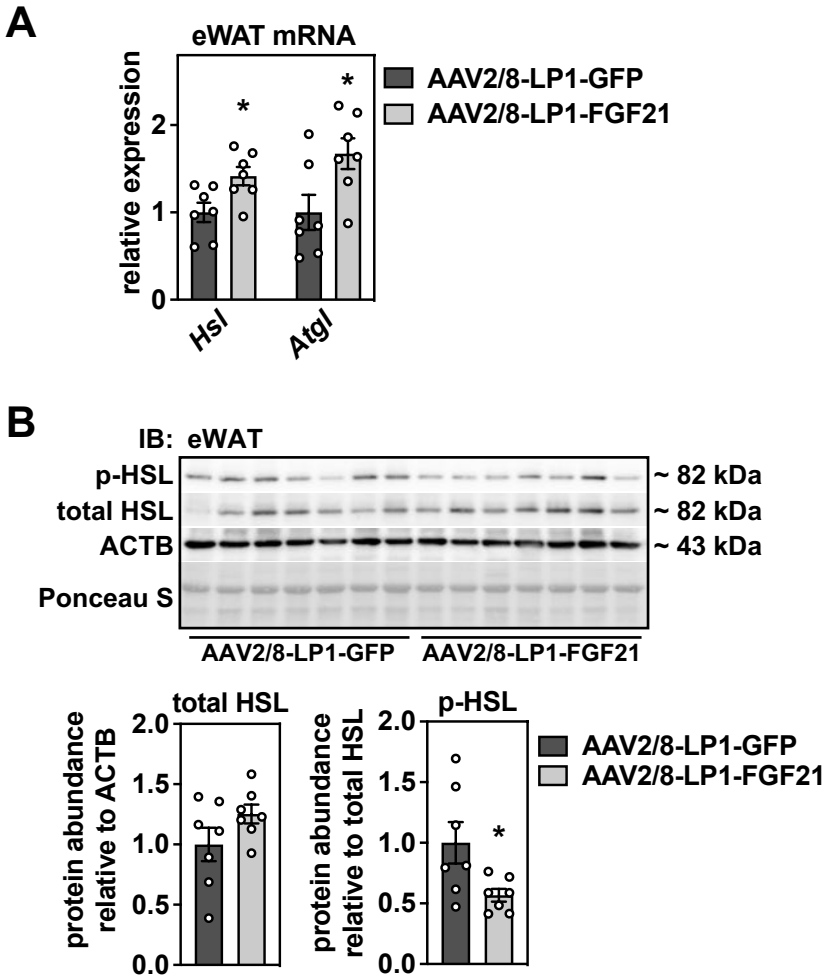

Figure 40: Liver-Specific AAV2/8-LP1-FGF21 Expression Increases Gene Expression of Lipases *Hsl* and *Atgl* but Decreases Phosphorylated HSL Protein Levels in eWAT. The mice were tail vein-injected with AAV2/8-LP1-GFP or AAV2/8-LP1-FGF21. Then, 24 days after injection, eWAT was harvested. (A) The mRNA expression levels of *Hsl* and *Atgl* were determined by qPCR. (B) eWAT was analyzed by immunoblotting for protein expression of p-HSL and total HSL and a densitometric analysis was performed using image processing software. The data is presented as individual data points and mean ± sem (n=7,7) and **P*<0.05 is considered statistically significant when compared to mice with liver-specific GFP expression.

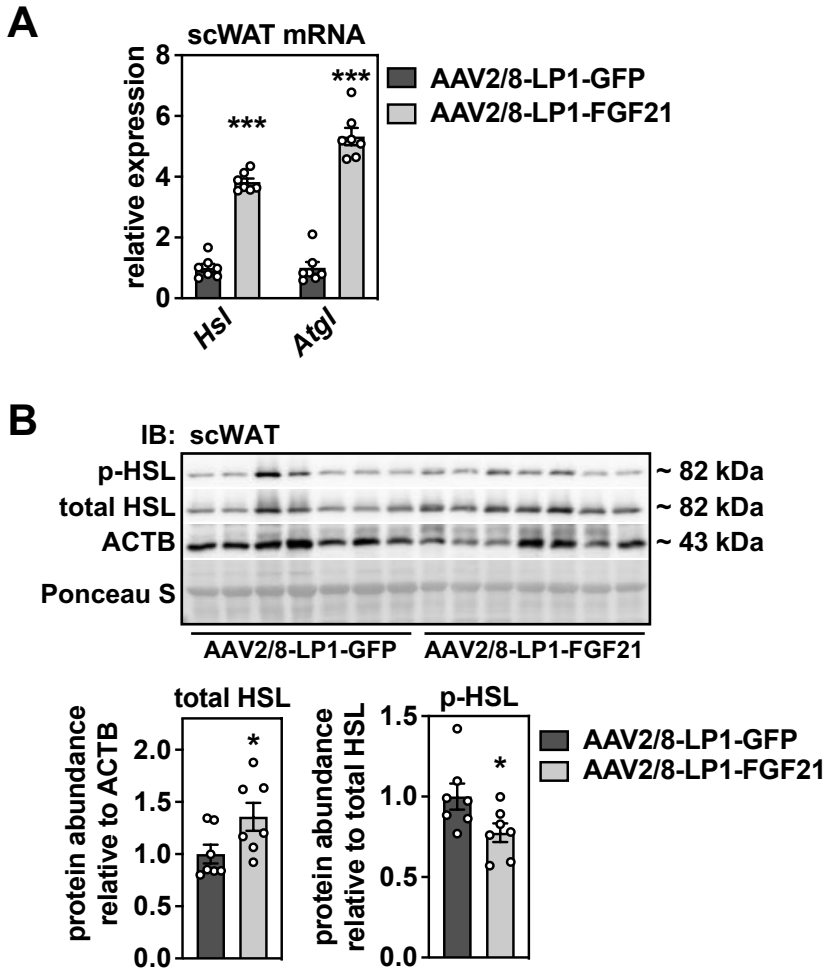

Figure 41: Liver-Specific AAV2/8-LP1-FGF21 Expression Increases Gene Expression of Lipases *Hsl* and *Atgl* but Decreases Phosphorylated HSL Protein Levels in scWAT. The mice were tail vein-injected with AAV2/8-LP1-GFP or AAV2/8-LP1-FGF21. Then, 24 days after injection, scWAT was harvested. (A) The mRNA expression levels of *Hsl* and *Atgl* were determined by qPCR. (B) scWAT was analyzed by immunoblotting for protein expression of p-HSL and total HSL and a densitometric analysis was performed using image processing software. The data is presented as individual data points and mean ± sem (n=7,7) and **P*<0.05 and ****P*<0.001 are considered statistically significant when compared to mice with liver-specific GFP expression.

4.3.8 The Effects of FGF21 on Browning

In order to assess the role of FGF21 in browning, both isolated white adipose tissues were tested regarding specific target genes and proteins. The eWAT was unable to be analyzed due to very low expression on mRNA and protein level. For this reason, the following section solely focusses upon the results of the scWAT analysis.

The gene expression of *Ucp1*, *Cidea*, and *Adrb3* was significantly upregulated (**Figure 42A**). *Ucp1* gene expression displayed an approximate 14-fold difference when comparing the mice overexpressing FGF21 (AAV-LP1-FGF21) to the control group (AAV-LP1-GFP). The following

protein expression analysis showed increased levels of UCP1 in the mice overexpressing FGF21 (AAV-LP1-FGF21), while the UCP1 levels in the control group (AAV-LP1-GFP) were almost undetectable (**Figure 42B**).

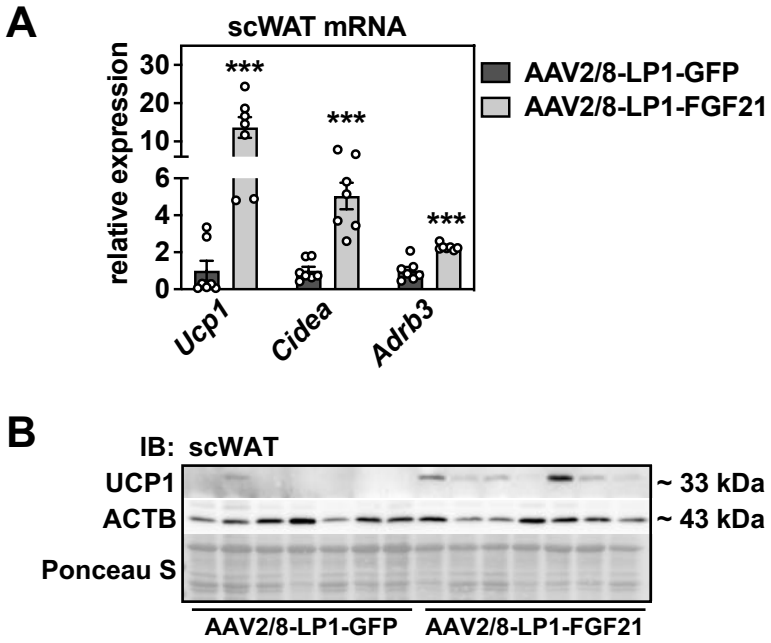

Figure 42: Liver-Specific AAV2/8-LP1-FGF21 Expression Increases Thermogenesis and Browning-Related Gene Expression and Increases Protein Levels of UCP1 in scWAT. The mice were tail vein-injected with AAV2/8-LP1-GFP or AAV2/8-LP1-FGF21. Then, 24 days after injection, scWAT was harvested. (A) The mRNA expression levels of *Ucp1, Cidea,* and *Adrb3* were determined by qPCR. (B) scWAT was analyzed by immunoblotting for protein expression of UCP1. The data is presented as individual data points and mean ± sem (n=7,7) and ****P*<0.001 is considered statistically significant when compared to mice with liver-specific GFP expression.

5 Discussion

5.1 Retinoid Homeostasis is Regulated by Glucagon and Insulin Signaling in the Feeding-Fasting Transition

The preliminary study on retinoid homeostasis in fasted mice revealed a striking regulation of hepatic *Rbp4* and *Ttr* mRNA expression as well as of their protein levels in the liver and serum. In addition to this, another study had shown that *Rbp4* mRNA is upregulated in fasting periods [214]. The present study aimed to illuminate the underlying mechanisms of these regulations.

Since PPARα is known to be one of the master regulators of fasting [202], the first step taken was to investigate the regulation of *Rbp4* and *Ttr* in primary murine hepatocytes upon exposure to the PPARα agonist WY. Neither *Rbp4* nor *Ttr* showed a response to two different concentrations of the PPARα agonist, and it was therefore concluded that the regulation of both proteins is independent of PPARα. This is supported by the observation that a fasting challenge can still induce the mRNA levels of *Rbp4* in PPARα knockout mice [214].

The following step involved investigating the influence of participants of retinoid metabolism – retinol and retinoic acid – in an experimental setup with primary murine hepatocytes. This step was selected since hepatic retinoic acid levels and retinoid acid signaling related genes had been shown to decrease during fasting [207]. The *Rbp4* and *Ttr* mRNA levels were unaltered by both stimuli. This indicates that changes in the amounts of retinoid metabolites that might occur during the fasting transition and as a result of the hypothesized reverse transport of retinoids during fasting are not responsible for alterations in *Rbp4* and *Ttr* regulation. This coincides with results from a study that investigated the influence of the dietary vitamin A status on *Rbp4* gene expression levels in mice. Neither retinol depletion nor retinol repletion caused alterations in the gene expression of *Rbp4* in the liver compared to the mice fed a normal chow [215]. Moreover, atRA was only able to reduce adipocyte mRNA levels of *Rbp4*, but not hepatic levels of *Rbp4* in another study [216]. In contrast, several studies were able to show that the mRNA expression level of *Rbp4* is inducible by atRA stimulation and that its secretion is inhibited *in vivo* and *in vitro* [217, 218]. The results presented in this study suggest that altered levels of retinol or atRA in the liver are not responsible for the regulation of *Rbp4* and *Ttr* gene expression in the feeding-fasting transition.

Subsequently, the focus shifted to whether the counteracting hormones insulin and glucagon and their signaling pathways are possible candidates for the regulation of RBP4 and TTR. For this very reason, a synthetic analogue of cAMP was used. Interestingly, the mRNA expression levels of both proteins were upregulated in a dose-dependent manner. The *Rbp4* gene

expression was significantly upregulated using the highest 8-Br-cAMP dose, while *Ttr* showed this significant change for all three tested concentrations. This is consistent with findings from previous studies that presented upregulated *Rbp4* mRNA expression in mouse hepatoma cell lines resulting from cAMP stimulation [219, 220]. However, the presented study provides new insights into cAMP's regulatory effect on *Rbp4* and *Ttr* mRNA expression by using primary murine hepatocytes, which represent a more physiological context for analyzing hepatic metabolism.

cAMP is known to be induced by stimulation of the glucagon receptor. Therefore, the next step was to expose primary murine hepatocytes to indicated doses of glucagon. The *Rbp4* gene expression was increased when 100 nM of glucagon were used. *Ttr* was not regulated. Upregulation of the *Rbp4* mRNA expression and of the hepatic protein content was also observed for an *in vivo* injection of glucagon [220]. The efficiency of glucagon in the experimental setup presented here was much lower compared to the synthetic and more stable 8-Br-cAMP that strongly influences the physiology of the isolated primary murine hepatocytes. In comparison, this makes glucagon's effects on *Rbp4* and *Ttr* seem less robust. This was also observed in the results of the *Pck1* mRNA analysis. 8-Br-cAMP is a synthetic derivative of physiologic cAMP. It activates protein kinase and has long-acting consequences for the cell, because it is resistant to cAMP phosphodiesterase [221].

Incubation with insulin and a FOXO1 knockdown study provided additional insights into mRNA regulations. Direct insulin incubation did not significantly alter the *Rbp4* mRNA expression, but revealed a trend of a dose-dependent decrease down to mRNA levels between 90% and 80% of the control values. This reduction was shown in multiple experiments performed within this study. Although this was not significant in the individual experiments, a collective analysis of all experiments clearly showed a significant reduction of the *Rbp4* mRNA expression levels by about 20%. The knockdown of FOXO1 effectively reduced *Rbp4* gene expression by about 50%. *Ttr* gene expression was decreased dose-dependently after insulin stimulation and remained unaltered in the FOXO1 knockdown study.

Ttr mRNA levels were downregulated in the fasting experiment of the preliminary study, but did not reveal conclusive results in the presented experiments. The results showed an upregulation caused by cAMP stimulation and showed a corresponding downregulation induced by insulin stimulation. However, these results are not supported by experimentally observed effects of glucagon on *Ttr* mRNA level. Moreover, the results do not provide an explanation for the *Ttr* regulation during fasting.

This study provides novel insights into the regulation of *Rbp4* mRNA expression. In the fed state, insulin secretion is enhanced by dietary carbohydrate intake, which, in turn, inhibits

FOXO1 by means of AKT phosphorylation. The inhibited FOXO1 activity results in repressed *Rbp4* gene expression. A hepatocyte-specific deletion of the insulin receptor also led to the identification of insulin as a repressor of hepatic *Rbp4* mRNA expression [214]. This contributes to the discovered upregulation of *Rbp4* mRNA levels during fasting, since insulin-mediated inhibition of FOXO1 in feeding, and, thus, of *Rbp4* mRNA expression, is diminished. Fasting has been shown to promote *Foxo1* gene expression owing to a mechanism involving the activation of PKA via cAMP [222]. This leads to the induction of CREB signaling and, eventually, to the upregulation of *Foxo1* gene expression. Additionally, a study showed that cAMP-mediated hepatic glucose production is partially dependent on the action of FOXO1 [223]. This suggests that *Rbp4* mRNA expression is also regulated by CREB and FOXO1 signaling during fasting. The increased *Rbp4* mRNA expression during fasting is supported by the action of glucagon through cAMP and the subsequent PKA activation, as indicated by the results of this study.

Therefore, it is concluded that the elevation of *Rbp4* gene expression during fasting is mediated by two mechanisms: 1) The upregulation of *Rbp4* caused by FOXO1 activation (which is induced by the inhibition of insulin-mediated FOXO1 suppression and induced by cAMP signaling via CREB). 2) Glucagon-mediated and cAMP-dependent upregulation of *Rbp4* during fasting.

The preliminary data showed that the hepatic RBP4 protein levels increased during fasting while the serum levels of RBP4 remained unaltered. This indicates that the increased gene expression leads to an elevated translation, however, the secretion remains unaltered due to the tightly regulated levels of RBP4 and retinol in the circulation and, ultimately, RBP4 protein accumulates in the liver. The experiments performed on primary murine hepatocytes in this study also revealed new insights into the protein expression levels. The use of the mimetic of fasting 8-Br-cAMP led to a strong decrease in RBP4 secretion. Surprisingly, the protein levels in the cell lysates did not increase to a corresponding extent, indicating degradation was taking place rather than accumulation. It is important to note that primary murine hepatocytes exposed to 8-Br-cAMP for 21 h displayed shrinkage, causing the shapes of their cells to change. This information combined with the observation that also TTR secretion decreases dose-dependently points towards overall reduced protein secretion in this setup. This is thought to be due to the extent the cell physiology is influenced by 8-Br-cAMP. Nonetheless, RBP4 secretion was inhibited more intensely compared to TTR secretion, and TTR displayed an accumulation in the cell lysates that reflected the reduced secretion of this protein. Overall, the cAMP exposure resulted in a strong decrease in RBP4 secretion, although no corresponding accumulation in the cell lysates became obvious. TTR's secretion was inhibited while this protein appeared to accumulate in the hepatocytes.

The usage of glucagon in the same experimental setup showed no significant changes, neither for protein levels in the hepatocytes, nor in the supernatant. Nonetheless, the results provided a visible trend that supported the findings for 8-Br-cAMP, namely decreasing levels of RBP4 and TTR in the supernatant, stable RBP4 levels in the cell lysates, and increasing TTR levels in the cell lysates. In contrast, glucagon's counterpart molecule – insulin – was able to reduce RBP4 levels in the cell lysates dose-dependently. The protein levels in the supernatant displayed a high standard deviation, but, overall, the trend showed a corresponding increase in secreted RBP4. TTR's secretion remained unchanged.

This provides new insights into the mechanism that involves the insulin and glucagon signaling pathways. TTR protein expression is not regulated by insulin stimulation, but, instead, displays decreased secretion and hepatocyte accumulation mediated by the cAMP signaling pathway. This indicates that TTR's secretion is inhibited in times of fasting due to cAMP signaling. The TTR levels in the bloodstream were found to have reduced during fasting in the preliminary study as well as in this study. Since the serum levels of retinol and RBP4 remained unaltered at the same time, a reduced secretion of RBP4-unbound TTR can be assumed, since the concentration of TTR in serum is more than twice as high as the concentration of RBP4. This implies that not all of the TTR can exit the liver while bound to RBP4, and the secretion of the RBP4-independent TTR has to be taken into consideration. RBP4, in contrast, is dependent on glucagon and insulin signaling. Insulin is thought to increase the secretion of RBP4 and, correspondingly, of retinol during feeding in order to distribute it to extra-hepatic tissues. During fasting, glucagon signaling inhibits the secretion of RBP4 via cAMP signaling.

Although primary murine hepatocytes represent a highly reliable option for investigating hepatic regulations *in vitro*, *in vivo* studies would introduce new insight into the proposed mechanism. The experimental setup using cell culture conditions does not enable other tissues to be included which might cause to overlook their contributing mechanisms. In addition to that, the hepatocytes were only isolated from male mice, which does not allow sex-related differences to be excluded. The used media in the experiments contained indicated concentrations of pyruvate and lactate, which are standard compounds used to simulate a fasting medium. It is not clear to what extent this medium already induces changes in the regulation of RBP4 and TTR. In future studies the effects of the stimulating compounds could be investigated independent of the fasting medium. This study suggests that RBP4 regulation and, partially, also TTR regulation are dependent on the presence of glucagon and insulin and their ratios during various metabolic states. The next step could be an experimental setup with varying ratios of insulin and glucagon to see if this balance can shift the outcome for RBP4 and TTR regulation regarding the mRNA expression and protein levels.

Overall, these *in vitro* results suggest that the fasting-mediated regulations of RBP4 and TTR

in the liver occur independent of changes in retinol and retinoic acid availability, and also suggest an independence of the fasting master-regulator PPARα. Both proteins, but especially RBP4, are regulated by a mechanism that is dependent on the presence of insulin and glucagon during feeding and fasting to maintain stable concentrations of circulating retinol and simultaneously manage hepatic retinyl ester stores and the availability for extrahepatic tissues.

5.2 Fasting Alters the Balance of holo-RBP4 and apo-RBP4 Levels in the Bloodstream

The presented study confirms the preliminary data regarding the serum RBP4 and TTR protein levels in fasted mice: RBP4 remained unaltered, while TTR was reduced by more than 50%. This study investigated retinol loading of RBP4 in times of fasting and showed in a non-denaturing immunoblot that while only about 1% of RBP4 appears in its apo-form in the fed state, about 8% is already detected as apo-RBP4 during fasting. This indicates that the secretion of RBP4 and, therefore, the detected levels of total RBP4 may not vary in times of fasting, but the degree of retinol binding in the bloodstream is altered. Interestingly, differences were detected hereby that were not suspected when looking at the stable concentrations of RBP4 or of retinol in the circulation.

The section on the immunoprecipitation of RBP4 in the serum of fed and fasted mice provided additional insights. Using the method established here, approximately 90% of the total RBP4 were precipitated from the serum with no differences identified between the feeding and fasting states. Moreover, the retinol detected in the supernatant and precipitate totaled 100% when added together, meaning no retinol was lost in the process. The retinol levels in the serum of fed and fasted mice before the immunoprecipitation were equally high, and less than 5% of retinol was detectable in the supernatant after the experiment. This coincides with current literature that confirms RBP4 as retinol's main transporter [224]. Since the RBP4 levels had not reduced 100% it was not surprising to find some remaining retinol in the supernatant after immunoprecipitation. Interestingly, the retinol levels in the supernatant after RBP4 had been removed by immunoprecipitation were significantly lower in the fasted state compared to the fed state. Accordingly, more retinol can be found in the precipitate that contains the RBP4-bound retinol. Thus, this suggests that more retinol is bound to RBP4 during fasting, meaning more holo-RBP4 can be found during fasting. This was surprising, because the non-denaturing immunoblot revealed that more apo-RBP4 can be found in the serum of fasted mice.

The immunoblot data suggest that apo-RBP4 levels increased during fasting. Like the preliminary study, this study found that the serum RBP4 levels as well as the levels of

circulating retinol remained unaltered during fasting. The hepatic *Rbp4* mRNA expression had increased during fasting. This finding is supported by the observation in the preliminary study that identified RBP4 accumulating in the liver. This suggests that hepatic *Rbp4* mRNA expression is increased which results in a higher translation of RBP4. During the fasting transition, the liver appears to keep retinoid stores stable, which, in turn, suggests the retinol export via RBP4 is not induced, causing RBP4 to accumulate in the liver instead. At the same time, circulating RBP4 and retinol levels remain constant. Based on the unaltered total RBP4 levels in the serum and the increased hepatic RBP4 levels, it was concluded that the liver does not induce RBP4 secretion, despite gene expression and translation being increased. The increased amount of apo-RBP4 suggests that the circulating retinol present during fasting is inevitably bound to other carrier proteins, since lipophilic retinol is dependent on transporters [1]. It has been suggested that albumin and other lipoproteins, especially those linked to lipolysis and fatty acid transport, are candidates that can serve this purpose [24, 48, 225].

An explanation for the elevated apo-RBP4 levels in the fasted state – especially since a hepatocyte-specific knockout of RBP4 resulted in undetectably low RBP4 levels in the serum [46] – could be that the amount of holo-RBP4 that is secreted by the liver is no different than in the fed state while the delivery of retinol to extra-hepatic tissues is enhanced. Thereafter, RBP4 remains in the bloodstream in the form of apo-RBP4, which would be detected at an elevated level in the described immunoblot. As mentioned in the initial hypothesis, an organism exposed to a fasting challenge is thought to induce the reverse transport of retinol to the liver, possibly even via other transporters. This would enable stable concentrations of retinoids in the serum and liver even though the delivery of retinol to extrahepatic tissues and apo-RBP4 levels are suggested to be elevated.

In this study only the serum levels were detected and no flux studies of the secretion were performed. This leaves room for another possible explanation for the observed increase in apo-RBP4 levels. If the RBP4 secreted by the liver was found to be only holo-RBP4 in mice [27-29, 48], one could speculate that the elevated levels of apo-RBP4 found here could originate from another organ. However, this would be surprising since the liver was identified as the principal source of serum RBP4 [46]. It is important to note that this mentioned study does not provide information regarding the sources of RBP4 during a fasted state, a state in which other organs might contribute to circulating RBP4 levels as well. A muscle-specific overexpression of RBP4 in RBP4 knockout mice showed that other tissues can generally contribute to circulating RBP4 levels during certain challenges [226]. In addition to that, successful *in vitro* secretion of RBP4 from adipocytes and fat pad explants has been shown in other studies [43, 46, 227]. While taking the fact that the expression levels of *Rbp4* in adipose tissue are 20% to 40% of those found in liver [43] into account, it could be speculated that the

fasting transition promotes adipocyte-derived secretion of RBP4. The secretion of RBP4 from adipose tissue has been suggested to take place in obesity and type 2 diabetes [228, 229], although this information must be reviewed critically due to the finding that circulating RBP4 derives from hepatocytes in lean and insulin resistant mice [46]. The possibility of adipocyte-derived RBP4 secretion during fasting could be tested by subjecting hepatocyte-specific RBP4-deleted mice to a fasting challenge. Until further experimental testing can be completed, this hypothesis remains a speculative attempt to explain these findings. The suggested changes in the role of adipose tissue further support the initial hypothesis of retinoids being mobilized from adipose tissue towards the liver to maintain the hepatic retinoid stores during fasting. In addition, RBP4 has been found capable of binding fatty acids and is speculated to be a potent fatty acid carrier [230-233]. Although these fatty acids are non-retinoid ligands, they were found in the binding pocket of RBP4. Since lipolysis is enhanced during fasting, it is possible to question the possibility of apo-RBP4 being secreted by adipose tissue to support the transport of fatty acids.

Thus far it remains unclear how apo-RBP4 can circulate without any other binding partner. RBP4 must be bound to retinol and TTR to be protected from renal filtration, however a TTR deficiency did not entirely inhibit the RBP4 secretion [66, 234]. The detection of apo-RBP4 on the shown non-denaturing blot indicates that at least some of the apo-RBP4 can circulate without immediate renal filtration.

In contrast, RBP4 immunoprecipitation pointed towards increased levels of holo-RBP4 in the bloodstream of fasted mice. Evidence exists that the ratio of retinol to RBP4 is decreased in case of obesity, suggesting elevated apo-RBP4 levels are present in obese humans [235-238]. Interestingly, a different study on obese mice found the exact opposite, namely increased holo-RBP4 levels [48]. The contradictory findings were thought to stem from the studies being based on different species, the method of data acquisition, and the evaluation thereof. While the first studies motioned used the ratio of retinol to RBP4, the second study utilized the visualization of both apo- and holo-RBP4 on a non-denaturing immunoblot. The latter is thought to be more accurate, since the ratio of retinol to RBP4 does not take the RBP4-independent retinol transport into consideration [48, 239].

Increased holo-RBP4 levels in serum during fasting – a result concluded from performed immunoprecipitation – suggest that retinol is especially dependent on the transportation by RBP4 in this metabolic state and that less apo-RBP4 is circulating. In mice, the RBP4 secreted by the liver is thought to be holo-RBP4 [27-29, 48]. It is assumed that the liver secretion of holo-RBP4 remains unaltered, but the delivery to target tissues does not. The elevated levels of holo-RBP4 lead to the suggestion that holo-RBP4 is less prone to releasing its ligand during fasting. All of this is suspected to occur to maintain the steady-state of hepatic and circulating

retinoid content.

The immunoprecipitation experiment resulted in a reduction of the RBP4 levels by about 88% in the supernatant, including dramatically reduced retinol levels. However, it was surprising that TTR was barely visible in the precipitate and remained highly detectable in the supernatant instead. RBP4, retinol, and TTR form a complex in the endoplasmic reticulum of the hepatocytes before they are secreted, and the affinity of TTR to RBP4 is especially high when it is bound to retinol [25, 26, 240, 241]. Nonetheless, the immunoprecipitation of RBP4 and, simultaneously, the precipitation of retinol cannot remove TTR either, which indicates that the experimental procedure influences the bond to TTR. Therefore, an influence on the RBP4 to retinol bond cannot be excluded. The immunoprecipitation lasts seven hours, making it possible for the retinol to have been redistributed between apo-RBP4 and holo-RBP4 during this time.

Both types of experiments performed in this study display discrepancies in their findings. Reasons for this can be sought after in the study design and methodical approach. The immunoblot was conducted with the mouse cohort elaborated upon in **Chapter 3.5.1**. These mice were 10 weeks old. Contrastingly, the cohort used for the immunoprecipitations described in **Chapter 3.5.2** were 25 to 26 weeks old. At both ages the mice are considered to be adult mice. Nonetheless, it is not possible to state that age-related differences did not play any role in the different outcomes of both experiments. Ideally, both types of analyses would be carried out with serum samples from each cohort in order to identify the age-related effects. The used antibody for immunoblotting and immunoprecipitation was designed specifically to be against RBP4 isolated from human urine. It is possible that this antibody has different affinities to apo-RBP4 and holo-RBP4 because of the bond to retinol and/or TTR. Additionally, as mentioned before, RBP4 can bind to other non-retinoid ligands that might disturb the antibody binding. Both methods only provide insight into the RBP4 levels in the serum at a certain point in time. It would be interesting to perform tracing studies to investigate the secretion of this protein rather than draw conclusions about secretory phenomena from serum levels. This would be especially worthwhile to look into, since the source of the detected RBP4 in fasting was thought to be the liver, but the results hinted at the possibility of other tissues contributing to the serum levels. However, this methodical approach of tracing RBP4 represents a great challenge and is not a standard procedure thus far. Moreover, a look into flux studies on the circulating retinol might help to shed more light on the presented hypothetical options of either increased delivery to target tissues or enhanced stability of holo-RBP4.

Overall, both methods – non-denaturing immunoblot and immunoprecipitation – provided insight into retinoid homeostasis regarding retinol-loading of RBP4 during fasting. However,

they remain inconclusive due to their results being contradictory and possible explanations are unable to be supported by sufficient experimental data just yet.

5.3 FGF21 Overexpression Alters Metabolic Homeostasis

The overexpression of FGF21 was successfully induced in the liver, the main source of circulating FGF21 [108], by a single administration of AAV. It promoted *Fgf21* gene expression, resulting in increased FGF21 secretion into the bloodstream. In contrast to physiologically induced FGF21 expression, this pharmacological approach strongly increased FGF21 serum levels, by more than 200-fold to be more specific. This led to decreasing body weight while the food intake remained unaltered. At the same time, the weight of several tissues reduced as well, including the liver and eWAT, but not scWAT. There are previous reports about increased serum FGF21 levels strongly reducing body weight without food intake having changed, respectively protecting from diet-induced weight gain and obesity [129, 130, 242-244]. A study that also used an AAV to overexpress FGF21 specifically in the liver reported a similar decrease in the body weight of obese mice after monitoring their weight for the first four weeks after AAV injection [242]. This was also independent of food intake. They found the masses of the liver, eWAT, and scWAT had reduced in obese mice by the end of their experiment, which came to a close after one year. One could speculate that the amount of time and the obesity of the mice contributed to changing the outcome of the organ weight measurements in contrast to the study here, especially because adipose tissue behaves as described in **Chapter 1.4.1** when a person or animal is obese. Some of these studies report adipose tissues and adipocyte sizes being reduced by FGF21 as well [114, 242]. The size of the adipocytes was not determined in this study. However, based on the data obtained, the hypothesis can be made that they will be smaller, which would then be consistent with the reports from the literature.

Unsurprisingly, the blood glucose had decreased in the mice fed *ad libitum*, which suggests better insulin sensitivity. This coincides with the findings from previous studies [129-131, 244-253]. The serum triglycerides were decreased in the FGF21 overexpression model, which also matched reports from literature [130, 131, 244, 254]. The levels of NEFAs in the serum had not changed. In the literature other studies showed different results with increasing [114] and also decreasing NEFA levels caused by FGF21 overexpression in their models [244] or as a result of FGF21 administration [255]. The NEFAs were only measured at the end of the experiment in the presented model, and changes in NEFA secretion could have been induced in the first days after AAV injection, which, in turn, may have normalized by the end of this experiment owing to a feedback mechanism. Interestingly, it was suggested in the literature that the elevated FGF21 serum levels are not responsible for the increase of NEFAs in the

serum, but that enhanced NEFA secretion intensifies PPARα signaling, eventually resulting in increasing FGF21 expression and secretion [256-258]. NEFAs are substrates for β-oxidation. The products created by this process are ketones, which were found to have increased in the serum of transgenic FGF21 mice [114], and β-oxidation was reported to be elevated in these mice as well [128]. Since the NEFA levels were not upregulated in this study, it is presumed that blood ketone levels remained unaltered because NEFAs were not available for β-oxidation. Consistent with previous studies, this study found that the elevated levels of FGF21 increase circulating levels of adiponectin [123, 124, 242, 244].

It is important to note, this study is limited to male mice. All results regarding the induced regulations upon FGF21 overexpression need to be reevaluated in female mice. In this study, elevated *Fgf21* gene expression and FGF21 serum levels were induced to an extent that is physiologically impossible. One could speculate that the FGF21 elevation during fasting is not strong enough to cause similar changes to those observed in this study. Furthermore, all organs as well as the serum were subject to experimental analysis 24 days after the injection of the AAV. All results of this study refer to this specific timepoint. It is not possible to draw a conclusion about short-term occurring effects within the first few days after injection. The same true for long-term effects after several months, since this was not investigated. Short-term and long-term analyses might provide additional insights into possible counter-regulations the organism is initiating when overexpressing FGF21 in the liver. All of this could influence not only the changes regarding the metabolic homeostasis described in this section, but also those on retinoid homeostasis (**Chapter 5.4**), on lipolytic enzymes (**Chapter 5.5**), and on browning (**Chapter 5.6**).

Overall, the metabolic effects of increased hepatic *Fgf21* gene expression and elevated FGF21 secretion overlap with most of the previous findings, underlining the reliability of the presented model.

5.4 FGF21 Induces Retinoid Homeostasis Alterations but Is Not the Cause of its Fasting-Mediated Changes

For the first time, FGF21's impact on retinoid homeostasis has been uncovered. The initial question of this study aimed to find out whether FGF21 secretion induces retinoid repartitioning from white adipose tissue to the liver during fasting. Similar to the findings for the fasted state, the retinol levels remained stable in serum of mice overexpressing FGF21. The current literature suggests the circulating retinol levels to be kept within narrow limits in order to maintain the physiological steady-state concentration [23]. As mentioned in **Chapter 5.1**, this study suggests this is regulated by a balance of insulin and glucagon signaling pathways.

While concentrations of retinol and retinyl esters in the liver increased due to the FGF21 overexpression, the overall retinol content in the whole organ revealed that the retinol and retinyl ester levels remained unaltered, since the liver weight of animals overexpressing FGF21 had decreased. This finding does not support the statement that FGF21 is secreted in times of fasting to promote reverse transport of retinoids from the liver, because one would otherwise expect to see increasing hepatic retinoid levels caused by the pharmacological FGF21 elevation. All mice of this study on FGF21 were fed *ad libitum* and, thus, did not experience a lack of retinoid intake caused by fasting. This contributed to the expectation of increased rather than decreased hepatic retinoid levels.

Nevertheless, the analysis of RAR target genes in the liver showed an upregulation of Cyp2c39 and *Rarβ2*, which could indicate that FGF21 induces catabolism by Cyp2c39 and promotes RAR stimulation. This leads to the assumption that retinoids are indeed transported reversely to the liver while, however, hepatic stores are maintained within narrow limits, leading to increased catabolism. This remains a speculation, because the retinoic acid levels were not measured.

Based on the findings that illustrated how eWAT and scWAT can play different metabolic roles, these two types of adipose tissue were analyzed separately [150-158]. Indeed, the retinoid concentrations and the calculation of total retinoid content resulted in different outcomes for both organs. In eWAT, the retinyl ester content per whole organ decreased, indicating FGF21 induced retinol secretion from eWAT. In contrast, scWAT, had significantly elevated retinol and retinyl ester concentrations, however, the total amount per whole organ showed only a non-significant trend of increased retinoid content. The differing results for eWAT and scWAT suggest that both types of adipose tissue not only fulfill different roles in the energy and glucose metabolism, but also in retinoid homeostasis. One could assume that the replenishment of retinoids in the liver is not conducted by the white adipose tissue in general, but more likely by eWAT. The scWAT retinoid content appears to be protected and functions as a highly relevant metabolic organ on its own. Strikingly, the amount of total retinoids depleted from eWAT was only around 1.5 µg per whole organ, while the amount of total retinoids usually found in the liver is more than 100-fold higher. This leads to the conclusion that eWAT-derived retinoids are not capable of fully replenishing of hepatic retinoid stores.

Having taken all of this into consideration, this study suggests that hepatic FGF21 overexpression and increased secretion induce a signal to export retinoids from eWAT, but not scWAT. The amount of retinoids in the liver is *per se* higher, and it is not possible to state whether the relatively small amount of retinoids mobilized from eWAT was transported to the liver or elsewhere. Whether only this small amount of retinol was actually reverse transported to the liver as a result of FGF21's action, and, in turn, whether FGF21 is not the only signal

induced during fasting to regulated retinoid homeostasis remains to be seen. The increased hepatic mRNA expression of RAR target genes points towards an enhanced transformation to retinoic acid, which could be due to the suggested reverse transport of retinol from eWAT, even if the total amount is only little as stated before. The retinoic acid metabolizing enzyme family CYP26 includes *Cyp26a1*, which is predominantly expressed in the liver, and *Cyp26b1*, which is predominantly expressed in extrahepatic tissues, such as white adipose tissues [259]. None of the following genes were regulated in eWAT: *Cyp26b1*, *Lrat*, *Rarβ2*, or the RBP4 receptor *Stra6*. This indicates that the retinyl esters are only converted to retinol and transported out of this tissue. This would include that they do not initiate any further RAR activation, supporting the notion that retinol is transported out of eWAT by means of the FGF21 signal.

In scWAT, not only the retinoid content was detected differently, but also the RAR target genes. Although not significant due to a high standard error of the mean, *Cyp26b1* expression levels displayed a trend of upregulation. Moreover, *Rarβ2* was upregulated significantly. This led to the conclusion that FGF21 overexpression alters RAR signaling in scWAT. When taking into account that retinol and retinyl ester content displayed an increasing trend, it is possible that scWAT was responding to this by promoting RAR signaling-related genes and their transcription.

This study thus shows that not only the liver, but also scWAT reacts to increased FGF21 availability by maintaining a constant retinol content and inducing retinoic acid signaling. The eWAT does not show this gene regulation. It is concluded from the retinoid content detected in eWAT that retinoids are liberated from its storage in eWAT. It remains unclear if these eWAT-derived retinoids reach the liver and/or scWAT. Therefore, it can be hypothesized that the functions of retinoids in the liver are tightly regulated to maintain physiological functions, and that the same also true for retinoids in scWAT. However, it should be mentioned that hepatic retinoid stores are more abundant that those in white adipose tissue and therefore display the more important tissue store for the organism.

The homeostasis of retinoids in this study needs to be also evaluated by investigating the main retinol binding and transport proteins since crosstalk and reverse transport are key points in the proposed hypothesis. Neither hepatic *Rbp4*, nor *Ttr* gene expression were upregulated and the serum levels of both proteins remained unaltered. RBP4 protein expression was upregulated in the liver. This could be explained by the almost significant and only slightly upregulated hepatic *Rbp4* gene expression (with a *P*-value of 0.06) that did not lead to increasing RBP4 serum levels, but, in turn, suggests unaltered secretion. To be more precise, it indicates an accumulation to maintain the retinoid content in the liver, not its mobilization. *Crbp1*, retinol's binding protein within the hepatocyte, did not show changes in its mRNA level,

supporting the notion that hepatic retinoid homeostasis is supposed to be kept in a constant state.

In both investigated white adipose tissues, the *Rbp4* gene expression increased, but the changes in scWAT were stronger than in eWAT. Surprisingly, this effect was not reflected in the protein levels in both tissues. This study hypothesizes that retinol is transported from adipose tissue to the liver, and the possibility arises that retinol is reverse transported by RBP4 originating from eWAT. However, it is known that the circulating RBP4 in mice is secreted solely by the liver [46]. When this and the unaltered RBP4 levels in eWAT are taken into account, it becomes clear that retinoids in this model are not mobilized from eWAT via RBP4. Another relevant retinol binding protein is CRBP1. It was not regulated on mRNA and protein level in eWAT and scWAT. All of this leads to the conclusion that the induced changes in retinoid content in eWAT and scWAT are not associated with alterations of the expression levels of RBP4 and CRBP1.

In addition to the limitations of this study mentioned in **Chapter 5.3**, a tracing study would provide interesting insights into the retinoid homeostasis. The results of this study combined with those of the preliminary study only allow for hypotheses about retinoids being transported from one organ to the other. It is not clear if white adipose tissue can release enough retinol to replenish hepatic stores. Therefore, it would be of great interest to find a way to detect the route of retinoids through the organism.

The question whether elevated FGF21 is the cause of altered retinoid homeostasis during fasting or one of the consequences – together with changes in retinoid distribution and signaling – of fasting arose after this study had been conducted. Overall, the following observations led to the conclusion that FGF21 elevation is not a cause for changes in retinoid homeostasis, but rather a consequence of fasting: the amounts of retinoids in the liver, serum, and scWAT were unaltered; a lack of alterations regarding the intra- and extracellular retinol binding proteins was observed; retinoid levels in eWAT were reduced; RAR signaling in scWAT and liver was induced. The changes in the amounts of missing retinoids in eWAT were rather small and not thought to be able to function as substitute for potentially lacking hepatic retinoids in the fasted state, especially when keeping in mind that hepatic *Fgf21* increases 28-fold during 12 h of fasting [114]. This increase was actually surpassed in the here presented study and confirmed to be approximately 200-fold higher. If FGF21 had been a cause of retinoid repartitioning, it would have been expected that FGF21 overexpression decreases the retinoid content in white adipose tissue and increases hepatic retinoid content. Thus, FGF21 is not thought to be causative for repartitioning of retinoids from white adipose tissue to the liver, however, FGF21 overexpression still promoted changes in RAR signaling, as well as the release of small amounts of retinol from eWAT with an unknown destination.

Finally, FGF21 turned out not to be the master regulator of retinol homeostasis during fasting, since it only induced minor changes that can only partially contribute to the regulation in the feeding-fasting transition. For this reason, other thus far unknown mechanisms that induce signaling towards adipose tissue for the reverse transport of retinoids during fasting will need to be investigated in the future.

5.5 FGF21 Promotes Retinyl Ester Mobilization from eWAT but Not an Increase in p-HSL Levels

In this study eWAT and scWAT were investigated separately, due to their at least partially distinct functions in metabolism [150-158]. The organ weight of scWAT did not change significantly and even showed a trend to increase that might have become more evident if the experiment had been carried out for a longer period of time. In contrast, the weight of eWAT decreased. FGF21 is a hormone which's expression and secretion increases during exposure to stresses [106]. The data presented here indicates that the induced FGF21 overexpression placed the organism into a pathological situation, thus promoting the preservation – if not expansion – of scWAT to induce protective pathways. The present study exposed a healthy mouse with a normal weight to pharmacologically elevated serum levels of FGF21 exceeding standard physiological elevations by far. This suggests that protective mechanisms were induced by the non-pathophysiological elevation of FGF21 achieved with the AAV injection.

This study recorded increased gene expression levels for *Hsl* and *Atgl* in eWAT and, especially, scWAT. The increased amount of circulating FGF21 is capable of interacting with the receptor complex FGFR1/β-klotho found on white adipose tissue, and can function as an endocrine hormone [110-112]. FGF21 can induce lipolysis, which coincides with the upregulated gene expression levels of *Hsl* and *Atgl* found here [114, 260]. In its by phosphorylation activated form, HSL has been proposed to not only hydrolyze triglycerides, but also retinyl esters [175]. Therefore, it was hypothesized that the overexpression of FGF21 would induce the activity of lipolytic enzymes and that would, in turn, cause HSL to promote retinyl ester hydrolysis. Increased levels of retinol would occur in white adipose tissue, which would result in a reverse transport to the liver. The analysis of total HSL in scWAT and eWAT showed significantly increased protein levels in scWAT and an increasing trend in eWAT. This was consistent with the findings of the gene expression analysis. Interestingly, p-HSL levels in relation to total HSL had decreased in both tissues. This indicated that the increased gene expression and transcription did not influence the phosphorylation of HSL and with that its activity. In a model of hepatocyte-specific overexpression of FGF21 mediated by a non-viral vector, the ratio of p-HSL to HSL did not increase in normal chow fed mice [244]. The

observation that the NEFA levels in the serum of FGF21-overexpressing mice remained unaltered coincides with the conclusion that FGF21 cannot induce lipolysis in the model presented here. However, as mentioned before, the serum NEFA levels were only measured at defined point in time, which means it is possible that in the NEFAs in the serum were elevated during the first days of FGF21's action, but then the organism initiated a feedback mechanism to normalize them.

The levels of p-HSL only allow for hypotheses to be made for the activity of this lipolytic enzyme. To address this, a measurement of its activity would provide new insights. Moreover, it would be interesting to establish a link between the increased gene regulation of *Hsl* and *Atgl*, the unaltered p-HSL levels, and the retinyl ester mobilization from eWAT. As mentioned above, flux studies on retinoids would be interesting to trace the shuttling. Additionally, the possibility of early mobilization cannot be neglected. It could be speculated that the retinyl esters had been mobilized earlier, possibly even with the help of p-HSL, however, a feedback mechanism had regulated these processes and made them undetectable after 24 days. In order to address this, other points in time would need to be analyzed.

In summary, the present data provides evidence of the upregulation of gene expression of the lipolytic enzymes *Hsl* and *Atgl*. FGF21-induced retinyl ester mobilization from eWAT was found, but without an apparent increase in p-HSL at the final time point.

5.6 FGF21 Overexpression Promotes Browning in Subcutaneous Adipose Tissue

The secretion of FGF21 as an endocrine hormone can be induced by several stresses in order to mediate a response mechanism and this includes a stress response to cold exposure [146]. Elevated FGF21 levels were shown to induce murine thermogenic gene expression and promote browning in scWAT, but not in eWAT [133, 146, 253, 261-263]. However, in a model of AAV-mediated overexpression of FGF21 in the liver, browning in white adipocytes was not observed [242]. They investigated the effect of FGF21 overexpression on browning over a time period of one year in obese mice fed a high-fat diet. The serum levels of FGF21 were about 18-fold increased. These findings contradict those obtained for the mice fed a normal chow in this study, which was only conducted over the course of 24 days, and resulted in a more than 200-fold elevation of FGF21's serum levels. Moreover, studies on human samples confirmed a correlation between cold exposure and FGF21 secretion and suggested there is a direct link to the adaptation to cold [264]. In this study the levels of FGF21 in the bloodstream increased due to liver-specific overexpression and the thermogenic target genes *Ucp1* and *Cidea* were found to have upregulated in scWAT, but remained barely detectable in eWAT. This indicates

that the process of browning was induced in scWAT by the hepatic FGF21 overexpression and therefore by the consequences of the elevated circulating levels of FGF21. In scWAT of the control group, the UCP1 protein was barely detectable, while the upregulated gene expression of *Ucp1* in scWAT of FGF21-overexpressing mice directly corresponded with the highly upregulated UCP1 protein levels in this tissue. The aforementioned study that also used an AAV-mediated overexpression of FGF21, observed that multilocular beige adipocytes within the scWAT and UCP1 protein expression in scWAT were not altered [242]. They concluded that browning was unaltered in their model. It is important to note that their model was carried out for a much longer time period and the FGF21 levels did not increase to a level comparable to the ones shown here.

The NEFA levels were not increased in the bloodstream in this study. In part, this could be explained by the increased utilization within scWAT for thermogenic signaling. This was also reflected by the upregulated *Adrb3* gene expression, which suggests there was increased β-adrenergic signaling upon FGF21 stimulation in scWAT.

The results indicate that the FGF21 secreted by the liver affects the adipocytes in scWAT and eWAT. Nonetheless, browning was more robustly induced in scWAT compared to eWAT, since UCP1 was induced in scWAT on protein and mRNA level. As mentioned in **Chapter 1.4.3**, cold exposure promotes browning to a higher extent in scWAT compared to eWAT, which was confirmed within this study.

Browning is not only promoted by stimulation with FGF21, but also by retinoids and retinoid signaling in white adipose tissue [265-267]. The stimulation of white adipocytes with atRA or 9-*cis* RA was shown to induce browning, indicated through the upregulation of specific browning markers, such as *Ucp1* and *Cidea* [184, 185, 268]. Moreover, it was found that increased retinaldehyde levels promote browning [265], and that browning is depended on the presence of RBP4 [269]. Taking this, the upregulated hepatic *Rbp4* gene expression and the increased RBP4 secretion upon cold exposure [269] into account, it was suggested that a functional retinol transport from the liver to adipose tissue is necessary for successful cold adaptation [23, 146, 269, 270]. This points out that not only the impaired FGF21 levels observed in the present study, but also the changes in retinoid homeostasis contribute to the promoted browning in scWAT. The significantly higher retinoid concentration detected in scWAT, and the trend of more retinoids being present per whole organ, indicate a mild change in the retinoid homeostasis of scWAT. Retinoic acid is a known inducer of browning as explained above. However, its levels were not measured in this study. It is hypothesized that the slightly increased presence of retinol and retinyl esters are accompanied by increased levels of retinoic acid. Moreover, genes related to RAR signaling were upregulated in scWAT in this study. Elevated RAR activity is suggested to induce thermogenesis, as it has been

shown to before [180-185]. As explained in **Chapter 5.4**, scWAT is not thought to mobilize its retinyl ester stores. This supports the idea that, like others, retinoids function within the thermogenic programming.

Overall, observations of upregulated thermogenic gene expression and increased UCP1 protein expression indicate that the elevated levels of FGF21 in the serum can easily induce browning in scWAT. Moreover, the slightly increased levels of retinol and of retinyl esters, and the induced RAR signaling in scWAT are suggested to multiply this effect. However, FGF21, in fact, is thought to contribute to a much higher extent to the regulation of browning in this model, since FGF21 was found about 200-fold increased in the serum, while the effects on the retinoid homeostasis were milder in comparison.

6 Summary

This study has uncovered novel insights into retinoid homeostasis during the feeding-fasting transition and offers a characterization of the contribution FGF21 makes to this process. The findings have been summarized in **Figure 43** to provide an overview of the biology of fasting regarding retinoid homeostasis.

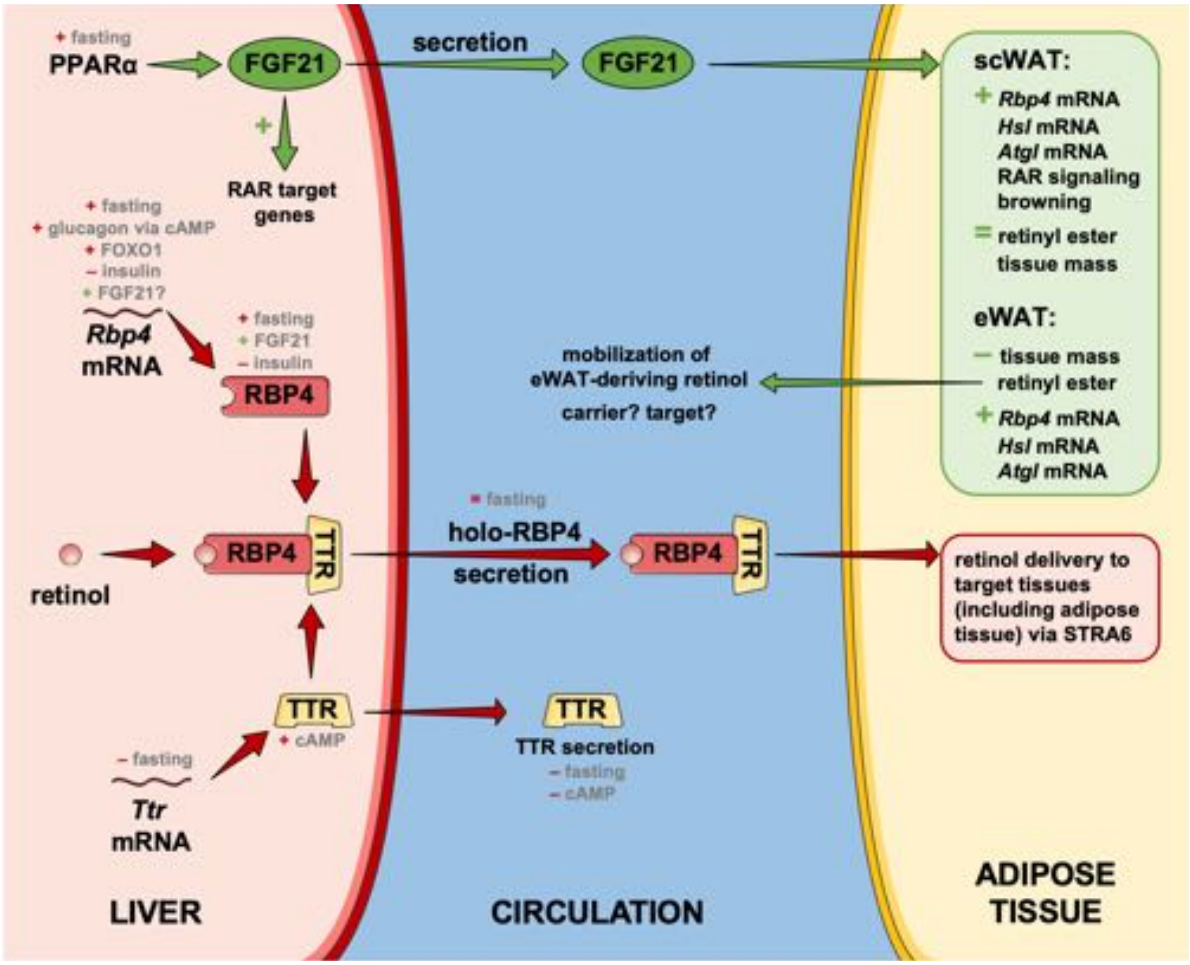

Figure 43: Graphical Summary: Schematic presentation of retinoid homeostasis in fasted mice, including novel findings of this study. The regulation of hepatic expression, translation, and secretion of the retinol transport-related proteins RBP4 and TTR are illustrated. The influence of the fasting-induced secretion of FGF21 and its regulatory effect in adipose tissues are shown.

Retinoids are provided by nutrition and the vast majority are transported to the liver, the main organ for storage and mobilization of retinoids. During fasting, retinoid stores in the liver are kept at a stable level despite lacking nutritional intake. Preliminary studies have shown that changes in the retinoid content of white adipose tissue occur as well as in the regulation of the proteins RBP4 and TTR, which are significant for the transport of retinol. This led to the

hypothesis that retinoids could be transported back to the liver from adipose tissue during the feeding-fasting transition in order to maintain the steady-state concentration in the liver and so as to ensure retinol-related physiological functions of the organism can continue.

One of the questions addressed within this study is the following. Which mechanism underlies the changes of hepatic mRNA expression and protein levels of RBP4 and TTR observed in the fasted state *in vivo*? In order to address this question and unravel the mechanism, an *in vitro* model of primary murine hepatocytes was selected. It was found that *Rbp4* mRNA expression is induced in times of fasting by glucagon via the cAMP signaling pathway. Moreover, the missing action of insulin promotes FOXO1 activity and, thereby, increases the mRNA expression of *Rbp4*, which is additionally thought to be enhanced by cAMP's inducing effect on FOXO1. The completed research verified that this has effects on the hepatic RBP4 protein levels, because fasting increases intracellular protein levels while insulin does the opposite. *Ttr* mRNA expression is downregulated during fasting and the protein secretion is inhibited by fasting due to cAMP signaling. Since there is a higher concentration of TTR in the bloodstream than RBP4, and the serum RBP4 levels remained unaltered in fasting periods, the suggestion was made that mainly the RBP4-independent secretion of TTR diminished. Overall, the gene and protein expression levels of RBP4 in particular, but also TTR, were regulated by the presence of insulin and glucagon. Their ratios shifted during the feeding-fasting transition in order to regulate the retinoid homeostasis and provide retinoids for physiological functions during metabolic changes.

Another question that this study aimed to answer was this: Are the concentrations of apo-RBP4 and holo-RBP4 in the bloodstream altered by fasting? This was of special interest since the export of hepatic retinol was thought to be diminished and repartitioning from adipose tissue suggested to be enhanced and, therefore, changes in the retinol loading of RBP4 were implied into this hypothesis. The liver secretes holo-RBP4 to transport retinol to extra-hepatic target tissues. During feeding-fasting transition, the serum levels of total RBP4 and retinol remained unaltered, which suggests that the organism was somehow maintaining a steady-state of retinoid homeostasis. This study used two different methods: non-denaturing immunoblot and newly established immunoprecipitation of RBP4. The goal was to detect differences in the apo-RBP4 and holo-RBP4 levels in the serum. The methods provided contradicting results and led to different conclusions.

The immunoblot results showed increased levels of apo-RBP4 in the bloodstream of fasted mice. This led to the hypothesis that retinol delivery to target tissues is enhanced and leaves RBP4 unloaded in the bloodstream. As serum retinol levels remained unaltered, this also hinted at the possibility of increased reverse transport via other transporters from extra-hepatic tissues. Another possible explanation for the increased apo-RBP4 levels in the bloodstream

could be a diminished release of hepatic holo-RBP4 and increased secretion of apo-RBP4 from other tissues. The immunoprecipitation results led to the conclusion that serum holo-RBP4 levels are elevated during fasting. This led to believing that holo-RBP4 released its ligand less frequently in the midst of the feeding-fasting transition. All of these hypotheses remain speculative until further research can be conducted. Flux studies would be especially helpful in order to trace the routes of RBP4 and retinol. Thus far, studies of this kind have not been carried out.

Finally, the role of FGF21 in retinoid homeostasis during fasting was investigated in order to answer the following question. Can the secretion of the hepatokine FGF21 promote crosstalk between the liver and adipose tissue and induce retinoid repartitioning from white adipose tissue to the liver? It was discovered that FGF21 is not secreted to alter retinoid metabolism in the proposed way, but still has an impact on the retinoid homeostasis of the liver and adipose tissue. FGF21 induces protein levels of RBP4 in the liver by promoting its mRNA expression. Regardless, the retinol and retinyl ester contents of the liver are not influenced by FGF21's action. The study found that FGF21 promotes scWAT preservation, and that includes its retinoid content. In both mentioned tissues, RAR signaling had been induced, suggesting increased retinoid metabolism within the particular tissue. eWAT retinoid content was reduced and it was thought to have been releasing the retinoids to a thus far unknown destination. The observed alterations in the liver, eWAT, and scWAT were shown to not be associated with major changes in the protein abundance of retinol binding and transport-related proteins RBP4, CRBP1, and TTR.

Whether FGF21's signal induces white adipose tissue lipolysis in the fasted state and whether retinyl esters are mobilized within this process was investigated. The quantification of retinoids in the adipose tissue indicated that retinoids were being mobilized from eWAT. FGF21 was shown to increase the mRNA expression of the lipolytic enzymes *Hsl* and *Atgl* in eWAT and scWAT, but the p-HSL protein levels remained unaltered. Based on these findings, a link was unable to be established between adipose tissue lipolysis and retinyl ester mobilization.

FGF21 was identified as an inducer of browning in scWAT, but not in eWAT. This was concluded from the elevated gene expression levels of thermogenic signaling-related genes *Ucp1* and *Cidea*, as well as the induced UCP1 protein levels in scWAT. Browning was also suggested to have been enhanced by impaired retinoid homeostasis in scWAT. The increased concentrations of retinoids and the trend of elevated total amount of retinoids per tissue combined with the impaired RAR signaling were suspected to advance browning in scWAT. However, the majority of the effect on browning was thought to have been mediated by the abnormally high, pharmacologically induced FGF21 levels.

Overall, this study uncovered new insights into the regulation of retinoid homeostasis during fasting, which involved the balanced signaling of glucagon and insulin, and, to a lesser extent, of FGF21. The study results confirmed that retinoid supply is of great importance for the organism. A close regulation thereof is maintained throughout various metabolic stresses. Among these stresses are fasting and increased FGF21 availability, which are both presented in this study. The impaired FGF21 signaling and altered retinoid homeostasis are both consequences of fasting rather than FGF21 playing a causative role in the observed fasting-related changes in retinoid homeostasis.

7 Literature

1. McCollum, E.V. and Davis, M., *The necessity of certain lipids during growth.* J. Biol. Chem, 1913. **15**: p. 167-175.
2. Blaner, W.S., *Retinol-binding protein: the serum transport protein for vitamin A.* Endocr Rev, 1989. **10**(3): p. 308-16.
3. Blaner, W.S., *STRA6, a cell-surface receptor for retinol-binding protein: the plot thickens.* Cell Metab, 2007. **5**(3): p. 164-6.
4. Morriss-Kay, G.M. and Sokolova, N., *Embryonic development and pattern formation.* Faseb j, 1996. **10**(9): p. 961-8.
5. Napoli, J.L., *Biochemical pathways of retinoid transport, metabolism, and signal transduction.* Clin Immunol Immunopathol, 1996. **80**(3 Pt 2): p. S52-62.
6. Blaner, W.S., et al., *Retinoic Acid Synthesis and Metabolism*, in *Retinoids: The Biochemical and Molecular Basis of Vitamin A and Retinoid Action*, H. Nau and W.S. Blaner, Editors. 1999, Springer Berlin Heidelberg: Berlin, Heidelberg. p. 117-149.
7. Blegvad, O., *Xerophthalmia, Keratomalacia and Xerosis Conjunctivae.* American Journal of Ophthalmology, 1924. **7**(2): p. 89-117.
8. Pirie, A., *Vitamin A deficiency and child blindness in the developing world.* Proc Nutr Soc, 1983. **42**(1): p. 53-64.
9. Petkovich, M., et al., *A human retinoic acid receptor which belongs to the family of nuclear receptors.* Nature, 1987. **330**(6147): p. 444-50.
10. Heyman, R.A., et al., *9-cis retinoic acid is a high affinity ligand for the retinoid X receptor.* Cell, 1992. **68**(2): p. 397-406.
11. Levin, A.A., et al., *9-cis retinoic acid stereoisomer binds and activates the nuclear receptor RXR alpha.* Nature, 1992. **355**(6358): p. 359-61.
12. Rühl, R., et al., *9-cis-13,14-Dihydroretinoic Acid Is an Endogenous Retinoid Acting as RXR Ligand in Mice.* PLoS Genet, 2015. **11**(6): p. e1005213.
13. Palczewski, K., et al., *Crystal structure of rhodopsin: A G protein-coupled receptor.* Science, 2000. **289**(5480): p. 739-45.
14. Goodman, D.W., Huang, H.S., and Shiratori, T., *Tissue Distribution and Metabolism of Newly Absorbed Vitamin A in the Rat.* J Lipid Res, 1965. **6**: p. 390-6.
15. Vogel, S., Gamble, M.V., and Blaner, W.S., *Biosynthesis, Absorption, Metabolism and Transport of Retinoids*, in *Retinoids: The Biochemical and Molecular Basis of Vitamin A and Retinoid Action*, H. Nau and W.S. Blaner, Editors. 1999, Springer Berlin Heidelberg: Berlin, Heidelberg. p. 31-95.
16. Quadro, L., et al., *Transplacental delivery of retinoid: the role of retinol-binding protein and lipoprotein retinyl ester.* Am J Physiol Endocrinol Metab, 2004. **286**(5): p. E844-51.
17. O'Byrne, S.M. and Blaner, W.S., *Retinol and retinyl esters: biochemistry and physiology.* J Lipid Res, 2013. **54**(7): p. 1731-43.
18. Napoli, J.L., *Functions of Intracellular Retinoid Binding-Proteins.* Subcell Biochem, 2016. **81**: p. 21-76.
19. Yamada, M., et al., *Biochemical characteristics of isolated rat liver stellate cells.* Hepatology, 1987. **7**(6): p. 1224-9.
20. Batten, M.L., et al., *Lecithin-retinol acyltransferase is essential for accumulation of all-*

trans-retinyl esters in the eye and in the liver. J Biol Chem, 2004. **279**(11): p. 10422-32.

21. Liu, L. and Gudas, L.J., *Disruption of the lecithin:Retinol acyltransferase gene makes mice more susceptible to vitamin A deficiency.* J Biol Chem, 2005. **280**: p. 40226-34.
22. O'Byrne S, M., et al., *Retinoid absorption and storage is impaired in mice lacking lecithin: Retinol acyltransferase (LRAT).* J Biol Chem, 2005. **280**(42): p. 35647-57.
23. Shirakami, Y., et al., *Hepatic metabolism of retinoids and disease associations.* Biochim Biophys Acta, 2012. **1821**(1): p. 124-36.
24. Haemmerle, G. and Lass, A., *Genetically modified mouse models to study hepatic neutral lipid mobilization.* Biochim Biophys Acta Mol Basis Dis, 2019. **1865**(5): p. 879-894.
25. Monaco, H.L., Rizzi, M., and Coda, A., *Structure of a complex of two plasma proteins: transthyretin and retinol-binding protein.* Science, 1995. **268**(5213): p. 1039-41.
26. Naylor, H.M. and Newcomer, M.E., *The structure of human retinol-binding protein (RBP) with its carrier protein transthyretin reveals an interaction with the carboxy terminus of RBP.* Biochemistry, 1999. **38**(9): p. 2647-53.
27. Bellovino, D., et al., *MMH cells: An in vitro model for the study of retinol-binding protein secretion regulated by retinol.* J Cell Physiol, 1999. **181**(1): p. 24-32.
28. Dixon, J.L. and Goodman, D.S., *Studies on the metabolism of retinol-binding protein by primary hepatocytes from retinol-deficient rats.* J Cell Physiol, 1987. **130**(1): p. 14-20.
29. Smith, J.E., Muto, Y., and Goodman, D.S., *Tissue distribution and subcellular localization of retinol-binding protein in normal and vitamin A-deficient rats.* J Lipid Res, 1975. **16**(4): p. 318-23.
30. Steinhoff, J.S., Lass, A., and Schupp, M., *Retinoid Homeostasis and Beyond: How Retinol Binding Protein 4 Contributes to Health and Disease.* Nutrients, 2022. **14**(6).
31. Taneja, R., et al., *Reexpression of retinoic acid receptor (RAR) gamma or overexpression of RAR alpha or RAR beta in RAR gamma-null F9 cells reveals a partial functional redundancy between the three RAR types.* Proc Natl Acad Sci U S A, 1995. **92**(17): p. 7854-8.
32. Chen, Y., et al., *Structure of the STRA6 receptor for retinol uptake.* Science, 2016. **353**(6302).
33. Kawaguchi, R., et al., *A membrane receptor for retinol binding protein mediates cellular uptake of vitamin A.* Science, 2007. **315**(5813): p. 820-5.
34. Kawaguchi, R., et al., *Receptor-mediated cellular uptake mechanism that couples to intracellular storage.* ACS Chem Biol, 2011. **6**(10): p. 1041-51.
35. Isken, A., et al., *RBP4 disrupts vitamin A uptake homeostasis in a STRA6-deficient animal model for Matthew-Wood syndrome.* Cell Metab, 2008. **7**(3): p. 258-68.
36. Kawaguchi, R., et al., *STRA6-catalyzed vitamin A influx, efflux, and exchange.* J Membr Biol, 2012. **245**(11): p. 731-45.
37. Alapatt, P., et al., *Liver retinol transporter and receptor for serum retinol-binding protein (RBP4).* J Biol Chem, 2013. **288**(2): p. 1250-65.
38. Kanai, M., Raz, A., and Goodman, D.S., *Retinol-binding protein: the transport protein for vitamin A in human plasma.* J Clin Invest, 1968. **47**(9): p. 2025-44.
39. Rask, L., et al., *The retinol-binding protein.* Scand J Clin Lab Invest Suppl, 1980. **154**: p. 45-61.

40. Rask, L., et al., *The complete amino acid sequence of human serum retinol-binding protein.* Ups J Med Sci, 1987. **92**(2): p. 115-46.

41. Newcomer, M.E., et al., *The three-dimensional structure of retinol-binding protein.* Embo j, 1984. **3**(7): p. 1451-4.

42. Zanotti, G. and Berni, R., *Plasma retinol-binding protein: structure and interactions with retinol, retinoids, and transthyretin.* Vitam Horm, 2004. **69**: p. 271-95.

43. Tsutsumi, C., et al., *Retinoids and retinoid-binding protein expression in rat adipocytes.* J Biol Chem, 1992. **267**(3): p. 1805-10.

44. Wu, C., Macleod, I., and Su, A.I., *BioGPS and MyGene.info: organizing online, gene-centric information.* Nucleic Acids Res, 2013. **41**(Database issue): p. D561-5.

45. Wu, C., et al., *BioGPS: an extensible and customizable portal for querying and organizing gene annotation resources.* Genome Biol, 2009. **10**(11): p. R130.

46. Thompson, S.J., et al., *Hepatocytes Are the Principal Source of Circulating RBP4 in Mice.* Diabetes, 2017. **66**(1): p. 58-63.

47. Fedders, R., et al., *Liver-secreted RBP4 does not impair glucose homeostasis in mice.* J Biol Chem, 2018.

48. Muenzner, M., et al., *Retinol-binding protein 4 and its membrane receptor STRA6 control adipogenesis by regulating cellular retinoid homeostasis and retinoic acid receptor alpha activity.* Mol Cell Biol, 2013. **33**(20): p. 4068-82.

49. Lee, S.A., et al., *Adipocyte-specific over-expression of retinol-binding protein 4 (RBP4) causes hepatic steatosis in mice.* Hepatology, 2016. **64**(5): p. 1534-1546.

50. Duan, W. and Schreiber, G., *Expression of retinol-binding protein mRNA in mammalian choroid plexus.* Comp Biochem Physiol B, 1992. **101**(3): p. 399-406.

51. MacDonald, P.N., Bok, D., and Ong, D.E., *Localization of cellular retinol-binding protein and retinol-binding protein in cells comprising the blood-brain barrier of rat and human.* Proc Natl Acad Sci U S A, 1990. **87**(11): p. 4265-9.

52. Soprano, D.R. and Blaner, W.S., *Plasma retinol-binding protein*, in *The Retinoids: Biology, Chemistry, and Medicine*, M.B. Sporn, A.B. Roberts, and D.S. Goodman, Editors. 1994: New York.

53. Soprano, D.R., Soprano, K.J., and Goodman, D.S., *Retinol-binding protein messenger RNA levels in the liver and in extrahepatic tissues of the rat.* J Lipid Res, 1986. **27**(2): p. 166-71.

54. Seibert, F.B. and Nelson, J.W., *Electrophoretic Study of the Blood Protein Response in Tuberculosis.* Journal of Biological Chemistry, 1942. **143**: p. 29-38.

55. Kabat, E.A., Moore, D.H., and Landow, H., *An Electrophoretc Study of the Protein Components in Cerebrospinal Fluid and their Relationship to the Serum Proteins.* J Clin Invest, 1942. **21**(5): p. 571-7.

56. Ingbar, S.H., *Pre-albumin: a thyroxinebinding protein of human plasma.* Endocrinology, 1958. **63**(2): p. 256-9.

57. Raz, A. and Goodman, D.S., *The interaction of thyroxine with human plasma prealbumin and with the prealbumin-retinol-binding protein complex.* J Biol Chem, 1969. **244**(12): p. 3230-7.

58. Felding, P. and Fex, G., *Cellular origin of prealbumin in the rat.* Biochim Biophys Acta, 1982. **716**(3): p. 446-9.

59. Aleshire, S.L., et al., *Localization of human prealbumin in choroid plexus epithelium.* J Histochem Cytochem, 1983. **31**(5): p. 608-12.

60. Smith, F.R. and Goodman, D.S., *The effects of diseases of the liver, thyroid, and kidneys on the transport of vitamin A in human plasma.* J Clin Invest, 1971. **50**(11): p. 2426-36.

61. Vranckx, R., et al., *Immunological quantitation of rat and mouse thyroxine-binding globulins. Ontogenesis and sex-dependence of the circulating levels of the thyroxine-binding globulins.* Acta Endocrinol (Copenh), 1990. **123**(6): p. 649-56.

62. Kanda, Y., et al., *The amino acid sequence of human plasma prealbumin.* J Biol Chem, 1974. **249**(21): p. 6796-805.

63. Bartalena, L., *Recent achievements in studies on thyroid hormone-binding proteins.* Endocr Rev, 1990. **11**(1): p. 47-64.

64. Blake, C.C., et al., *Strjcture of human plasma prealbumin at 2-5 A resolution. A preliminary report on the polypeptide chain conformation, quaternary structure and thyroxine binding.* J Mol Biol, 1974. **88**(1): p. 1-12.

65. Andrea, T.A., et al., *Binding of thyroid hormones and analogues to the human plasma protein prealbumin.* Biochemistry, 1980. **19**(1): p. 55-63.

66. van Bennekum, A.M., et al., *Biochemical basis for depressed serum retinol levels in transthyretin-deficient mice.* J Biol Chem, 2001. **276**(2): p. 1107-13.

67. Goodman, D.S., *Vitamin A and retinoids in health and disease.* N Engl J Med, 1984. **310**(16): p. 1023-31.

68. Noy, N., Slosberg, E., and Scarlata, S., *Interactions of retinol with binding proteins: studies with retinol-binding protein and with transthyretin.* Biochemistry, 1992. **31**(45): p. 11118-24.

69. Wei, S., et al., *Studies on the metabolism of retinol and retinol-binding protein in transthyretin-deficient mice produced by homologous recombination.* J Biol Chem, 1995. **270**(2): p. 866-70.

70. Bernal, J., *Thyroid hormones and brain development.* Vitam Horm, 2005. **71**: p. 95-122.

71. Cheng, S.Y., Leonard, J.L., and Davis, P.J., *Molecular aspects of thyroid hormone actions.* Endocr Rev, 2010. **31**(2): p. 139-70.

72. Saltiel, A.R., *Insulin signaling in health and disease.* J Clin Invest, 2021. **131**(1).

73. Banting, F.G., Best, C.H., and Macleod, J.J.R., *The internal secretion of the pancreas.* Am. J. Physiol., 1922. **59**: p. 479.

74. Kido, Y., Nakae, J., and Accili, D., *Clinical review 125: The insulin receptor and its cellular targets.* J Clin Endocrinol Metab, 2001. **86**(3): p. 972-9.

75. Kasuga, M., et al., *Insulin stimulates tyrosine phosphorylation of the insulin receptor in a cell-free system.* Nature, 1982. **298**(5875): p. 667-669.

76. Ablooglu, A.J. and Kohanski, R.A., *Activation of the Insulin Receptor's Kinase Domain Changes the Rate-Determining Step of Substrate Phosphorylation.* Biochemistry, 2001. **40**(2): p. 504-513.

77. Kahn, C.R., et al., *The insulin receptor and its substrate: molecular determinants of early events in insulin action.* Recent Prog Horm Res, 1993. **48**: p. 291-339.

78. Sun, X.J., et al., *Structure of the insulin receptor substrate IRS-1 defines a unique signal transduction protein.* Nature, 1991. **352**(6330): p. 73-77.

79. Lavan, B.E., Lane, W.S., and Lienhard, G.E., *The 60-kDa Phosphotyrosine Protein in Insulin-treated Adipocytes Is a New Member of the Insulin Receptor Substrate Family *.* Journal of Biological Chemistry, 1997. **272**(17): p. 11439-11443.

80. Sun, X.J., et al., *Role of IRS-2 in insulin and cytokine signalling.* Nature, 1995. **377**(6545): p. 173-177.

81. Gustafson, T.A., et al., *Phosphotyrosine-dependent interaction of SHC and insulin receptor substrate 1 with the NPEY motif of the insulin receptor via a novel non-SH2 domain.* Molecular and Cellular Biology, 1995. **15**(5): p. 2500-2508.

82. Sasaoka, T., et al., *Evidence for a functional role of Shc proteins in mitogenic signaling induced by insulin, insulin-like growth factor-1, and epidermal growth factor.* J Biol Chem, 1994. **269**(18): p. 13689-94.

83. Sun, Y., et al., *Signaling pathway of MAPK/ERK in cell proliferation, differentiation, migration, senescence and apoptosis.* J Recept Signal Transduct Res, 2015. **35**(6): p. 600-4.

84. McCormick, F., *How receptors turn Ras on.* Nature, 1993. **363**(6424): p. 15-16.

85. Myers, M.G., Jr., et al., *Insulin receptor substrate-1 mediates phosphatidylinositol 3'-kinase and p70S6k signaling during insulin, insulin-like growth factor-1, and interleukin-4 stimulation.* J Biol Chem, 1994. **269**(46): p. 28783-9.

86. Backer, J.M., et al., *Phosphatidylinositol 3'-kinase is activated by association with IRS-1 during insulin stimulation.* The EMBO Journal, 1992. **11**(9): p. 3469-3479.

87. Alessi, D.R., et al., *Characterization of a 3-phosphoinositide-dependent protein kinase which phosphorylates and activates protein kinase B alpha.* Current Biology, 1997. **7**(4): p. 261-269.

88. Stephens, L., et al., *Protein Kinase B Kinases That Mediate Phosphatidylinositol 3,4,5-Trisphosphate-Dependent Activation of Protein Kinase B.* Science, 1998. **279**(5351): p. 710-714.

89. Farmer, S.R., *The Forkhead Transcription Factor Foxo1: A Possible Link between Obesity and Insulin Resistance.* Molecular Cell, 2003. **11**(1): p. 6-8.

90. Nakae, J., et al., *The forkhead transcription factor Foxo1 (Fkhr) confers insulin sensitivity onto glucose-6-phosphatase expression.* The Journal of Clinical Investigation, 2001. **108**(9): p. 1359-1367.

91. Burgering, B.M.T. and Coffer, P.J., *Protein kinase B (c-Akt) in phosphatidylinositol-3-OH kinase signal transduction.* Nature, 1995. **376**(6541): p. 599-602.

92. Janah, L., et al., *Glucagon Receptor Signaling and Glucagon Resistance.* Int J Mol Sci, 2019. **20**(13).

93. Elrick, H., Witten, T.A., and Arai, Y., *Glucagon treatment of insulin reactions.* N Engl J Med, 1958. **258**(10): p. 476-80.

94. Habegger, K.M., et al., *The metabolic actions of glucagon revisited.* Nat Rev Endocrinol, 2010. **6**(12): p. 689-97.

95. Ramnanan, C.J., et al., *Physiologic action of glucagon on liver glucose metabolism.* Diabetes Obes Metab, 2011. **13 Suppl 1**(Suppl 1): p. 118-25.

96. Cohen, P., *Activation and phosphorylation of the subunits of phosphorylase kinase.* Biochem J, 1972. **130**(1): p. 5p-6p.

97. Titanji, V.P., Zetterqvist, O., and Engstroöm, L., *Regulation in vitro of rat liver pyruvate kinase by phosphorylation-dephosphorylation reactions, catalyzed by cyclic-AMP dependent protein kinases and a histone phosphatase.* Biochim Biophys Acta, 1976. **422**(1): p. 98-108.

98. El-Maghrabi, M.R., et al., *Regulation of rat liver fructose 2,6-bisphosphatase.* J Biol Chem, 1982. **257**(13): p. 7603-7.

99. Exton, J.H., *Mechanisms of hormonal regulation of hepatic glucose metabolism.* Diabetes Metab Rev, 1987. **3**(1): p. 163-83.

100. Jiang, G. and Zhang, B.B., *Glucagon and regulation of glucose metabolism.* Am J Physiol Endocrinol Metab, 2003. **284**(4): p. E671-8.

101. Miller, R.A. and Birnbaum, M.J., *Glucagon: acute actions on hepatic metabolism.* Diabetologia, 2016. **59**(7): p. 1376-1381.

102. Petersen, M.C., Vatner, D.F., and Shulman, G.I., *Regulation of hepatic glucose metabolism in health and disease.* Nat Rev Endocrinol, 2017. **13**(10): p. 572-587.

103. Nishimura, T., et al., *Identification of a novel FGF, FGF-21, preferentially expressed in the liver.* Biochim Biophys Acta, 2000. **1492**(1): p. 203-6.

104. Beenken, A. and Mohammadi, M., *The FGF family: biology, pathophysiology and therapy.* Nat Rev Drug Discov, 2009. **8**(3): p. 235-53.

105. Beenken, A. and Mohammadi, M., *The structural biology of the FGF19 subfamily.* Adv Exp Med Biol, 2012. **728**: p. 1-24.

106. BonDurant, L.D. and Potthoff, M.J., *Fibroblast Growth Factor 21: A Versatile Regulator of Metabolic Homeostasis.* Annu Rev Nutr, 2018. **38**: p. 173-196.

107. Fon Tacer, K., et al., *Research resource: Comprehensive expression atlas of the fibroblast growth factor system in adult mouse.* Mol Endocrinol, 2010. **24**(10): p. 2050-64.

108. Markan, K.R., et al., *Circulating FGF21 is liver derived and enhances glucose uptake during refeeding and overfeeding.* Diabetes, 2014. **63**(12): p. 4057-63.

109. Hsuchou, H., Pan, W., and Kastin, A.J., *The fasting polypeptide FGF21 can enter brain from blood.* Peptides, 2007. **28**(12): p. 2382-6.

110. Kurosu, H., et al., *Tissue-specific expression of betaKlotho and fibroblast growth factor (FGF) receptor isoforms determines metabolic activity of FGF19 and FGF21.* J Biol Chem, 2007. **282**(37): p. 26687-26695.

111. Suzuki, M., et al., *betaKlotho is required for fibroblast growth factor (FGF) 21 signaling through FGF receptor (FGFR) 1c and FGFR3c.* Mol Endocrinol, 2008. **22**(4): p. 1006-14.

112. Lee, S., et al., *Structures of β-klotho reveal a 'zip code'-like mechanism for endocrine FGF signalling.* Nature, 2018. **553**(7689): p. 501-505.

113. Badman, M.K., et al., *Hepatic fibroblast growth factor 21 is regulated by PPARalpha and is a key mediator of hepatic lipid metabolism in ketotic states.* Cell Metab, 2007. **5**(6): p. 426-37.

114. Inagaki, T., et al., *Endocrine regulation of the fasting response by PPARalpha-mediated induction of fibroblast growth factor 21.* Cell Metab, 2007. **5**(6): p. 415-25.

115. Iroz, A., et al., *A Specific ChREBP and PPARα Cross-Talk Is Required for the Glucose-Mediated FGF21 Response.* Cell Rep, 2017. **21**(2): p. 403-416.

116. Fisher, F.M., et al., *A critical role for ChREBP-mediated FGF21 secretion in hepatic fructose metabolism.* Mol Metab, 2017. **6**(1): p. 14-21.

117. von Holstein-Rathlou, S., et al., *FGF21 Mediates Endocrine Control of Simple Sugar Intake and Sweet Taste Preference by the Liver.* Cell Metab, 2016. **23**(2): p. 335-43.

118. Iizuka, K., Takeda, J., and Horikawa, Y., *Glucose induces FGF21 mRNA expression through ChREBP activation in rat hepatocytes.* FEBS Lett, 2009. **583**(17): p. 2882-6.

119. Sánchez, J., Palou, A., and Picó, C., *Response to carbohydrate and fat refeeding in*

the expression of genes involved in nutrient partitioning and metabolism: striking effects on fibroblast growth factor-21 induction. Endocrinology, 2009. **150**(12): p. 5341-50.

120. BonDurant, L.D., et al., *FGF21 Regulates Metabolism Through Adipose-Dependent and -Independent Mechanisms.* Cell Metab, 2017. **25**(4): p. 935-944.e4.

121. Ding, X., et al., *βKlotho is required for fibroblast growth factor 21 effects on growth and metabolism.* Cell Metab, 2012. **16**(3): p. 387-93.

122. Xu, J., et al., *Acute glucose-lowering and insulin-sensitizing action of FGF21 in insulin-resistant mouse models--association with liver and adipose tissue effects.* Am J Physiol Endocrinol Metab, 2009. **297**(5): p. E1105-14.

123. Holland, W.L., et al., *An FGF21-adiponectin-ceramide axis controls energy expenditure and insulin action in mice.* Cell Metab, 2013. **17**(5): p. 790-7.

124. Lin, Z., et al., *Adiponectin mediates the metabolic effects of FGF21 on glucose homeostasis and insulin sensitivity in mice.* Cell Metab, 2013. **17**(5): p. 779-89.

125. Jensen-Cody, S.O., et al., *FGF21 Signals to Glutamatergic Neurons in the Ventromedial Hypothalamus to Suppress Carbohydrate Intake.* Cell Metab, 2020. **32**(2): p. 273-286.e6.

126. Talukdar, S., et al., *FGF21 Regulates Sweet and Alcohol Preference.* Cell Metab, 2016. **23**(2): p. 344-9.

127. Flippo, K.H. and Potthoff, M.J., *Metabolic Messengers: FGF21.* Nat Metab, 2021. **3**(3): p. 309-317.

128. Potthoff, M.J., et al., *FGF21 induces PGC-1alpha and regulates carbohydrate and fatty acid metabolism during the adaptive starvation response.* Proc Natl Acad Sci U S A, 2009. **106**(26): p. 10853-8.

129. Coskun, T., et al., *Fibroblast growth factor 21 corrects obesity in mice.* Endocrinology, 2008. **149**(12): p. 6018-27.

130. Kharitonenkov, A., et al., *FGF-21 as a novel metabolic regulator.* J Clin Invest, 2005. **115**(6): p. 1627-35.

131. Kharitonenkov, A., et al., *The metabolic state of diabetic monkeys is regulated by fibroblast growth factor-21.* Endocrinology, 2007. **148**(2): p. 774-81.

132. Xu, J., et al., *Fibroblast growth factor 21 reverses hepatic steatosis, increases energy expenditure, and improves insulin sensitivity in diet-induced obese mice.* Diabetes, 2009. **58**(1): p. 250-9.

133. Douris, N., et al., *Central Fibroblast Growth Factor 21 Browns White Fat via Sympathetic Action in Male Mice.* Endocrinology, 2015. **156**(7): p. 2470-81.

134. Owen, B.M., et al., *FGF21 acts centrally to induce sympathetic nerve activity, energy expenditure, and weight loss.* Cell Metab, 2014. **20**(4): p. 670-7.

135. Flippo, K.H., et al., *FGF21 signaling in glutamatergic neurons is required for weight loss associated with dietary protein dilution.* Sci Rep, 2020. **10**(1): p. 19521.

136. Hill, C.M., et al., *FGF21 Signals Protein Status to the Brain and Adaptively Regulates Food Choice and Metabolism.* Cell Rep, 2019. **27**(10): p. 2934-2947.e3.

137. Lan, T., et al., *FGF19, FGF21, and an FGFR1/β-Klotho-Activating Antibody Act on the Nervous System to Regulate Body Weight and Glycemia.* Cell Metab, 2017. **26**(5): p. 709-718.e3.

138. De Sousa-Coelho, A.L., et al., *FGF21 mediates the lipid metabolism response to amino acid starvation.* J Lipid Res, 2013. **54**(7): p. 1786-97.

139. Laeger, T., et al., *FGF21 is an endocrine signal of protein restriction.* J Clin Invest, 2014. **124**(9): p. 3913-22.

140. Maida, A., et al., *A liver stress-endocrine nexus promotes metabolic integrity during dietary protein dilution.* J Clin Invest, 2016. **126**(9): p. 3263-78.

141. Gosby, A.K., et al., *Protein leverage and energy intake.* Obes Rev, 2014. **15**(3): p. 183-91.

142. Raubenheimer, D. and Simpson, S.J., *Protein Leverage: Theoretical Foundations and Ten Points of Clarification.* Obesity (Silver Spring), 2019. **27**(8): p. 1225-1238.

143. Sørensen, A., et al., *Protein-leverage in mice: the geometry of macronutrient balancing and consequences for fat deposition.* Obesity (Silver Spring), 2008. **16**(3): p. 566-71.

144. Chartoumpekis, D.V., et al., *Brown adipose tissue responds to cold and adrenergic stimulation by induction of FGF21.* Mol Med, 2011. **17**(7-8): p. 736-40.

145. Hondares, E., et al., *Thermogenic activation induces FGF21 expression and release in brown adipose tissue.* J Biol Chem, 2011. **286**(15): p. 12983-90.

146. Fisher, F.M., et al., *FGF21 regulates PGC-1α and browning of white adipose tissues in adaptive thermogenesis.* Genes Dev, 2012. **26**(3): p. 271-81.

147. Luong, Q., Huang, J., and Lee, K.Y., *Deciphering White Adipose Tissue Heterogeneity.* Biology (Basel), 2019. **8**(2).

148. Tchkonia, T., et al., *Mechanisms and metabolic implications of regional differences among fat depots.* Cell Metab, 2013. **17**(5): p. 644-656.

149. Frayn, K.N., et al., *Integrative physiology of human adipose tissue.* Int J Obes Relat Metab Disord, 2003. **27**(8): p. 875-88.

150. Fox, C.S., et al., *Abdominal Visceral and Subcutaneous Adipose Tissue Compartments.* Circulation, 2007. **116**(1): p. 39-48.

151. Gastaldelli, A., et al., *Metabolic Effects of Visceral Fat Accumulation in Type 2 Diabetes.* The Journal of Clinical Endocrinology & Metabolism, 2002. **87**(11): p. 5098-5103.

152. Ghaben, A.L. and Scherer, P.E., *Adipogenesis and metabolic health.* Nature Reviews Molecular Cell Biology, 2019. **20**(4): p. 242-258.

153. Kissebah, A.H., et al., *Relation of Body Fat Distribution to Metabolic Complications of Obesity.* The Journal of Clinical Endocrinology & Metabolism, 1982. **54**(2): p. 254-260.

154. Ishikawa, K., et al., *Subcutaneous fat modulates insulin sensitivity in mice by regulating TNF-alpha expression in visceral fat.* Horm Metab Res, 2006. **38**(10): p. 631-8.

155. Mauer, M.M., Harris, R.B., and Bartness, T.J., *The regulation of total body fat: lessons learned from lipectomy studies.* Neurosci Biobehav Rev, 2001. **25**(1): p. 15-28.

156. Lottati, M., et al., *Greater omentectomy improves insulin sensitivity in nonobese dogs.* Obesity (Silver Spring), 2009. **17**(4): p. 674-80.

157. Muzumdar, R., et al., *Visceral adipose tissue modulates mammalian longevity.* Aging Cell, 2008. **7**(3): p. 438-40.

158. Weber, R.V., et al., *Subcutaneous lipectomy causes a metabolic syndrome in hamsters.* Am J Physiol Regul Integr Comp Physiol, 2000. **279**(3): p. R936-43.

159. Zechner, R., et al., *FAT SIGNALS-lipases and lipolysis in lipid metabolism and signaling.* Cell Metab, 2012. **15**(3): p. 279-91.

160. Jenkins, C.M., et al., *Identification, cloning, expression, and purification of three novel human calcium-independent phospholipase A2 family members possessing*

triacylglycerol lipase and acylglycerol transacylase activities. J Biol Chem, 2004. **279**(47): p. 48968-75.

161. Villena, J.A., et al., *Desnutrin, an adipocyte gene encoding a novel patatin domain-containing protein, is induced by fasting and glucocorticoids: ectopic expression of desnutrin increases triglyceride hydrolysis.* J Biol Chem, 2004. **279**(45): p. 47066-75.

162. Zimmermann, R., et al., *Fat mobilization in adipose tissue is promoted by adipose triglyceride lipase.* Science, 2004. **306**(5700): p. 1383-6.

163. Vaughan, M., Berger, J.E., and Steinberg, D., *Hormone-Sensitive Lipase and Monoglyceride Lipase Activites in Adipose Tissue.* J Biol Chem, 1964. **239**: p. 401-9.

164. Osuga, J., et al., *Targeted disruption of hormone-sensitive lipase results in male sterility and adipocyte hypertrophy, but not in obesity.* Proc Natl Acad Sci U S A, 2000. **97**(2): p. 787-92.

165. Haemmerle, G., et al., *Hormone-sensitive lipase deficiency in mice causes diglyceride accumulation in adipose tissue, muscle, and testis.* J Biol Chem, 2002. **277**(7): p. 4806-15.

166. Tornqvist, H. and Belfrage, P., *Purification and some properties of a monoacylglycerol-hydrolyzing enzyme of rat adipose tissue.* J Biol Chem, 1976. **251**(3): p. 813-9.

167. Karlsson, M., et al., *cDNA cloning, tissue distribution, and identification of the catalytic triad of monoglyceride lipase. Evolutionary relationship to esterases, lysophospholipases, and haloperoxidases.* J Biol Chem, 1997. **272**(43): p. 27218-23.

168. Zechner, R., et al., *Adipose triglyceride lipase and the lipolytic catabolism of cellular fat stores.* J Lipid Res, 2009. **50**(1): p. 3-21.

169. Lass, A., et al., *Adipose triglyceride lipase-mediated lipolysis of cellular fat stores is activated by CGI-58 and defective in Chanarin-Dorfman Syndrome.* Cell Metab, 2006. **3**(5): p. 309-19.

170. Sztalryd, C., et al., *Perilipin A is essential for the translocation of hormone-sensitive lipase during lipolytic activation.* J Cell Biol, 2003. **161**(6): p. 1093-103.

171. Anthonsen, M.W., et al., *Identification of novel phosphorylation sites in hormone-sensitive lipase that are phosphorylated in response to isoproterenol and govern activation properties in vitro.* J Biol Chem, 1998. **273**(1): p. 215-21.

172. Stralfors, P. and Belfrage, P., *Phosphorylation of hormone-sensitive lipase by cyclic AMP-dependent protein kinase.* J Biol Chem, 1983. **258**(24): p. 15146-52.

173. Strålfors, P., Björgell, P., and Belfrage, P., *Hormonal regulation of hormone-sensitive lipase in intact adipocytes: identification of phosphorylated sites and effects on the phosphorylation by lipolytic hormones and insulin.* Proc Natl Acad Sci U S A, 1984. **81**(11): p. 3317-21.

174. Yeaman, S.J., *Hormone-sensitive lipase--a multipurpose enzyme in lipid metabolism.* Biochim Biophys Acta, 1990. **1052**(1): p. 128-32.

175. Ström, K., et al., *Hormone-sensitive lipase (HSL) is also a retinyl ester hydrolase: evidence from mice lacking HSL.* Faseb j, 2009. **23**(7): p. 2307-16.

176. Cannon, B. and Nedergaard, J., *Brown adipose tissue: function and physiological significance.* Physiol Rev, 2004. **84**(1): p. 277-359.

177. Enerbäck, S., et al., *Mice lacking mitochondrial uncoupling protein are cold-sensitive but not obese.* Nature, 1997. **387**(6628): p. 90-4.

178. Klingenberg, M. and Huang, S.G., *Structure and function of the uncoupling protein from brown adipose tissue.* Biochim Biophys Acta, 1999. **1415**(2): p. 271-96.

179. Seale, P., Kajimura, S., and Spiegelman, B.M., *Transcriptional control of brown adipocyte development and physiological function--of mice and men.* Genes Dev, 2009. **23**(7): p. 788-97.

180. Alvarez, R., et al., *Both retinoic-acid-receptor- and retinoid-X-receptor-dependent signalling pathways mediate the induction of the brown-adipose-tissue-uncoupling-protein-1 gene by retinoids.* Biochem J, 2000. **345 Pt 1**(Pt 1): p. 91-7.

181. Alvarez, R., et al., *A novel regulatory pathway of brown fat thermogenesis. Retinoic acid is a transcriptional activator of the mitochondrial uncoupling protein gene.* J Biol Chem, 1995. **270**(10): p. 5666-73.

182. Berry, D.C., et al., *Retinoic acid upregulates preadipocyte genes to block adipogenesis and suppress diet-induced obesity.* Diabetes, 2012. **61**(5): p. 1112-21.

183. Rabelo, R., et al., *A complex retinoic acid response element in the uncoupling protein gene defines a novel role for retinoids in thermogenesis.* Endocrinology, 1996. **137**(8): p. 3488-96.

184. Mercader, J., Palou, A., and Bonet, M.L., *Induction of uncoupling protein-1 in mouse embryonic fibroblast-derived adipocytes by retinoic acid.* Obesity (Silver Spring), 2010. **18**(4): p. 655-62.

185. Puigserver, P., et al., *In vitro and in vivo induction of brown adipocyte uncoupling protein (thermogenin) by retinoic acid.* Biochem J, 1996. **317 (Pt 3)**(Pt 3): p. 827-33.

186. Rial, E., et al., *Retinoids activate proton transport by the uncoupling proteins UCP1 and UCP2.* Embo j, 1999. **18**(21): p. 5827-33.

187. Petrovic, N., et al., *Chronic Peroxisome Proliferator-activated Receptor γ (PPARγ) Activation of Epididymally Derived White Adipocyte Cultures Reveals a Population of Thermogenically Competent, UCP1-containing Adipocytes Molecularly Distinct from Classic Brown Adipocytes *.* Journal of Biological Chemistry, 2010. **285**(10): p. 7153-7164.

188. Cousin, B., et al., *Occurrence of brown adipocytes in rat white adipose tissue: molecular and morphological characterization.* J Cell Sci, 1992. **103 (Pt 4)**: p. 931-42.

189. Nedergaard, J., et al., *UCP1: the only protein able to mediate adaptive non-shivering thermogenesis and metabolic inefficiency.* Biochimica et Biophysica Acta (BBA) - Bioenergetics, 2001. **1504**(1): p. 82-106.

190. Abreu-Vieira, G., et al., *Cidea improves the metabolic profile through expansion of adipose tissue.* Nat Commun, 2015. **6**: p. 7433.

191. Barbatelli, G., et al., *The emergence of cold-induced brown adipocytes in mouse white fat depots is determined predominantly by white to brown adipocyte transdifferentiation.* Am J Physiol Endocrinol Metab, 2010. **298**(6): p. E1244-53.

192. Barneda, D., et al., *Dynamic changes in lipid droplet-associated proteins in the "browning" of white adipose tissues.* Biochim Biophys Acta, 2013. **1831**(5): p. 924-33.

193. Cinti, S., *Adipose Organ Development and Remodeling.* Compr Physiol, 2018. **8**(4): p. 1357-1431.

194. Cinti, S., *Reversible physiological transdifferentiation in the adipose organ.* Proc Nutr Soc, 2009. **68**(4): p. 340-9.

195. Himms-Hagen, J., et al., *Multilocular fat cells in WAT of CL-316243-treated rats derive directly from white adipocytes.* Am J Physiol Cell Physiol, 2000. **279**(3): p. C670-81.

196. Rosenwald, M., et al., *Bi-directional interconversion of brite and white adipocytes.* Nat Cell Biol, 2013. **15**(6): p. 659-67.

197. Vitali, A., et al., *The adipose organ of obesity-prone C57BL/6J mice is composed of mixed white and brown adipocytes.* J Lipid Res, 2012. **53**(4): p. 619-29.

198. Lee, Y.H., Petkova, A.P., and Granneman, J.G., *Identification of an adipogenic niche for adipose tissue remodeling and restoration.* Cell Metab, 2013. **18**(3): p. 355-67.

199. Lee, Y.H., et al., *In vivo identification of bipotential adipocyte progenitors recruited by β3-adrenoceptor activation and high-fat feeding.* Cell Metab, 2012. **15**(4): p. 480-91.

200. Schulz, T.J., et al., *Identification of inducible brown adipocyte progenitors residing in skeletal muscle and white fat.* Proc Natl Acad Sci U S A, 2011. **108**(1): p. 143-8.

201. Wu, J., et al., *Beige adipocytes are a distinct type of thermogenic fat cell in mouse and human.* Cell, 2012. **150**(2): p. 366-76.

202. Kersten, S., et al., *Peroxisome proliferator-activated receptor alpha mediates the adaptive response to fasting.* J Clin Invest, 1999. **103**(11): p. 1489-98.

203. Gu, J., et al., *Identification of functional peroxisome proliferator-activated receptor α response element in the human Ppsig gene.* Biochemistry (Moscow), 2011. **76**(2): p. 253-259.

204. Sun, Y., et al., *Identification and characterization of a novel mouse peroxisome proliferator-activated receptor alpha-regulated and starvation-induced gene, Ppsig.* Int J Biochem Cell Biol, 2008. **40**(9): p. 1775-91.

205. Weber, P., et al., *Retinol Saturase: More than the Name Suggests.* Trends Pharmacol Sci, 2020. **41**(6): p. 418-427.

206. Obrochta, K.M., Kane, M.A., and Napoli, J.L., *Effects of diet and strain on mouse serum and tissue retinoid concentrations.* PLoS One, 2014. **9**(6): p. e99435.

207. Klyuyeva, A.V., et al., *Changes in retinoid metabolism and signaling associated with metabolic remodeling during fasting and in type I diabetes.* J Biol Chem, 2021. **296**: p. 100323.

208. Yamamoto, Y., Zolfaghari, R., and Ross, A.C., *Regulation of CYP26 (cytochrome P450RAI) mRNA expression and retinoic acid metabolism by retinoids and dietary vitamin A in liver of mice and rats.* Faseb j, 2000. **14**(13): p. 2119-27.

209. White, J.A., et al., *Identification of the Retinoic Acid-inducible All-trans-retinoic Acid 4-Hydroxylase *.* Journal of Biological Chemistry, 1996. **271**(47): p. 29922-29927.

210. Salavert, A. and Iynedjian, P.B., *Regulation of phosphoenolpyruvate carboxykinase (GTP) synthesis in rat liver cells. Rapid induction of specific mRNA by glucagon or cyclic AMP and permissive effect of dexamethasone.* J Biol Chem, 1982. **257**(22): p. 13404-12.

211. Guo, S., et al., *Phosphorylation of serine 256 by protein kinase B disrupts transactivation by FKHR and mediates effects of insulin on insulin-like growth factor-binding protein-1 promoter activity through a conserved insulin response sequence.* J Biol Chem, 1999. **274**(24): p. 17184-92.

212. Wang, L., et al., *Systematic Evaluation of AAV Vectors for Liver directed Gene Transfer in Murine Models.* Molecular Therapy, 2010. **18**(1): p. 118-125.

213. Andreola, F., et al., *Mouse Liver CYP2C39 Is a Novel Retinoic Acid 4-Hydroxylase: ITS DOWN-REGULATION OFFERS A MOLECULAR BASIS FOR LIVER RETINOID ACCUMULATION AND FIBROSIS IN ARYL HYDROCARBON RECEPTOR-NULL MICE *.* Journal of Biological Chemistry, 2004. **279**(5): p. 3434-3438.

214. Smati, S., et al., *Regulation of hepatokine gene expression in response to fasting and feeding: Influence of PPAR-α and insulin-dependent signalling in hepatocytes.*

Diabetes Metab, 2020. **46**(2): p. 129-136.

215. Soprano, D.R., Smith, J.E., and Goodman, D.S., *Effect of retinol status on retinol-binding protein biosynthesis rate and translatable messenger RNA level in rat liver.* J Biol Chem, 1982. **257**(13): p. 7693-7.

216. Mercader, J., et al., *All-trans retinoic acid decreases murine adipose retinol binding protein 4 production.* Cell Physiol Biochem, 2008. **22**(1-4): p. 363-72.

217. Amengual, J., et al., *Lecithin:retinol acyltransferase is critical for cellular uptake of vitamin A from serum retinol-binding protein.* J Biol Chem, 2012. **287**(29): p. 24216-27.

218. Jessen, K.A. and Satre, M.A., *Mouse retinol binding protein gene: cloning, expression and regulation by retinoic acid.* Mol Cell Biochem, 2000. **211**(1-2): p. 85-94.

219. Jessen, K.A. and Satre, M.A., *Induction of mouse retinol binding protein gene expression by cyclic AMP in Hepa 1-6 cells.* Arch Biochem Biophys, 1998. **357**(1): p. 126-30.

220. Chiefari, E., et al., *The cAMP-HMGA1-RBP4 system: a novel biochemical pathway for modulating glucose homeostasis.* BMC Biol, 2009. **7**: p. 24.

221. Ogreid, D., et al., *Comparison of the two classes of binding sites (A and B) of type I and type II cyclic-AMP-dependent protein kinases by using cyclic nucleotide analogs.* Eur J Biochem, 1989. **181**(1): p. 19-31.

222. Wondisford, A.R., et al., *Control of Foxo1 Gene Expression by Co-activator P300.* Journal of Biological Chemistry, 2014. **289**(7): p. 4326-4333.

223. Matsumoto, M., et al., *Impaired regulation of hepatic glucose production in mice lacking the forkhead transcription factor Foxo1 in liver.* Cell Metab, 2007. **6**(3): p. 208-16.

224. Steinhoff, J.S., Lass, A., and Schupp, M., *Biological Functions of RBP4 and Its Relevance for Human Diseases.* Front Physiol, 2021. **12**: p. 659977.

225. Krasinski, S.D., et al., *Postprandial plasma vitamin A metabolism in humans: a reassessment of the use of plasma retinyl esters as markers for intestinally derived chylomicrons and their remnants.* Metabolism, 1990. **39**(4): p. 357-65.

226. Quadro, L., et al., *Muscle expression of human retinol-binding protein (RBP). Suppression of the visual defect of RBP knockout mice.* J Biol Chem, 2002. **277**(33): p. 30191-7.

227. Wei, S., et al., *Retinyl ester hydrolysis and retinol efflux from BFC-1beta adipocytes.* J Biol Chem, 1997. **272**(22): p. 14159-65.

228. Graham, T.E., et al., *Retinol-binding protein 4 and insulin resistance in lean, obese, and diabetic subjects.* N Engl J Med, 2006. **354**(24): p. 2552-63.

229. Yang, Q., et al., *Serum retinol binding protein 4 contributes to insulin resistance in obesity and type 2 diabetes.* Nature, 2005. **436**(7049): p. 356-62.

230. Perduca, M., et al., *Human plasma retinol-binding protein (RBP4) is also a fatty acid-binding protein.* Biochim Biophys Acta, 2018. **1863**(4): p. 458-466.

231. Huang, H.J., et al., *Identification of a Non-Retinoid Compound and Fatty Acids as Ligands for Retinol Binding Protein 4 and Their Implications in Diabetes.* 2010.

232. Nanao, M., et al., *Crystal Structure of Rbp4 Bound to Oleic Acid.* 2010.

233. Cioffi, C.L., et al., *Design, Synthesis, and Pre-Clinical Efficacy of Novel Non-Retinoid Antagonists of Retinol Binding Protein 4 in the Mouse Model of Hepatic Steatosis.* J Med Chem, 2019.

234. Frey, S.K., et al., *Isoforms of retinol binding protein 4 (RBP4) are increased in chronic*

diseases of the kidney but not of the liver. Lipids Health Dis, 2008. **7**: p. 29.

235. Norseen, J., et al., *Retinol-binding protein 4 inhibits insulin signaling in adipocytes by inducing proinflammatory cytokines in macrophages through a c-Jun N-terminal kinase- and toll-like receptor 4-dependent and retinol-independent mechanism.* Mol Cell Biol, 2012. **32**(10): p. 2010-9.

236. Aeberli, I., et al., *Serum retinol-binding protein 4 concentration and its ratio to serum retinol are associated with obesity and metabolic syndrome components in children.* J Clin Endocrinol Metab, 2007. **92**(11): p. 4359-65.

237. Ortega-Senovilla, H., de Oya, M., and Garcés, C., *Relationship of NEFA concentrations to RBP4 and to RBP4/retinol in prepubertal children with and without obesity.* Journal of Clinical Lipidology, 2019. **13**(2): p. 301-307.

238. Mills, J.P., Furr, H.C., and Tanumihardjo, S.A., *Retinol to retinol-binding protein (RBP) is low in obese adults due to elevated apo-RBP.* Exp Biol Med (Maywood), 2008. **233**(10): p. 1255-61.

239. Quadro, L., et al., *Impaired retinal function and vitamin A availability in mice lacking retinol-binding protein.* Embo j, 1999. **18**(17): p. 4633-44.

240. Bellovino, D., et al., *Retinol binding protein and transthyretin are secreted as a complex formed in the endoplasmic reticulum in HepG2 human hepatocarcinoma cells.* Exp Cell Res, 1996. **222**(1): p. 77-83.

241. Frey, S.K., et al., *Factors that influence retinol-binding protein 4-transthyretin interaction are not altered in overweight subjects and overweight subjects with type 2 diabetes mellitus.* Metabolism, 2009. **58**(10): p. 1386-92.

242. Jimenez, V., et al., *FGF21 gene therapy as treatment for obesity and insulin resistance.* EMBO Mol Med, 2018. **10**(8).

243. Lewis, J.E., et al., *Whole-body and adipose tissue-specific mechanisms underlying the metabolic effects of fibroblast growth factor 21 in the Siberian hamster.* Mol Metab, 2020. **31**: p. 45-54.

244. Yano, K., et al., *Hepatocyte-specific fibroblast growth factor 21 overexpression ameliorates high-fat diet-induced obesity and liver steatosis in mice.* Lab Invest, 2022. **102**(3): p. 281-289.

245. Adams, A.C., et al., *LY2405319, an Engineered FGF21 Variant, Improves the Metabolic Status of Diabetic Monkeys.* PLoS One, 2013. **8**(6): p. e65763.

246. Berglund, E.D., et al., *Fibroblast growth factor 21 controls glycemia via regulation of hepatic glucose flux and insulin sensitivity.* Endocrinology, 2009. **150**(9): p. 4084-93.

247. Camporez, J.P., et al., *Cellular mechanisms by which FGF21 improves insulin sensitivity in male mice.* Endocrinology, 2013. **154**(9): p. 3099-109.

248. Charoenphandhu, N., et al., *Fibroblast growth factor-21 restores insulin sensitivity but induces aberrant bone microstructure in obese insulin-resistant rats.* J Bone Miner Metab, 2017. **35**(2): p. 142-149.

249. Hale, C., et al., *Lack of overt FGF21 resistance in two mouse models of obesity and insulin resistance.* Endocrinology, 2012. **153**(1): p. 69-80.

250. Hecht, R., et al., *Rationale-Based Engineering of a Potent Long-Acting FGF21 Analog for the Treatment of Type 2 Diabetes.* PLoS One, 2012. **7**(11): p. e49345.

251. Stanislaus, S., et al., *A Novel Fc-FGF21 With Improved Resistance to Proteolysis, Increased Affinity Toward β-Klotho, and Enhanced Efficacy in Mice and Cynomolgus Monkeys.* Endocrinology, 2017. **158**(5): p. 1314-1327.

252. Véniant, M.M., et al., *Long-acting FGF21 has enhanced efficacy in diet-induced obese mice and in obese rhesus monkeys.* Endocrinology, 2012. **153**(9): p. 4192-203.

253. Emanuelli, B., et al., *Interplay between FGF21 and insulin action in the liver regulates metabolism.* J Clin Invest, 2014. **124**(2): p. 515-27.

254. Gaich, G., et al., *The Effects of LY2405319, an FGF21 Analog, in Obese Human Subjects with Type 2 Diabetes.* Cell Metabolism, 2013. **18**(3): p. 333-340.

255. Schlein, C., et al., *FGF21 Lowers Plasma Triglycerides by Accelerating Lipoprotein Catabolism in White and Brown Adipose Tissues.* Cell Metab, 2016. **23**(3): p. 441-53.

256. Hotta, Y., et al., *Fibroblast growth factor 21 regulates lipolysis in white adipose tissue but is not required for ketogenesis and triglyceride clearance in liver.* Endocrinology, 2009. **150**(10): p. 4625-33.

257. Mai, K., et al., *Free fatty acids link metabolism and regulation of the insulin-sensitizing fibroblast growth factor-21.* Diabetes, 2009. **58**(7): p. 1532-8.

258. Mai, K., et al., *Physiological modulation of circulating FGF21: relevance of free fatty acids and insulin.* Am J Physiol Endocrinol Metab, 2010. **299**(1): p. E126-30.

259. Topletz, A.R., et al., *Comparison of the function and expression of CYP26A1 and CYP26B1, the two retinoic acid hydroxylases.* Biochem Pharmacol, 2012. **83**(1): p. 149-63.

260. Chen, W., et al., *Growth Hormone Induces Hepatic Production of Fibroblast Growth Factor 21 through a Mechanism Dependent on Lipolysis in Adipocytes.* Journal of Biological Chemistry, 2011. **286**(40): p. 34559-34566.

261. Pereira, M.P., et al., *A low-protein, high-carbohydrate diet increases browning in perirenal adipose tissue but not in inguinal adipose tissue.* Nutrition, 2017. **42**: p. 37-45.

262. Adams, A.C., et al., *Fundamentals of FGF19 & FGF21 action in vitro and in vivo.* PLoS One, 2012. **7**(5): p. e38438.

263. Hondares, E., et al., *Hepatic FGF21 expression is induced at birth via PPARalpha in response to milk intake and contributes to thermogenic activation of neonatal brown fat.* Cell Metab, 2010. **11**(3): p. 206-12.

264. Lee, P., et al., *Mild cold exposure modulates fibroblast growth factor 21 (FGF21) diurnal rhythm in humans: relationship between FGF21 levels, lipolysis, and cold-induced thermogenesis.* J Clin Endocrinol Metab, 2013. **98**(1): p. E98-102.

265. Kiefer, F.W., et al., *Retinaldehyde dehydrogenase 1 regulates a thermogenic program in white adipose tissue.* Nat Med, 2012. **18**(6): p. 918-25.

266. Mercader, J., et al., *Remodeling of white adipose tissue after retinoic acid administration in mice.* Endocrinology, 2006. **147**(11): p. 5325-32.

267. Villarroya, F., Iglesias, R., and Giralt, M., *Retinoids and retinoid receptors in the control of energy balance: novel pharmacological strategies in obesity and diabetes.* Curr Med Chem, 2004. **11**(6): p. 795-805.

268. Ribot, J., et al., *Retinoic acid administration and vitamin A status modulate retinoid X receptor alpha and retinoic acid receptor alpha levels in mouse brown adipose tissue.* Mol Cell Biochem, 2004. **266**(1-2): p. 25-30.

269. Fenzl, A., et al., *Intact vitamin A transport is critical for cold-mediated adipose tissue browning and thermogenesis.* Mol Metab, 2020: p. 101088.

270. D'Ambrosio, D.N., Clugston, R.D., and Blaner, W.S., *Vitamin A Metabolism: An Update.* Nutrients, 2011. **3**(1): p. 63-103.